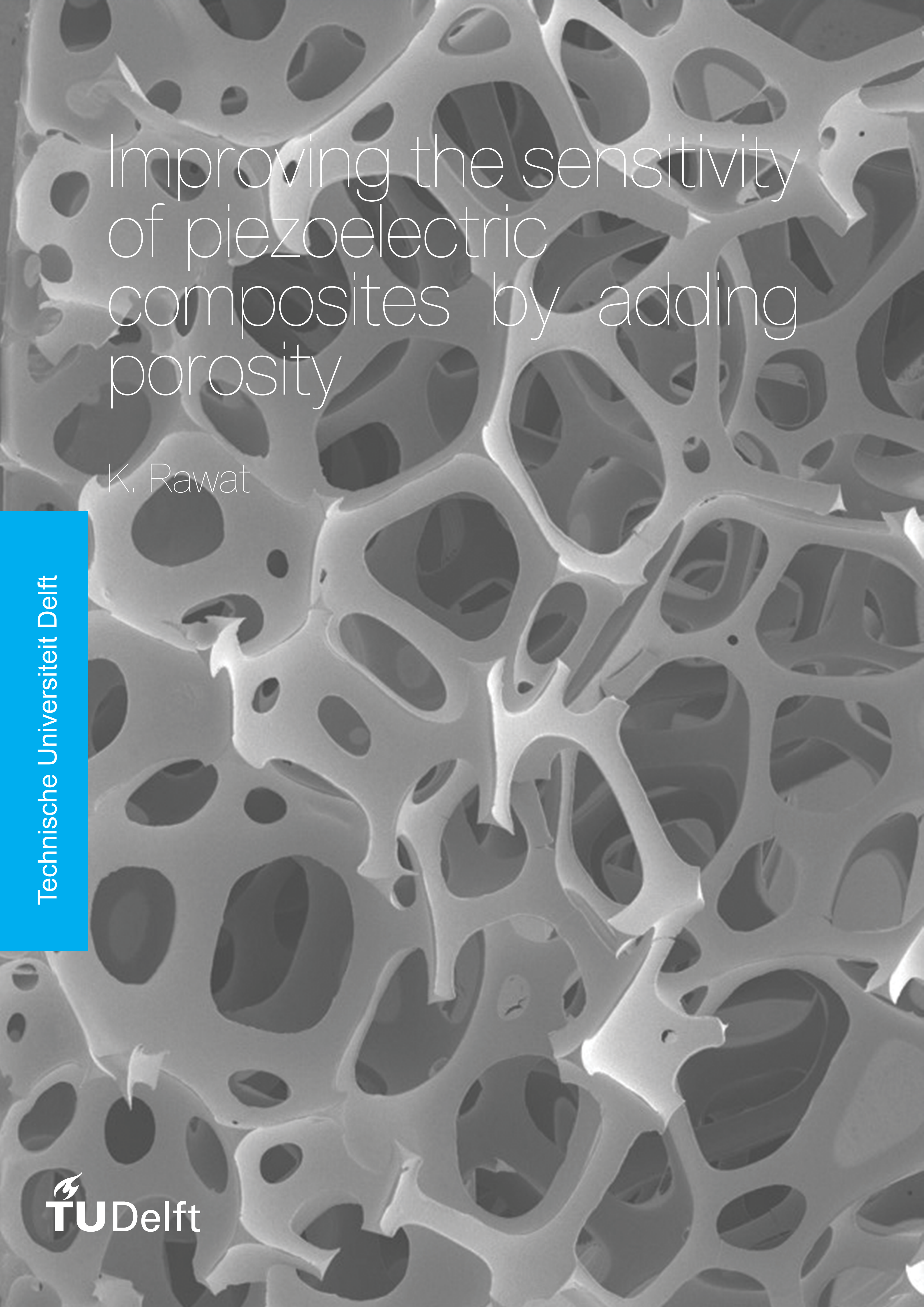

Improving the sensitivity of piezoelectric composites by adding porosity

K. Rawat

Technische Universiteit Delft

TUDelft

Improving the sensitivity of piezoelectric composites by adding porosity

by

Krishna Rawat

to obtain the degree of Master of Science
at the Delft University of Technology,
to be defended publicly on Tuesday 23^{rd} November, 2021 at 10:30 AM.

Student number:	5039908	
Thesis committee:	Prof. dr. ir. S. van der Zwaag,	TU Delft, Chair
	Dr. K. Masania,	TU Delft
	Dr. M. Nijemeisland,	TU Delft
	Dr. T. Mahon,	TU Delft, Daily supervisor

Preface

This MSc thesis concludes the work done within the Novel Aerospace Materials (NovAM) group, part of the Aerospace Structures and Materials (ASM) Department at TU Delft's Faculty of Aerospace Engineering. The whole process now in theory concludes my time as a engineering student, spanning seven fun and interesting years of my life. You experience a lot of ups and downs throughout the whole process, but the whole journey makes it worth the hassle and is something I am grateful for.

Finalizing this master thesis was a difficult task, and it could not have been completed without the help of a lot of people. First, I would like to start with my thesis supervisor, Dr. Tadhg Mahon for giving me an opportunity to work on this topic of research and guiding me throughout this process. He is an incredibly resourceful person who is also easy to talk to. Thanks for giving me the freedom to explore while also providing excellent feedback on the experimental work. Also, I thank him a lot for the feedback provided on the drafts I sent to him (which were a lot!). I would also like to thank Dr. Sybrand van der Zwaag for helping me finalize the thesis on time and giving it a better overall structure. His knowledge and insight on a wide field of research gave me a better understanding of the topic I'm working on and helped me a lot during the final phase of my thesis work. I would also like to express my gratitude to Anton Tuluk, for his incredible insight into piezoelectric systems and for the help provided with the dielectric and piezoelectric measurement setups.

I want to thank ir. Durga Mainali for the help provided in the chemical lab as well as the with the SEM. I would also like to thank Dr. Marlies Nijemeisland for help in the physical lab with the DMA setup. I also express my thanks to Shanta Visser for helping me with my administrative queries and for setting up the monthly progress meetings with my supervisor. Lastly, I want to thank all the NovAM members who have been incredibly fun to be with throughout this whole process. The NovAM meetings as well as the daily coffee/lunch discussions have helped a lot with my work and helped me relax after stressful days. I especially want to give thanks to my fellow master and PhD students: Siddharth, Nikhil, Mark, Caspar, Anuj, Sera, Willem, Dimos, Satya, Hugo and a lot more, who have been incredibly fun to be with and I will miss all the coffee breaks we had together.

At last, I thank my parents Ram and Tejeswari and my sister Bhavna for the incredible support they have provided me throughout my life. A special thanks for teaching me all the important cooking recipes and techniques I mastered during the past year. Love you all.

K. Rawat
Delft, November 2021

Abstract

Piezoelectric materials have the ability to convert mechanical to electrical energy (direct effect) and vice versa. They are readily used in the aerospace, automobile, telecommunication industry etc. as both sensors and actuators. For this work, the focus is on the sensor application, which utilizes the direct piezoelectric effect. With the rapidly growing technological demands, sensors should be flexible enough to adapt to different applications while also having adequate sensing capabilities. Currently, lead- and lead-based piezoelectrics are used in the industry due to their excellent piezoelectric properties. However, due to their toxic nature, research has been ongoing into more lead-free systems which are capable of replicating the performance of these lead-based systems. In this work, we aim to improve the sensing capabilities of lead-free piezoelectric composites. To further improve their performance, reducing the dielectric constant (ε) of the composite is the main strategy of this work that is achieved by fabricating a porous composite structure. The reduction in permittivity leads to an increase in the piezoelectric voltage constant (g), which defines the sensitivity of the piezoelectric composite.

The main focus of this work is to optimize a polymer and polymer foaming technique to obtain a high level of porosity, while also retaining adequate mechanical properties. The next step is to achieve a high poling efficiency for the composite in order to obtain good piezoelectric properties. For the polymer system, polyvinyl alcohol (PVA) is selected as the matrix due to its excellent film-forming ability as well as its relatively high dielectric properties (compared to polymers). The direct foaming technique is used for this work, due to its simplicity and its reproducibility. For the lead-free ceramic system, Barium Titanate ($BaTiO_3$) and Sodium Potassium Niobate doped with Lithium (KNLN3) are selected as they have good piezoelectric properties, and have been used in piezoelectric composites extensively. As a porous piezoelectric composite is used in this work, contact poling is replaced by the corona poling method to prevent localized dielectric breakdowns and non-uniform poling.

With the direct foaming technique, foams with porosities in the range of 90-95 % are obtained, resulting in a drastic reduction in the permittivity of the composite. Such a high porosity level also results in a much softer composite. The optimization of the corona poling process is done by selecting the adequate poling temperature and the grid voltage, which is found to be 110 °C and 6 kV respectively. The effective piezoelectric charge coefficient is measured using Al plates as electrodes, to prevent the soft composites from compressing locally. The foam composites exhibit remarkably high g_{33} values exceeding the 1000 mV.m/N mark, almost double the best sensor used in the industry currently (PVDF). This is attributed to the high poling efficiency and the reduced dielectric permittivity of the composite. This opens up a vast number of possibilities for future systems based on porous structures to be used as sensors that can showcase good piezoelectric properties as well as being more flexible.

Contents

List of Figures

1

Introduction

A material system composed of multiple distinct phases with each phase having its own functionality can be called a multifunctional materials system (MFMS). Effective incorporation of these distinct phases can lead to a wide range of properties, allowing the user to tailor the system to closely fit the application. An important subgroup of these systems is Stimuli-Responsive Materials (SRM), which have the ability to alter their physical/chemical properties in response to an external stimulus [1] and as such see extensive use in sensors. In particular, SRMs that produce a change in the electrical properties of the material in response to a stimulus are especially valuable as such changes are easy to measure when compared to other outputs. Perhaps the most well-known example of such SRMs are the piezoelectric materials [2].

To define piezoelectric materials and their subsets, we start with the introduction of dielectrics. A dielectric material is an electrical insulator with the ability to be polarized under the application of an electric field. Some important dielectric properties are defined in the following text, which is also useful in defining the electrical behaviour of ferroelectrics/piezoelectrics. The dielectric permittivity of a material is defined as the charge storage capacity or the degree of the polarizability of a dielectric. Whereas the dielectric constant or the relative dielectric permittivity (ε_r) is the absolute permittivity of the material divided by the permittivity of vacuum ($\varepsilon_0 = 8.854 \times 10^{-12}$ F/m). It is defined as

$$\varepsilon_r = \frac{\varepsilon}{\varepsilon_0} \tag{1.1}$$

Under an AC field, the dielectric constant has a real and an imaginary component that captures the phase lag between the applied electric field and the resulting electric polarization.

$$\varepsilon = \varepsilon' - i\varepsilon'' \tag{1.2}$$

In an ideal dielectric, there is only displacement of charges due to polarization. The current(I) leads voltage (V) by 90 °. In the real world, all materials are lossy, there is always a small charge flow through the material. In this case, the current leads voltage by an angle less than 90 °, offset by a lag angle (δ). The value of the loss tangent ($\tan\delta$) indicates the dielectric losses dissipated due to heat and is described as the imaginary part of the permittivity divided by the real part of permittivity. The loss tangent factor expresses/describes the usefulness of the dielectric, the lower the value the better.

$$\tan\delta = \frac{\varepsilon''}{\varepsilon'} \tag{1.3}$$

The dielectric strength describes the ability of a dielectric to endure high electric fields without breakdown. It defines the working limits of a dielectric to be used as a capacitor, as the material breaks down above this limit and conducts current. It is defined as the applied voltage per unit thickness of the dielectric, and is an important parameter for piezoelectrics during their poling process.

Piezoelectric materials are a subset of dielectrics that display a change in polarization under a mechanical force (direct effect) or a change in stress/strain behaviour under the influence of an electric field (inverse effect). The piezoelectric phenomenon is observed due to the interaction between the electrical and mechanical states, in crystalline materials/phases without a centre of symmetry [3]. Jacques and Pierre Curie [4] discovered the direct piezoelectric effect in 1880. When certain crystals (Tourmaline, Rochelle salt, quartz etc.) were pressed, a charge was generated in specific positions on the crystal surface. As this effect was only observed in some crystals, the crystallographic symmetry of the system played an important role. The inverse piezoelectric effect was predicted by Lippmann in 1881 and experimentally proven by the Curie brothers in the same year [2].

Atomically, during the direct effect, there is a shift in the centres of the positive and negative charges with respect to each other under the influence of the applied mechanical force, resulting in an electric dipole. The build-up of these dipoles across the material develops a macroscopic electric charge, which can be utilized in an electric circuit. The direct effect is utilized in piezoelectric sensors as there is a linear relationship between the applied mechanical deformation and the change in polarization. The converse effect is observed when mechanical stress, proportional to the applied electric field, is induced in the piezoelectric material. This electric field induced mechanical deformation is utilized in actuators [3]. The linear matrix equations defining the piezoelectric behaviour are shown below in Equation 1.4.

$$\begin{pmatrix} x \\ D \end{pmatrix} = \begin{pmatrix} S^E & d_t \\ d & \varepsilon^T \end{pmatrix} \begin{pmatrix} X \\ E \end{pmatrix} \tag{1.4}$$

The strain *x* and electric displacement *D*, are variables dependent on the stress *X* and electric field *E*. *S* is the elastic compliance, ε is the dielectric permittivity and *d* the piezoelectric charge constant, while the superscripts denote the quantities kept constant during their measurement and subscripts represent the transpose of the tensor [3]. Piezoelectric ceramics display cylindrical symmetry about the poling axis, allowing only three independent d_{ij} components. The poling axis is defined as the '3' direction and the '1' is therefore perpendicular to the poling direction by definition. Thus, the piezoelectric charge coefficient can be defined as :

$$d_{ij} = \frac{e_{ij}}{C_{ij}} \tag{1.5}$$

C_{ij} is the elastic modulus and e_{ij} is the piezoelectric stress modulus at the constant electric field. The piezoelectric voltage constant g_{ij} is defined as the open-circuit voltage generated when stress is applied over a piezoelectric material. It is an important parameter for evaluating the material's sensing and energy harvesting capabilities.

$$g_{ij} = \frac{d_{ij}}{\varepsilon_{ij}} \tag{1.6}$$

where *d* is the piezoelectric charge constant and ε is the dielectric constant of the material. The symmetry of the crystal structure affects the d_{ij} components in the piezoelectric constitutive equation. The three important modes of operation are the longitudinal (d_{33}), transverse (d_{31}) and shear (d_{15}) modes.

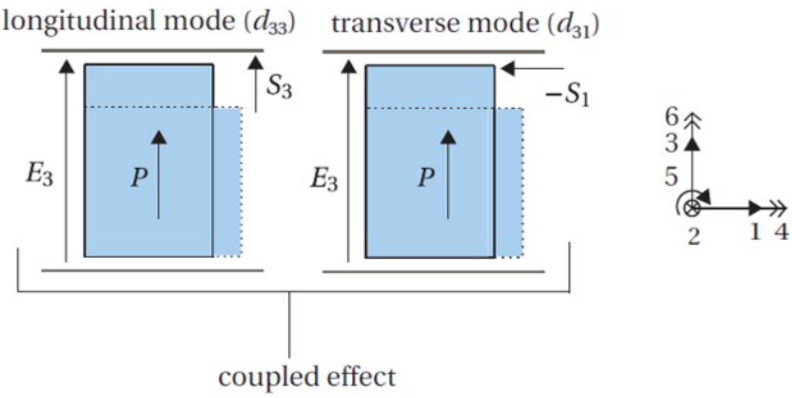

Figure 1.1: Longitudinal (d_{33}) and transverse (d_{31}) mode of operation for piezoelectric [3]

In the d_{33} mode, both the electric field and the deformation are parallel to the direction of polarization (‘3’ direction). While in d_{31} mode, the electric field is parallel to the direction of polarization, while the deformation is perpendicular to it. These two modes are coupled together via the Poisson constant (ν) and are shown in Figure 1.1.

$$d_{31} = -\nu d_{33} \tag{1.7}$$

Another important coefficient to define the functionality/usefulness of the piezoelectric behaviour is the electromechanical coupling coefficient (k). It defines the efficiency of a unit volume piezoelectric material to convert mechanical energy to electrical energy and vice versa. A real-life system cannot achieve full efficiency, so the coupling coefficient always has a value less than one [3].

$$k^2 = \frac{mechanical\,energy\,converted\,to\,electrical\,energy}{mechanical\,input} = \frac{d_{ij}^2}{S_{ij}^E \varepsilon_{ij}^T} \tag{1.8}$$

As the samples are in general poled and probed along their ‘3’-direction, the piezoelectric behaviour is defined by their longitudinal operation mode (d_{33} and g_{33}). Measurement of the d_{33} component is usually done via the direct method, also known as the Berlincourt method. In this method, a disc-shaped piezoelectric material is placed between two spherical probes to measure the direct piezoelectric behaviour. This method requires the measurement to be done under a constant electric field i.e., short-circuit conditions. The measurements are performed quasi-statically due to the issues caused by thermal drift. In the quasi-static method, a small oscillating force, usually at 110 Hz, is applied to a sample that is clamped with a static pre-load to hold it in place. The charge generated is measured and divided by the amplitude of the oscillating force. The static pre-load has to be at least twice the amplitude of the AC force and is required for stable measurements to prevent the sample from rattling [5]. The schematics are shown in Figure 1.2.

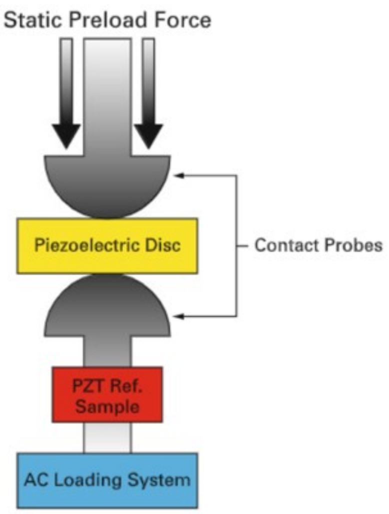

Figure 1.2: Force head schematic for measuring the direct behaviour of the piezoelectric [5]

Out of the twenty crystal classes that show piezoelectric behaviour, ten of them also exhibit pyroelectric behaviour. Pyroelectrics are a subset of piezoelectrics, that exhibit a spontaneous polarisation even before an external force acts on them. These materials will spontaneously change their polarization with a change in temperature due to variations in the positions of charged species with temperature. They are polar dielectrics with a non-centrosymmetric structure, meaning not all piezoelectrics exhibit pyroelectric behaviour. Ferroelectrics are a further subset of pyroelectrics and are able to spontaneously change their direction of polarization under an electric field. As ferroelectrics exhibit both piezoelectric and pyroelectric behaviour, they are multifunctional material systems [6]. Since both ferroelectrics and pyroelectrics are polar, they retain a spontaneous polarization in the absence of an electric field. This relationship between ferroelectrics, pyroelectrics, piezoelectrics and dielectrics is shown in Figure 1.3.

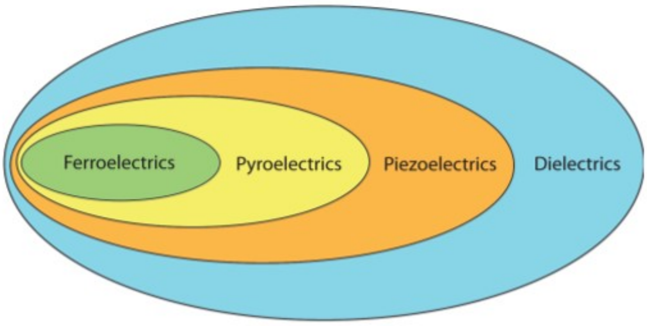

Figure 1.3: Relationship between piezoelectric, pyroelectric and ferroelectric properties [6]

Piezoelectric, pyroelectric and ferroelectric materials undergo a paraelectric phase transition above a certain temperature known as the Curie temperature (T_C). This transition is named for the analogous magnetic → paramagnetic transition observed in ferromagnetic materials. Ferroelectrics that undergo this transition lose their piezoelectric behaviour as the paraelectric phase retains a centrosymmetric crystal structure. As the crystal is cooled through its Curie temperature, the unit cell loses its symmetric structure resulting in the formation of electric dipoles through ferroelectric distortion. Regions with uniform polarizations are formed, which have dipoles aligned in the same direction. These regions are known as Weiss domains, separated by domain walls and a schematic representation is shown in Figure 1.4. The maximum operating temperature of piezoelectric material is therefore considered to be half the value of T$_C$ when expressed in °C.

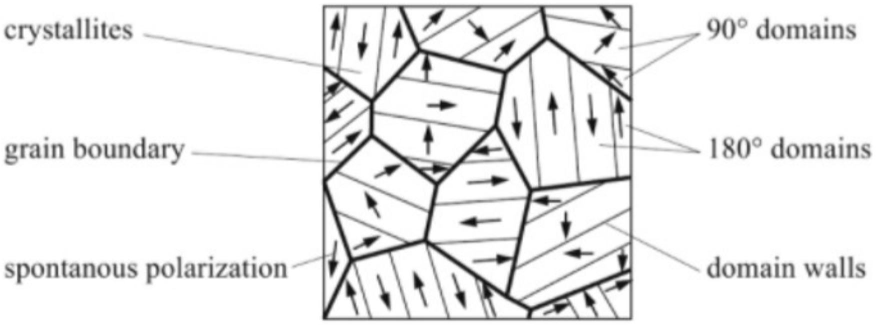

Figure 1.4: Polycrystalline structure of ferroelectrics below their T_C [7]

Piezoelectrics are generally classified into 4 systems: single crystals, polycrystalline ceramics, polymers and composites. A brief introduction of the main classes is given in the following sections to define their piezoelectric behaviour

1.1. Polycrystalline ceramics

Polycrystalline ceramics are the most commonly used form of piezoelectrics as they have good piezoelectric properties and are easy to form into virtually any size and shape. These ceramics are generally isotropic on the macroscopic scale, therefore a large electric field is required to align all the Weiss domains and introduce anisotropy and macroscopic charge. As such, only ferroelectric materials are useful in this form as the polarisation of directions cannot be changed in purely pyroelectric or piezoelectric materials. Some common examples of polycrystalline ceramics are lead zirconium titanate (PZT), barium titanate ($BaTiO_3$) and sodium potassium niobate (KNN). They generally have very high values of dielectric constant and piezoelectric charge constant.

Many ferroelectrics crystallize in the perovskite crystal structure with the general formula ABO_3. This structure is shown in Figure 1.5. A^{2+} and B^{4+} are cations, generally of very different sizes, and the O^{2-} oxygen anion bonds to both A and B. The ideal cubic structure obtained at T>T$_C$, has the B^{4+} cation situated in the centre of an O^{2-} octahedron. In this configuration, the centres of the positive and negative charges coincide and the material does not exhibit piezoelectricity. At T<T$_C$, the material may adopt a range of structures but most commonly tetragonal, rhombohedral or orthorhombic. The B^{4+} ions move away from the centre along the c-direction, changing the centres of the positive and negative charges, creating a permanent dipole moment.

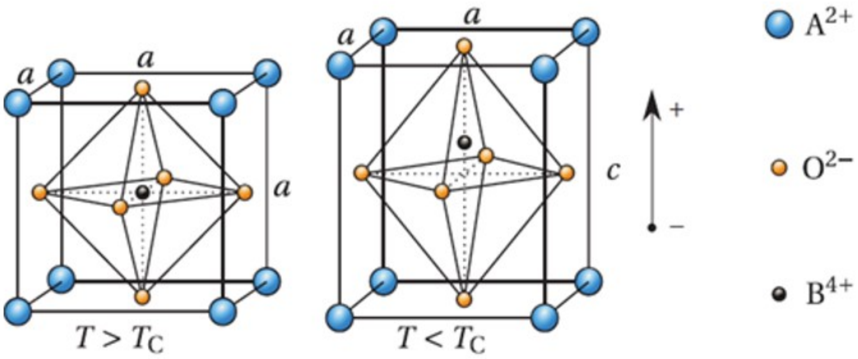

Figure 1.5: Perovskite unit cell above T_C (left) and below T_C (right) [3]

As the polarisation directions of the domains are random, given a large number of domains present in a material the poling directions will statistically cancel to prevent any macroscopic charge. Poling treatment is thus required to introduce artificial anisotropy by reorienting the domains. During the poling process, domains closely aligned to the poling direction grow at the expense of others. Once the field is removed, the dipoles stay partly locked in the polarization direction, resulting in a remnant polarization (P_r). Remnant polarization is retained due to the permanent deformation as a result of strain build-up during the reorientation of the domains [3]. A typical hysteresis loop of polarization vs. field (so-called P-E loops) for a ferroelectric ceramic is shown below in Figure 1.6. Surface topology can affect the poling efficiency due to the difference in local electric fields brought about by changes in the sample thickness from surface roughness. The amount of electric field that can permeate through the material; hence the dielectric behaviour of the piezoelectric controls the poling response.

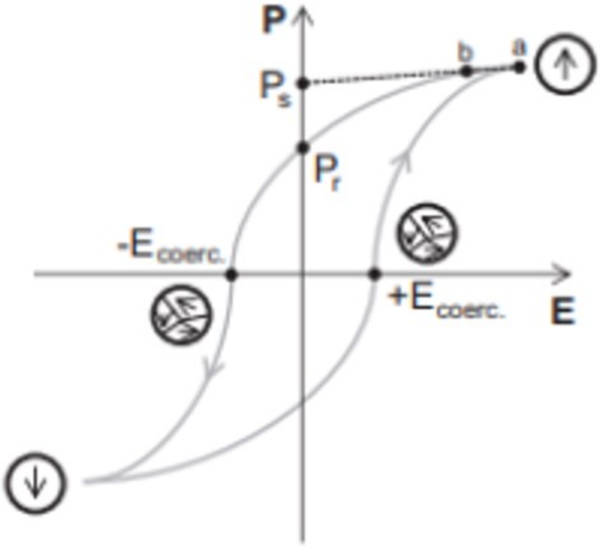

Figure 1.6: P-E Hysteresis loop in a ferroelectric during poling

To align the dipoles in a ferroelectric via poling, switching of domains is required. There are two distinctive groups: 180° (anti-parallel) and non-180° domains [8]. The switching of 180° domains is much easier as their strains are almost similar to the already aligned domains. While for non-180 ° domains, switching is much more difficult due to differences in strains. Since the polarization and strains are coupled together, the remnant polarization is limited by them. There are also certain strain limitations that affect the switching behaviour of these ferroelectrics during poling. For polycrystalline ceramics, the movement of domains inside different grains is constrained by the neighbouring grains. During the re-alignment process, switching of non-180 ° domains is possible only if there is no significant difference in strains at the grain boundaries.

The work done by Li et al. [9] showed that there is almost no switching of non-180° domains in ceramics such as $BaTiO_3$ and PZT, and is only possible at the morphotropic phase boundary (MPB) for PZT where there is a co-existence of at least three phases (monoclinic, rhombohedral and tetragonal). For $BaTiO_3$, on average less than 15% of non-180 ° domains are reoriented during the poling process [10], [11]. For thin films bound to a substrate, there is also a limit on switching. The film is constrained by the substrate, not allowing for dimensional changes under an applied electric field. The ferroelectric is thus not poled completely as there is no strain accommodation. These factors contribute to the much lower remnant polarization observed for $BaTiO_3$ ceramics and is shown in the hysteresis loops in Figure 1.7.

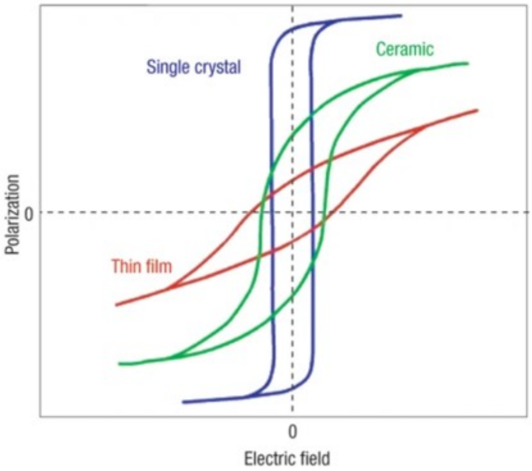

Figure 1.7: Hysteresis loops for ferroelectric single crystal, ceramic and thin films [8]

Currently, PZT systems are still the best performing polycrystalline ceramics in the industry, although their toxic nature has led to a search for other lead-free solutions. The use of toxic lead-oxide precursors during the fabrication process which volatilizes during the high-temperature calcination and sintering process, and the difficulty in disposing of this material has major implications on the environment and human health [12]. A lot of work has therefore been done on finding lead-free systems which have good piezoelectric properties and have been discussed in the following subsections.

1.1.1. Barium Titanate

The ferroelectric phenomena were first discovered in barium titanate during World War II. It crystallizes in the perovskite crystal structure and retains a tetragonal configuration upon cooling down from its Curie temperature of 120 °C. The next phase transition occurs at 0 °C to orthorhombic, and at -80 °C to rhombohedral. The spontaneous polarization is a result of the shifts of the Ti^{4+} and O^{2-} ions from their positions, relative to the $Ba^{2}+$ ions. This change in positions affects the unit cell parameters. The different crystal structures and the transition temperatures are shown below in Figure 1.8.

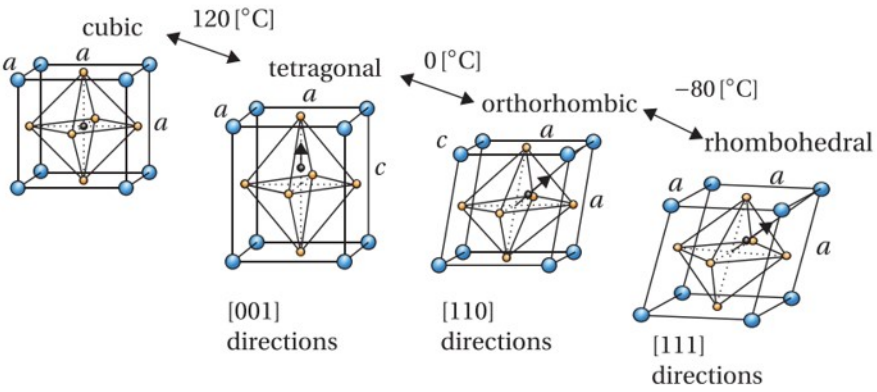

Figure 1.8: Representation of $BaTiO_3$ crystal structures and their transitions at different temperatures [3]

The dielectric and the piezoelectric properties of barium titanate are mainly dependent on the grain size and temperature [13]. Larger grains have much lower piezoelectric and dielectric values as a result of back-switching [14]. Although at very small grain sizes, the effect of reduced lattice distortion results in a significant lowering of piezoelectric properties [15]. Thus, there is an optimum size range where the piezoelectric properties can be maximized. For barium titanate, it lies between 1-2.3 µm, and grains in the region of 10-100 nm exhibit paraelectric behaviour [16], [17]. The effect of grain size on the dielectric and piezoelectric properties is showcased in Figure 1.9. As the operating temperature for ferroelectrics is generally considered to be half its T_C in °C, the use of barium titanate based ceramics is limited by the application temperature. Thus it is often used in polymer-ceramic composites since the polymer system limits the operating temperature in general.

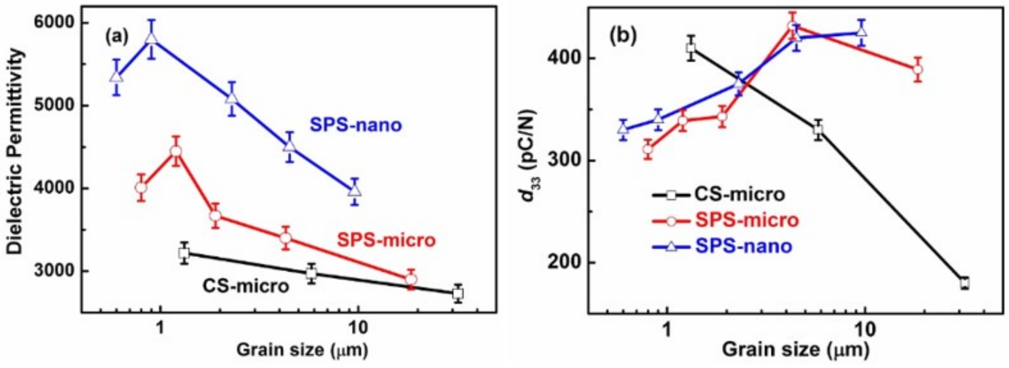

Figure 1.9: Dielectric permittivity (left) and d_{33} vs grain size for poled $BaTiO_3$ ceramics fabricated using conventional and SPS techniques (using micro and nano-sized powders) [16]

1.1.2. KNLN3

Other than $BaTiO_3$, one of the most promising candidates to replace PZT is Sodium Potassium Niobate (KNN) doped with Li. KNN is based on the morphotropic phase boundary of antiferroelectric $NaNbO_3$ and ferroelectric $KNbO_3$ with an equimolar composition. It has a high Curie temperature around 400 °C, allowing for its use in high temperature applications [18], [19]. The doping of KNN with Li substitution allows for an increase in the Curie temperature as well as grain size. It also reduces the temperature required for the orthorhombic to tetragonal phase transition (T_{O-T}) [19]–[22]. The highest value of d_{33} obtained for pure Li doped KNN ceramics is around 200 pC/N, which is much lower than that obtained for PZT systems. However, its lower dielectric permittivity makes it suitable for use in composites, as there is a lower permittivity mismatch between the ceramic and polymer phase.

1.2. Polymers

Piezoelectric polymers, the most important of which is PVDF (poly-vinylidene difluoride), contain a number of crystalline phases, not all of which exhibit piezoelectric properties. Kawai [23] was the first person to discover the ferroelectric behaviour of β-PVDF. In the β-conformation , all the fluorine atoms are on the same side of the backbone, resulting in a net polarization. The non-piezoelectric α-form is, however, most stable at room temperature. The structures of the α and β forms are shown in Figure 1.10. Here, the piezoelectric effect is attributed to the intertwined polymer chain molecules which, under the influence of an applied electric field, attract and repel each other. Due to this, the piezopolymers obtain a negative value of d_{33}, as they have a different structure-property relation to that of piezoceramics. The crystalline phase controls the piezoelectric response, therefore many steps are taken during production to maximise the proportion of the crystalline phase (stretching, controlled annealing and the addition of co-polymers). The addition of trifluoroethylene (TFE) as a copolymer results in crystallinity up to 90% greatly enhancing the piezoelectric properties of the polymer [3].

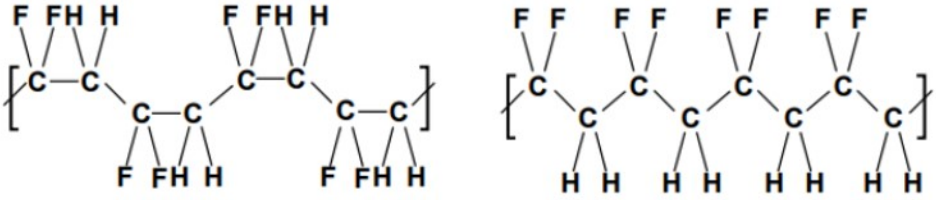

Figure 1.10: α-form (left) and β-form right of PVDF

A comparison of the piezoelectric charge and voltage constants for piezoelectric ceramics and polymer systems is shown below in Table 1.1. Although piezoceramics retain a very high d_{33} in comparison to piezopolymers, their relative permittivity greatly reduces the sensing properties (g_{33}). On the other hand, due to their relatively low permittivity and decent d_{33} values, piezopolymers have an extremely high g_{33} value, making them extremely useful as sensors. It is worth noting that mechanical properties such as Young's modulus and yield strength are generally given as a range, and not a specific value for these polymers. This is because PVDF is a viscoelastic material. Its stress-strain response is time dependant, making it difficult to identify the elastic behaviour with just a single value. The polymer is sometimes assumed to be linearly viscoelastic, but only within certain stress levels [24].

Table 1.1: Comparing the piezoelectric properties of piezoceramics and piezopolymers [3]

	PVDF film	**Copolymer**	**Soft PZT**	**BaTiO$_3$**
Density [10^3 kg/m^3]	1.78	1.82	7.90	5.70
Dielectric constant ε_r [-]	12	8	1800-4000	1800
d_{33} [pC/N]	-30	-38	400-900	190
g_{33} [mV.m/N]	-330	-540	20-25	5

1.3. Composites

A piezocomposite consists of two or more phases in which at least one is piezoelectric when properly processed. It offers substantial advantages over conventional piezoelectric materials in sensing applications. These include excellent flexibility, good electromechanical coupling factor, low acoustic impedance and a low dielectric constant [25]. A study by Lee et al. [26] found that a higher value of the electromechanical coupling factor can be obtained for a lower elastic modulus of the polymer. Although, a very low elastic modulus allows easy deformation of the composite. By designing the material, we can tailor the properties to a specific application which is more difficult with a single material [27]. Another advantage over ceramic materials is their resistance to brittle failure under large cyclic strains when using a flexible polymeric matrix [28].

The connectivity of the different phases plays an important role in their electrical and mechanical properties. The phases can be inter-connected in 0, 1, 2 or 3 dimensions, where 0 is defined as random. A simple two-phase system can, thus, have 10 different arrangements, described as an X-Y composite with X showing the dimensionality of connectivity for the filler phase and Y for the matrix phase. The simplest such configuration being the 0-3 composite, consisting of a random distribution of piezoelectric particles in a 3D polymer matrix [29]. The different possible arrangements are depicted in Figure 1.11. More complex “structured” composites can improve the properties by increasing the connectivity within the ceramic phase. A structured composite is one that shows interconnectivity of the active phase (e.g., 1-3, 2-3 or 3-3).

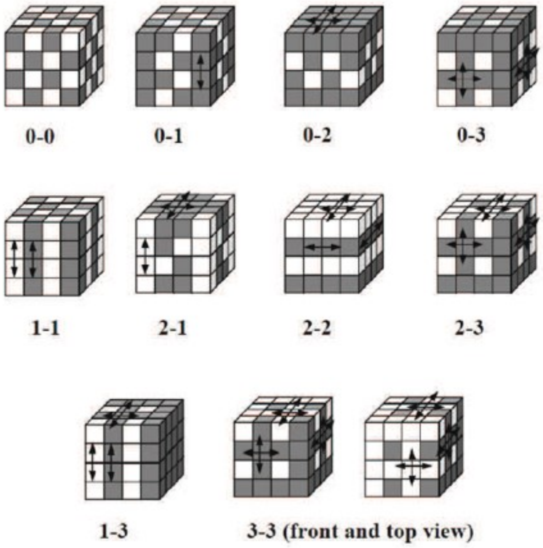

Figure 1.11: Interconnectivity of the phases [3]

Figure 1.12 shows that the piezoelectric voltage constant (g_{33}) of the structured composite reaches a maximum value at lower volume fractions than the random composite. While, at higher loading, the g_{33} of the structured composite converges with the random composite. For cases where high stiffness of the composite is required, a higher loading is required which may favour the random systems due to their comparatively simple synthesis.

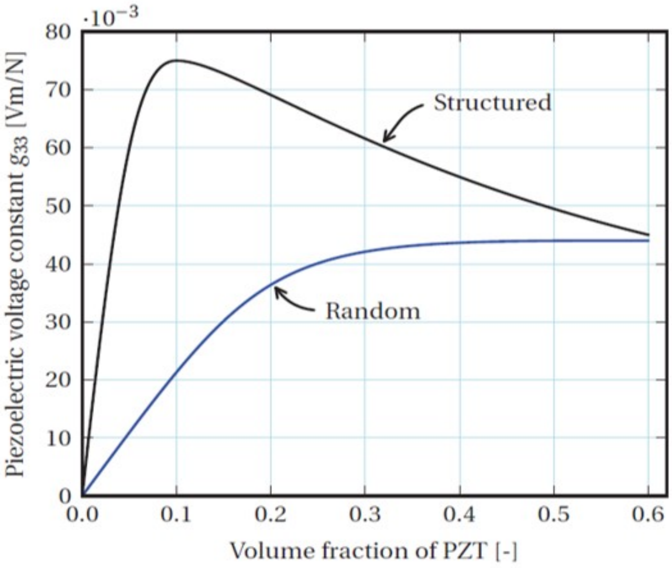

Figure 1.12: The g_{33} values for structured and random samples of PZT [3]

The structuring process can be done by either using templates or via dielectrophoresis to form chain-like structures aligned in one direction [3], [30]–[33]. This quasi 1-3 structuring to form chains is shown below in Figure 1.13. The ceramic particles are aligned under the influence of an AC field and the chain-formation process is dependent on the strength and frequency of the applied field. The viscosity of the polymer matrix also plays a role in counteracting the dielectrophoretic force and hence is another parameter to be considered while optimizing this process [32]. The improvement in performance for the quasi 1-3 structured composites is due to the reduction in inter-particle distance of the active piezoceramics resulting in a much better electromechanical coupling [33]. This alignment technique is only valuable at lower ceramic loadings, as, at higher loadings, the system converges to a random composite [22], [31], [34].

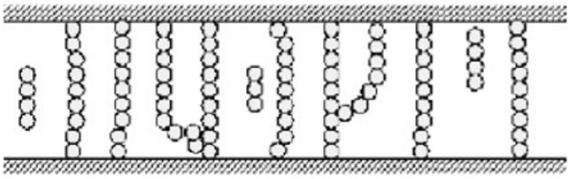

Figure 1.13: Chain-like structuring of ceramic particles at low loadings due to dielectrophoresis [32]

The connectivity of the different phases commands the piezoelectric response as well as the mechanical properties of these composites. The composites in general are either too brittle or relatively ductile with low piezoelectric properties as shown in Figure 1.14. For further improvement, the next generation of composites to be used as sensors should have good mechanical ductility as well as having decent piezoelectric properties. This is explored in the next section by fabricating a porous structure, which will greatly improve the electro-mechanical properties of the composite.

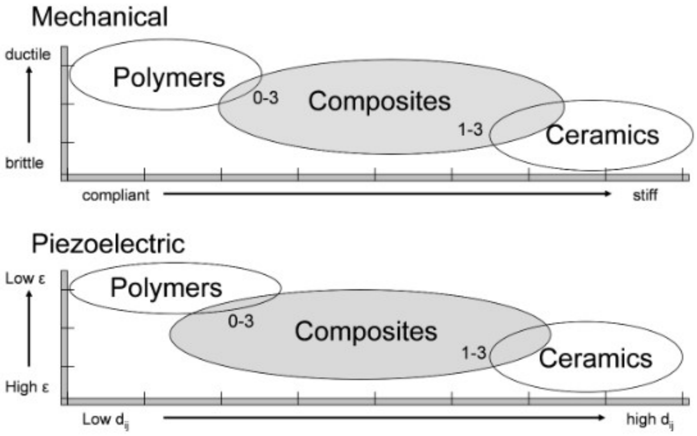

Figure 1.14: Mechanical and piezoelectric properties of different piezoelectric systems [31]

1.3.1. Porous composites

Recent trends in the electronic industry are heading towards the use of ultra-low permittivity dielectrics with permittivity values below 2.2 [35]. The easiest way of obtaining such low values is by fabricating a porous microstructure, due to the fact that air has a permittivity close to one. There are a number of techniques that can be used to obtain a porous structure: thermal decomposition, blowing agents, direct foaming, supercritical foaming etc. These techniques allow the end-user to have control over the pore structure (closed vs open-cell), pore size, pore interconnectivity and the overall porosity of the polymer matrix.

There is an obvious connection between the porosity and the dielectric permittivity of the polymer. A mixed connectivity model could be used to describe the dielectric behaviour of polymer foam. The model uses the serial (0-3) and parallel (1-3) arrangement to specify the connectivity of the pores. The serial connectivity is used for the uniform distribution of pores inside the structure, while the parallel connectivity for pores elongated along the thickness direction [36]. With the increase in porosity, we observe a linear decrease in the permittivity values. If there is a uniform distribution of these pores throughout the polymer matrix, this decrease is known to be exponential. Thus, a major reduction in the permittivity is expected in a polymer with homogeneously distributed pores in comparison to a non-porous/dense polymer [37], [38].

Another important factor to consider is that this inherent change in the microstructure due to the introduction of porosity will also have a major effect on the mechanical properties of the foam. Since, there already is a big mismatch in Young's modulus of the ceramic filler and the polymer matrix, the introduction of porosity also modifies the electromechanical response of the porous composite. For a structured composite, the interaction between the aligned ceramic particles and the polymer matrix will differ from that of a random composite. A random composite can be modelled using a mix of serial and parallel connectivity between the ceramic and polymer matrix, while a 1-3 structured composite shows parallel connectivity [31]. Serial connectivity between the two phases leads to lower stresses applied on the ceramic, as the polymer matrix acts as a stress absorber. While, in the case of parallel connectivity, the polymer-ceramic interface contributes to the stress transfer leading to stress concentrations on the ceramic particles [39]–[41]. This results in higher strains applicable on the piezoactive ceramic and will improve the piezoelectric response [6], although care has to be taken so that the porous composite stays in its linear elastic region.

As we already know from Equation 1.6, the piezoelectric voltage constant (g_{33}) is used to describe the sensitivity of a piezoelectric. A piezoelectric with a high d_{33} in general also has a very high permittivity. Therefore, in order to improve the sensing properties, the dielectric permittivity of the composite is the critical property that plays a major role in improving the sensing behaviour. This is where the overall porosity becomes the key component in improving the voltage response of the composite, considering there is no substantial change in the d_{33}.

Work done by Hamideh et al. [6] showed the effect of introducing porosity in a piezoelectric composite. A 2-component polyurethane was selected as the polymer matrix and porosity was induced by the reaction of water with diisocyanate which liberates CO_2. The addition of water as a chemical blowing agent was used to foam the polymer matrix. PZT was used as the ceramic filler with d_{50} = 1.8 µm to fabricate random (0-3) and dielectrophoretic structured (quasi 1-3) composites.

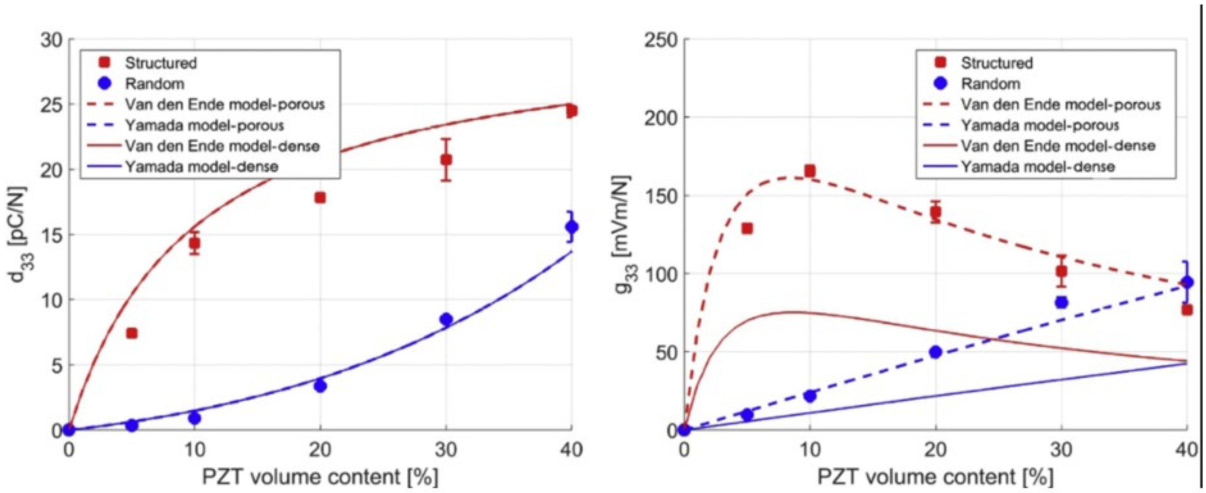

Figure 1.15: Variation of d_{33} (left) and g_{33} (right) with PZT vol.% for random and structured composites. Dashed lines are made using Yamada (0-3) and Van den Ende (1-3) model [6]

The piezoelectric charge (d_{33}) and voltage (g_{33}) response for the porous composites is shown above in Figure 1.15 for both random and structured porous PZT-PU composite with increasing ceramic loading. The g_{33} of the structured porous composite peaks at a low ceramic loading of 10 vol.% and obtains a value (166 mV.m/N) almost double that of a structured bulk/non-porous composite (70-90 mV.m/N) [42]. This major improvement is attributed to the decrease in permittivity by fabrication of foam with 60% porosity. The reduction in the stiffness of the porous composite is also a contributing factor for the improved piezoelectric performance, as explained previously.

However, porosity is not only limited to the polymer phase, it can also be induced in the active piezoceramic phase or at the interface of the two phases [32], [43], as can be seen in Figure 1.16.

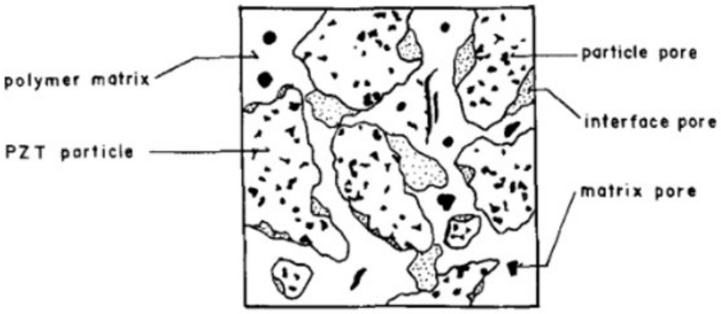

Figure 1.16: Types of porosities in a PZT-polymer composite [43]

Lee and Kim [43] studied the effects of the different types of porosities present in a random (0-3) PZT-polymer composite and their influence on the dielectric and piezoelectric properties. Samples were fabricated using the compression molding technique. According to the study, the pressure applied during the compression molding process controls the interface porosity of the composites. This may also be due to the polymer not properly binding the ceramic filler due to poor adhesion. The interface porosity had a major effect on the reduction in both the dielectric and the piezoelectric properties. The d_{33} suffered a much sharper drop in value, mainly due to the fact that the interface porosity acts as a stress absorber, resulting in lower stresses applied to the piezoceramic. This resulted in the subsequent reduction of g_{33} of the composite. The drop in the d_{33} and relative permittivity with change in interface porosity is shown below in Figure 1.17. Another important factor to consider is that the interface porosity also leads to the formation of insulation barriers around the active piezoceramic phase. The insulation barriers significantly reduce the poling efficiency of the composite, thereby reducing the overall piezoelectric properties [32].

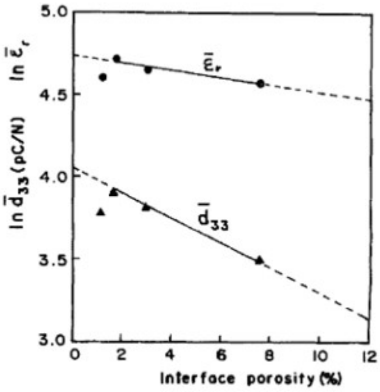

Figure 1.17: Permittivity and d_{33} vs interface porosity for the PZT-polymer composite [43]

Meanwhile, porosity in the ceramic phase results in an exponential decrease of its dielectric and piezoelectric properties. In a pure ceramic, the reduction in piezoelectric behaviour is compensated by the reduced dielectric properties. However, in a composite, the dielectric properties are defined by the contribution from both phases (although still matrix dominated). While the ceramic accounts for the piezoelectric properties. In this case, the reduced permittivity is not able to make up for the low piezoelectric properties, resulting in much lower g_{33} values [43]. Therefore, a random (0-3) composite behaviour at low ceramic loadings is similar to that of a porous ceramic dispersed inside a 3D-interconnected polymer network.

The poling efficiency is also affected by the interconnectivity of the ceramic particles. The work done by Ma and Wang [30] indicates the presence of a depolarizing field in random (0-3) composites, which is not present in structured (1-3) composites. This depolarization field results in almost no switching of domains during the poling process, leading to very low piezoelectric properties. This effect is shown in Figure 1.18.

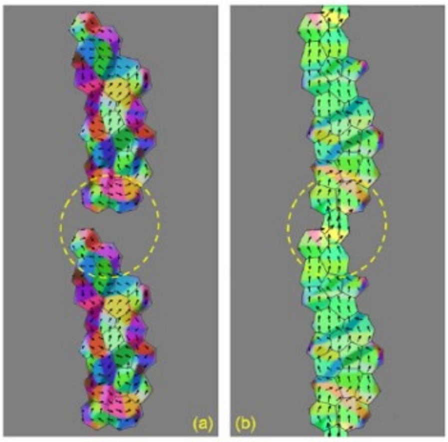

Figure 1.18: Distribution of polarization in simulated (a) disconnected and (b) interconnected piezoelectric particles [30]

Electret behaviour

A consequence of poling dielectric composites is the formation of quasi-permanent charges either in the bulk or on the surface of the material (real charges), or in frozen and aligned dipoles (dipolar charges) present in bulk. This behaviour is termed electret behaviour and is possible for all dielectric materials. Application of a high enough electric field results in either polarization of dipoles or injection of charge carriers or both at the same time. This means that a poled ferroelectric can also be considered to be an electret. The difference lies in the charge decay mechanism, which is dependent on the stability of these electrets. This present work is mainly related to the formation of electro-electrets created during the corona poling process [44], as it is the process used for this study. A brief description of the corona poling process is given in the following paragraphs.

In the corona poling process, the bottom electrode is a vacuum deposited-metallic film while the top electrode is a metallic wire with a pointed end. This point-plate asymmetric geometry reduces the voltage required to overcome the dielectric breakdown strength of air and form a corona discharge between the two electrodes. The lower voltage also prevents the corona from damaging the dielectric by exceeding its breakdown strength. A point electrode results in an inhomogeneous electric field distribution, decreasing in strength as you move radially away from the point source. This also affects the distribution of charges deposited on the surface of the dielectric. To overcome this phenomenon, a metallic grid is used to distribute the field more uniformly over the surface. Although, the potential of the grid has to be of the same bias but a much lower value in comparison to the point electrode. A high value of the grid electrode results in the formation of a parasitic corona between the grid and the sample, thereby reducing the efficiency of the poling process. Uniform field distribution is observed when the surface potential of the piezoelectric composite matches that of the grid. The schematic of a point-grid-plate corona poling setup is shown below in Figure 1.19.

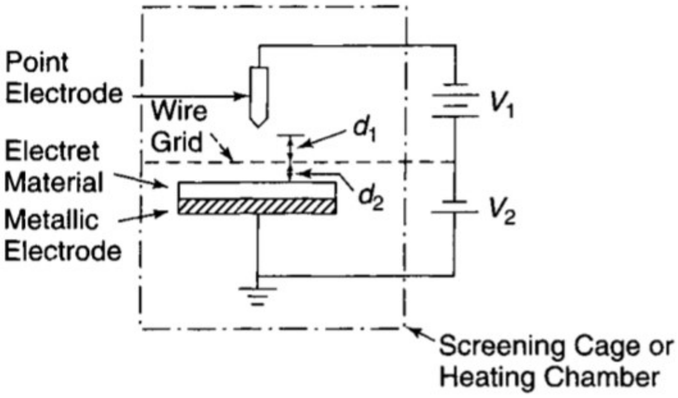

Figure 1.19: Schematic illustration of the corona poling setup [44]

It is also advised to perform the poling process at elevated temperatures, in order to improve the thermal stability of the charges deposited on the surface, as they are now captured in deep traps. In addition to that, the thermal treatment also improves the stability of these electrets by annealing them. Poling inside a heating chamber also prevents any interference from any outside sources and acts as a screening cage.

Some porous non-polar polymer foams show similar behaviour to ferroelectrics when subjected to a high enough electric field, and are therefore called ‘ferroelectrets’ [45]. The gas present inside the pores (usually > 1 μm) can undergo electrical breakdown to form microplasma discharges when poled using the corona poling method [46]. Their ferroelectric like behaviour is attributed to the formation of quasi-dipoles in the oppositely charged layers between the pores as shown in Figure 1.20(A). This asymmetric structure is similar to that in ferroelectrics, where dipoles are formed in the atomic scale due to their non-centrosymmetric crystal structure. Therefore, ferroelectrets also exhibit similar switching and polarization reversal characteristics under a high enough electric field. The theoretical hysteresis loop is shown in Figure 1.20(B).

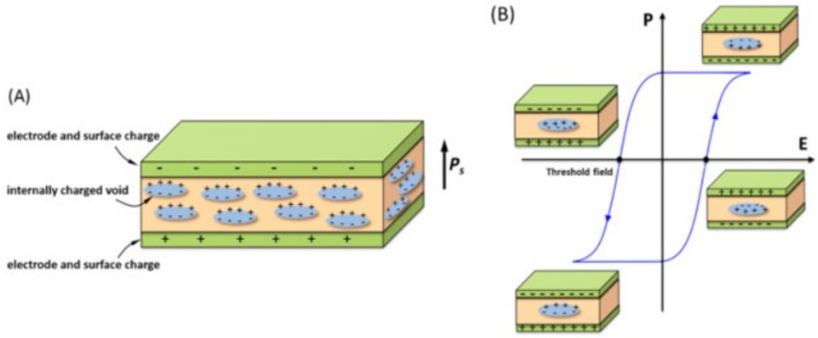

Figure 1.20: (A) Oppositely charged voids in a ferroelectret and (B) hysteresis loop for a single pore ferroelectret [47]

Cellular polypropylene ferroelectret can achieve d_{33} values in the range of 495-600 pC/N [45], [48], which is comparable to the values obtained by soft PZT (400-900 pC/N) [3], [49] and much higher than for pure polymers such as PVDF. A porous structure also results in a much lower dielectric permittivity as well as a more compliant composite. To maximize the ferroelectric-like behavior, the pores should have a lens/ellipse like shape, with aspect ratios greater than 4. These lens shaped voids have a much lower elastic stiffness along the polarization direction, generating a better electromechanical response. The piezoelectric response and the elastic stiffness along the polarization direction at different densities is shown below in Figure 1.21 for ferroelectret foams. However, for sensing applications there is a lower limit defined for the elastic stiffness. This is due to the fact the deformations undergone by the foam should be elastically reversible, in order to obtain reproducible properties [50].

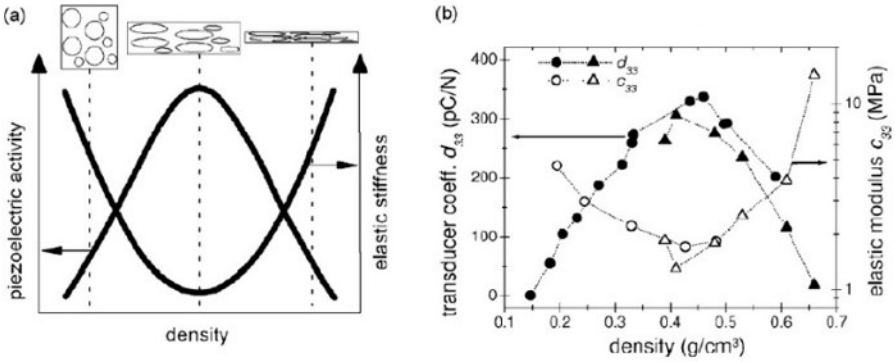

Figure 1.21: (a) Schematic illustration [51] and (b) Experimental [52] d_{33} and elastic stiffness data for Polypropylene electrets at different foam densities

Mechanical properties

The mechanical response of these porous structures is much different in comparison to bulk composites. To measure the piezoelectric properties of these foams, the samples are loaded quasi-statically under compression. Therefore, there is a need to define the deformation mechanism of these foam composites before using them as sensors. The deformation mechanism is dependent on a number of factors, mainly the load case and the type of polymer selected [53]. The compressive stress-strain curve for polymeric foams illustrates three distinct regions [54], [55] and is shown in Figure 1.22.

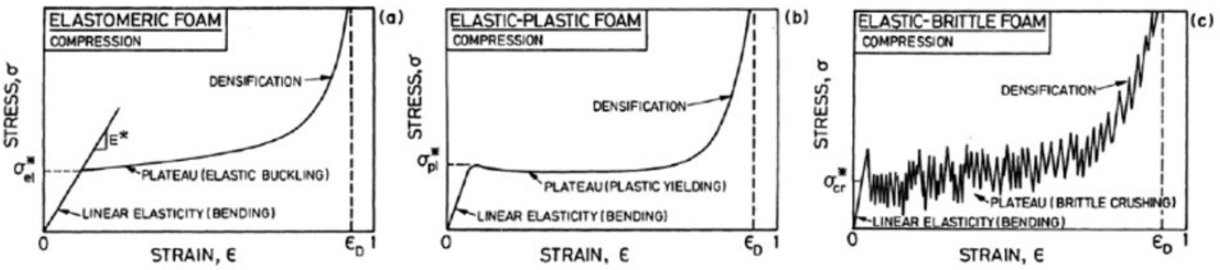

Figure 1.22: Compressive stress-strain curves for (a) Elastomeric foam (b) Elastic-plastic foam and (c) Elastic-Brittle foam showing the three distinct regions [54]

The linear elastic region is attributed to face stretching of the cells inside the foam. While the plateau region is associated with the collapse of the cellular structure. In elastomeric foams, the plateau is defined by the elastic buckling of the cell walls, plastic yielding due to the development of hinges in elastic-plastic foams and brittle crushing in elastic-brittle foams. In general, the linear elastic behaviour is limited to 5% strain for these foams, beyond that characterization of the non-linear behaviour is required in order to execute precise sensing measurements [54], [55].

1.4. Material and fabrication process selection

As mentioned previously, the piezoelectric voltage constant (g_{33}) is a function of the d_{33} and ε values of the piezoelectric system. The complex, multiphase, nature of composites thus allows for more tuning of the g_{33} than in bulk, single-phase piezoelectric materials. For example, a reduction in the dielectric constant of a composite can be achieved by varying the matrix material or even adding tertiary, low-dielectric constant, phases. In this work we will pursue the latter option, exploring routes to add a low dielectric phase in the form of air (pores) to piezoelectric composites resulting in so-called porous tri-phase composites.

The polymer matrix and the foaming technique used will define the porosity as well as the mechanical response of the composite. While the selection of the active ceramic material affects the piezoelectric behaviour. A consequence of selecting the polymer matrix is also the fact that there is a big mismatch between the dielectric properties of the polymer and the ceramic phase. This means that the dielectric properties of the polymer will affect the poling efficiency and thereby the piezoelectric response of the composite. Another consequence of a porous structure is the presence of interface porosity, which is not ideal as explained in subsection 1.3.1. To eliminate the possibility of interface porosity, it is better to select a polymer-ceramic combination that has good interfacial adhesion. Using the corona poling setup, could in theory also improve the piezoelectric response due to the formation of electrets. Therefore, polymer selection plays a major in defining the overall piezoelectric response of the composite.

From the polymer list, PVDF could be considered as an option for the composite. Although, as explained in section 1.2 and from Table 1.1, PVDF has a negative d_{33} as it has a different structure-property relation to that of piezoceramics. This results in a reduced piezoelectric behaviour as their properties will counteract each other [56], [57]. A specialized poling technique could be used to pole the two phases in the opposite direction in order for the piezoelectric properties to be enhanced, but it would be time-consuming and not that efficient.

For the production of piezoelectric composite foams, a number of possible foaming methods and polymers were analyzed and, in the end, it was determined from the literature that Polyvinyl alcohol (PVA) offered a high probability of success without the need of specialist equipment or dangerous chemicals. Before the results of producing piezoelectric foams from these materials is discussed, it is helpful to consider some of the literature on this material. To that end, this section will discuss the PVA polymer, the production of foams from PVA, and some of the key features of PVA to consider when working with it.

PVA is a semicrystalline synthetic polymer with excellent film-forming ability [58]. It is used in food packaging and medical applications due to its bio-compatibility as well as having a low environmental impact. It cannot be produced directly and is instead prepared by hydrolysis of polyvinyl acetate (PVAc), with the degree of hydrolysis (DH) defining the percentage of acetate groups converted to hydroxyl groups. The degree of hydrolysis along with the molecular weight of PVA greatly affect the water solubility as well as the mechanical properties of the composite. Low DH values (<95 %) display an increase in solubility due to having more hydrophobic acetate groups that do not participate in the intra/inter-molecular H-bonding as shown in Figure 1.23. Lower molecular weight PVA also has reduced mechanical strength [59]. PVA is one of the most studied polymers for interlayer dielectrics owing to its excellent dielectric strength and high dielectric permittivity [60]–[63]. Due to its superior ionic conductivity, it has been used a lot in fuel cells and electrochromic applications [64]. However, as a result of its highly hydrophilic nature, it is susceptible to aggregation due to hydrogen bonding via its polyhydroxygroups [65].

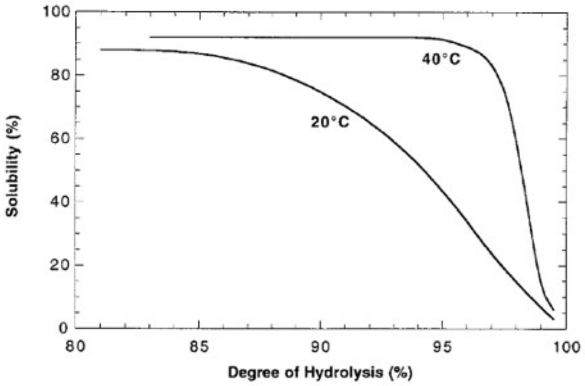

Figure 1.23: Solubility vs degree of hydrolysis at 20 °C and 40 °C [59]

PVA films are generally quite brittle which can make them difficult to process. Plasticizers can be introduced to improve film flexibility as well as reduce the surface roughness of the processed films. A compatible plasticizer does not exhibit phase separation. In PVA, plasticizers collect in the amorphous regions of the polymer, causing an increase in their free volume and a lowering of the glass transition temperature [58].

While a number of different routes are available for the production of PVA foams, the most commonly used are solution-based [66], [67]. This solution-based foaming technique is in general quite complex and not cost-efficient. In the case where a chemical crosslinker is used, it is also difficult to remove the toxic residue after the crosslinking step, which limits its application in the biomedical field. Although for commercial applications it is generally crosslinked as it is a water-soluble polymer. A newer and much cleaner technique is to use supercritical CO_2 as a blowing agent in addition to a plasticizer. The addition of the plasticizer is done to increase the solubility of CO_2 and therefore control the microstructure and the porosity of the foams [68], [69]. Although the requirement of a continuous extrusion setup and provision of supercritical CO_2 is not feasible in this study.

Instead, a novel way of fabricating PVA foams is by making a particle stabilized foam using non-adsorbing/hydrophilic PVA particles as stabilizing agents. This is possible with the use of spherical monodispersed PVA particles which are driven to form ordered layers through stratification (step-wise film thinning). There is also a reduced possibility of drainage, ensuring better stability of foam structure [70] during the drying process. The simplicity of this method made it attractive for the production of the foams studied in this work and thus the particle stabilized foam method will be used to produce the PVA foam composites.

1.5. Research objective

The aim of this work is to improve the sensing capabilities of piezoelectric composites, i.e., to increase the g_{33} of the composites. To further improve the piezoelectric voltage constant (g_{33}), the most promising approach is to reduce the dielectric constant of the composite. Therefore, this project will focus on the reduction of the dielectric constant (ε) of the composites by the inclusion of air.

Previous work done by Kevin and Hamideh [6] showed the improvement in the sensing capabilities of a piezoelectric composite by fabricating a porous structure. For further improvement, different systems and poling techniques can be used which are formulated by the research questions posed :

- Is it possible to fabricate a porous polymer matrix with an anisotropic cellular morphology to significantly reduce the dielectric permittivity?
- Is it possible to charge the cellular polymer matrix using the corona poling process to further enhance the piezoelectric response of the composites?

- What is the influence of the particle size and volume fraction of the lead-free piezoelectric ceramic on cellular morphology as well as the distribution of the filler in the polymer matrix?
- How does the dielectric properties of the polymer matrix influence the poling process and the piezoelectric properties of the composite?
- What is the effect of porosity on the electromechanical response of the foams?

To answer all of these questions, the following steps will be taken in this study. The piezoelectric ceramics are selected on the basis of being lead-free and having good piezoelectric properties. Barium titanate ($BaTiO_3$) is the first ferroelectric to be discovered and has been studied extensively throughout history. Therefore, its dielectric and piezoelectric properties are well defined in the literature. The second piezoelectric ceramic selected is KNLN3, as it has a very good piezoelectric response and a much lower dielectric constant than $BaTiO_3$. The combination of a higher piezoelectric charge constant (d_{33}) and a lower permittivity, should in theory improve the voltage response (g_{33}) of the composite.

To repeat the work done by Hamideh [6] in the initial experiments, polyurethane is used as the polymer matrix. The introduction of pores is done in the same way, by a side reaction between the diisocyanate component and water to release CO_2. The fabrication process is similar to the previous study, but the poling process is different. The samples will be poled using the corona poling method to understand the difference in the poling mechanism and to check if there is a possibility of charging the pores via the formation of electrets. The whole process is described in Appendix A along with the results and discussion.

Poly(vinyl alcohol) (PVA) is selected as the main polymer system to be investigated due to its excellent film-formingg ability. PVA is a polar, semi-crystalline, water-soluble polymer used in food packaging and medical applications due to its non-toxic nature. PVA is also extensively used as a flexible interlayer-dielectric due to its relatively high permittivity (compared to polymers) at low frequencies and high temperatures as well as having a very high dielectric breakdown strength. The excellent dielectric properties make it suitable to be used as the polymer matrix in the composite. A reduced dielectric mismatch between the two phases should result in a higher poling efficiency of the active-piezoelectric ceramic and an improved piezoelectric response. The selection of PVA is also based on the fact that it is already used as a binder in the production of piezoelectric ceramics due to its good interfacial adhesion properties. Fabrication of the porous structure is done using a direct-foaming technique. The effect of porosity on the poling efficiency and the electromechanical response of these foams will be studied in this work. The formation of electrets during the poling process will also be investigated.

2

Experimental methods

This chapter is dedicated to the experimental work as well as characterization techniques used to investigate the properties of the individual phases as well as the composite. The preparation of the ceramic fillers used is described in section 2.1, while section 2.2 dedicated to the fabrication of the porous composite. The section 2.3 is devoted to the techniques used to characterize the properties of the individual phases as well as the porous composite. The poling method used to align the dipoles and improve the piezoelectric properties is discussed in section 2.4. We end this chapter with the humidity chamber setup in section 2.5, to define its effect on the electromechanical properties of the foam composites.

2.1. Ceramic production

The production method of the piezoelectric ceramic selected for this study have been discussed in this section. Barium Titanate ($BaTiO_3$) is obtained from Inframat Advanced Materials^{TM}, USA with an average particle size of 300 nm and near-spherical particle morphology. The density of the obtained BaTiO3 is 5.85 g/cm^3.

The in-house $(K_{0.5}Na_{0.5})_{0.97}Li_{0.03}Nb_{O3}$ (KNLN3) is also produced with varying particle sizes (< 25 µm and 25-63 µm). The production of KNLN3 is adapted from previous work done by Sundaram Sivaganga Anandakrishnan [71]. The first step during the ceramic production is the mixing of raw materials: K_2CO_3, Na_2CO_3, Li_2CO_3 (stored in hot-air ovens at 220 ˚C to reduce moisture absorption) and Nb_2O_5. The raw materials were taken based on the stoichiometric ratios of the raw material elements in $(K_{0.5}Na_{0.5})_{0.97}Li_{0.03}Nb_{O3}$. The mixture is poured into a 6.5 kg ball-mill with about 20 g of 5 mm diameter yttria stabilized zirconia milling balls. The ball-mill is filled with isopropanol to about 1 cm below the brim for lubrication during milling. The mill is then fitted into a planetary ball-mill (Retsh PM 100) and mixed for 12 hours at 150 RPM with 10-minute breaks every 20 minutes to prevent overheating. The long mixing time at low RPM is done to ensure complete mixing of the components. After mixing, the contents of the ball-mill were dried on a hot-plate at 60 ˚C. After the mixing procedure, the mixture was put in a high temperature oven (L5/13 with Controller B410 manufactured by Nabertherm) and calcined for 2 hours at 950 °C with a heating rate of 5 °C/min.

After the first calcination, the mixture ends up as a compacted mass in the alumina crucible. It is taken out and hand-milled using an agate mortar and pestle. The hand-milling is done to reduce the sintered ceramic into smaller particles/powder without running the risk of over milling that can occur with a planetary ball-mill. This powder is sieved through a 125 µm mesh size sieve and any remaining material is reground until the entire powder has passed through the sieve. Sieving is done with the help of an auto-shaker (Haver EML digital plus – Test sieve shaker manufactured by Haver and Boecker). The phase purity of this sample is checked by X-ray powder diffraction measurements and, if needed, a small excess of K_2CO_3 and Na_2CO_3 is added to compensate for evaporation prior to the second calcination.

After sieving, the ceramic powder is put in an alumina crucible and calcined a second time. The second calcination is done at 925 ˚C, dwelling time of 10 hours, temperature ramp of 1 ˚C/min, and free cooled in the oven for all samples. The sample comes out as a partially sintered, soft powder, as the second calcination is mostly done for grain growth and the formation of agglomerates. Hand-milling is then repeated to reduce the bulk mass that is got from the second calcination to workable powders. Then the powder is passed through a series of sieves with mesh sizes of; 63 µm and 25 µm. The size fractions between each sieve were kept separated and only the particles with sizes below 63 µm and 25 µm were chosen for investigation.

2.2. Composite production

From section 1.4 (Figure 1.23) we already know the effect of degree of hydrolysis (DH) and molecular weight (M.W.) on the solubility of PVA in water and its mechanical properties. To take advantage of this, PVA with 88% DH and M.W. 20-30,000 is selected. A lower degree of hydrolysis results in a higher solubility of PVA at room temperature (RT), while a lower molecular weight results in lower mechanical properties. The lower mechanical properties can be used to exploit the modulus mismatch between the polymer and the ceramic phase, by increasing the applied/apparent stress on the piezoelectric filler and obtaining a higher piezoelectric charge coefficient (d_{33}).

To observe the effect of the viscosity of wet foam, PVA is mixed with different amounts of H_2O. PVA1 foam is made by using a 1:4 wt. ratio of PVA:H_2O, while PVA2 uses a 1:3 wt. ratio. The wet foam with the higher PVA concentration is naturally more viscous, affecting the pore size and morphology. The polymer is foamed using the direct foaming processing inside the speed mixer, followed by the addition of the ceramic phase. The ceramics are then homogeneously distributed to prevent agglomeration, before being cast on an aluminium substrate at a height of 2 mm. The speed mixing and the tape-casting setup is shown below in Figure 2.1.

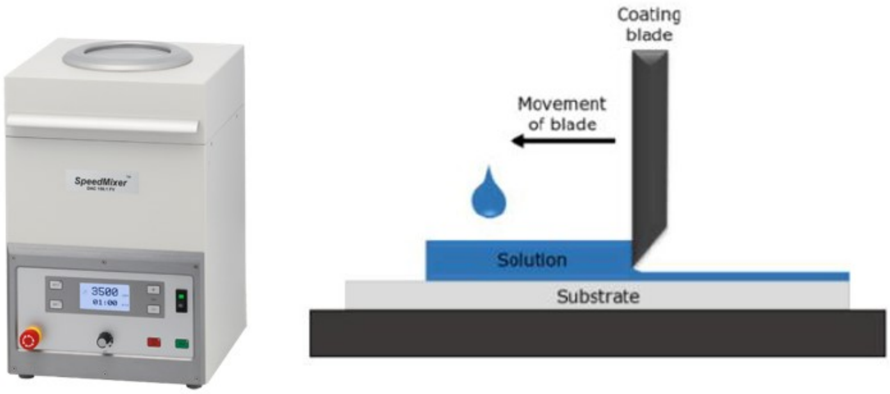

Figure 2.1: Speed-mixer (left) and tape-casting setup (right)

The processing steps are the same for PVA1 and PVA2 foams. PVA is added to distilled water in the specified ratios and kept for 5 min kept for 10 min for PVA to dissolve a bit without using the speed mixer. Then, it is mixed in a speed mixer (SM) at 3500 rpm for 5 min and rested for 1 min. By now, a high percentage of PVA has been dissolved, making the solution more viscous and improving the foaming properties of the slurry. This is then followed by another round of speed mixing at 3500 rpm for 5 min, resulting in a thick slurry. The addition of the ceramic is done in 5 steps (1 min each), to prevent sedimentation of the denser ceramic particles. The foaming process is shown step by step in Figure 2.2.

Figure 2.2: PVA1 in distilled water after 10 min rest (top-left), 5 min SM (top-right), 10 min SM (bottom-left) and after adding $BaTiO_3$ ceramic powder in steps and SM (bottom-right)

For the first set of trials, PVA1 and PVA2 foams are made with $BaTiO_3$ (BT) as the ceramic filler. This is due to the fact that it has a very consistent particle size in the range of 300 nm, which should not have a major effect on the overall porosity of the foams. Foams are also made using KNLN3 as the ceramic filler but only at a high loading since the particle size plays a major role in the porosity of this foam composite. The final foam is then tape-cast on an Aluminum substrate coated with a release agent and either cured/dried in an oven at 60 °C for 3h, or left to cure overnight at RT. The tape-casting process is shown below in Figure 2.3.

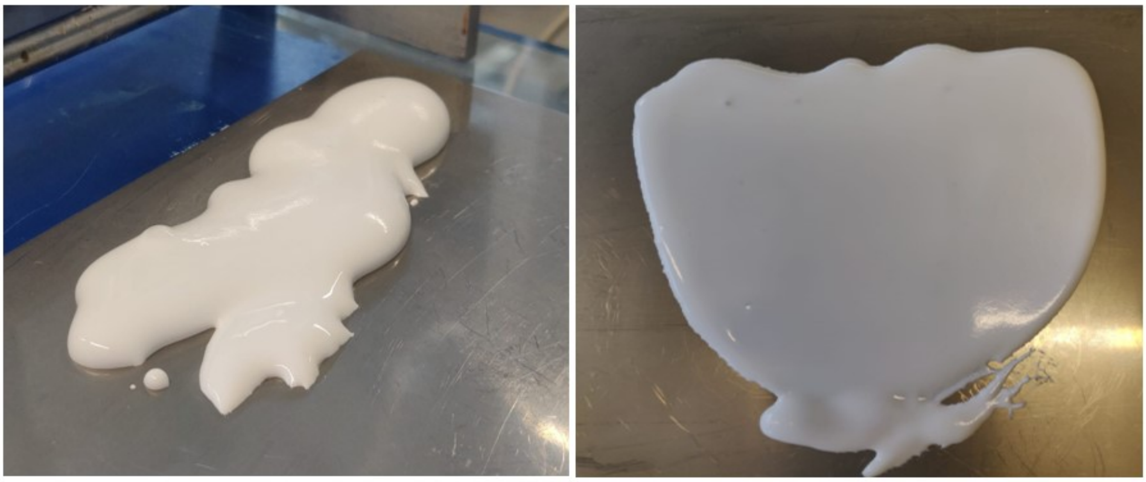

Figure 2.3: Foam before (left) and after (right) tape-casting

A plasticizer may also be added during the foam production process. The addition of a plasticizer reduces the T_g and affects the curing cycle as well as the mechanical properties of the final foams. Benzyl butyl phthalate (BBP) (40 wt.%) is added as the plasticizer to observe the changes. With the temperature set at 60 °C, foams with the plasticizer take about 10 hours to cure, while the ones without cure in 3 hrs. The surface roughness and the mechanical properties are affected by the curing cycle and the amount of plasticizer added. The plasticizer reduces the T_g of the composite as well as making the ceramic distribution more homogeneous. The curing cycle is also affected by the addition of the plasticizer, as it affects the rate of evaporation of water from the foam during the drying cycle. The foams cured with and without the plasticizer are shown in Figure 2.4. To avoid confusion in further sections, the nomenclature of foams is defined in the following manner: Ceramic-PVA with ceramic/PVA mass ratios (vol.% of ceramic). For example a foam with 32.2 vol.% BT loading is called: BT-PVA 70/30 (32 vol.% BT).

(a) Without plasticizer, RT cure (b) Without plasticizer, 60 °C cure (c) With plasticizer, 60 °C cure

Figure 2.4: BT-PVA1 70/30 foams

2.3. Characterization techniques

The different material characterization techniques used will be discussed in the following subsections.

2.3.1. XRD

X-Ray diffraction (XRD) is an analytical technique used for phase-identification of crystalline samples. A hot filament produces electrons that accelerate towards the target. These electrons have enough energy to remove electrons from the inner shells, driving electrons from the outer shells to fill this energy gap. The subsequent X-ray spectra produced from this are then focused, through a monochromator on the sample and the diffracted beam is detected by the diffractometer. The diffraction spectrum produced is based on Bragg's Law, which states that :

$$n\lambda = 2d \sin\theta \tag{2.1}$$

Where n is the order of interference, λ is the wavelength, d is the lattice spacing and θ is the diffraction angle. Data post-processing is done in FullProf and Origin Pro. Rigaku Miniflex Benchtop powder XRD 600 setup (Figure 2.5) is used for the characterization of the ceramic powders and composites. The scan is done from 20-80° at a step width of 0.005° and speed of 1°/min.

Figure 2.5: XRD setup

2.3.2. Microstructure analysis

A scanning electron microscope (SEM) is used to analyze the microstructure of the sample. An intense electron beam is focused on the sample which interacts with the sample surface. The collision of the incident electron beam with the surface emits electrons and X-Rays. These emitted secondary electrons and X-Rays are then used to provide information about the topography, morphology and composition of the sample surface. The SEM in use is a JEOL JSM-7500F (Figure 2.6 left) which uses a field emission source to emit electrons. The normal SEI and LEI lenses are used to get images of the sample microstructure. To detect compositional changes in the specimen, the SEM is used in backscattered mode (COMPO).

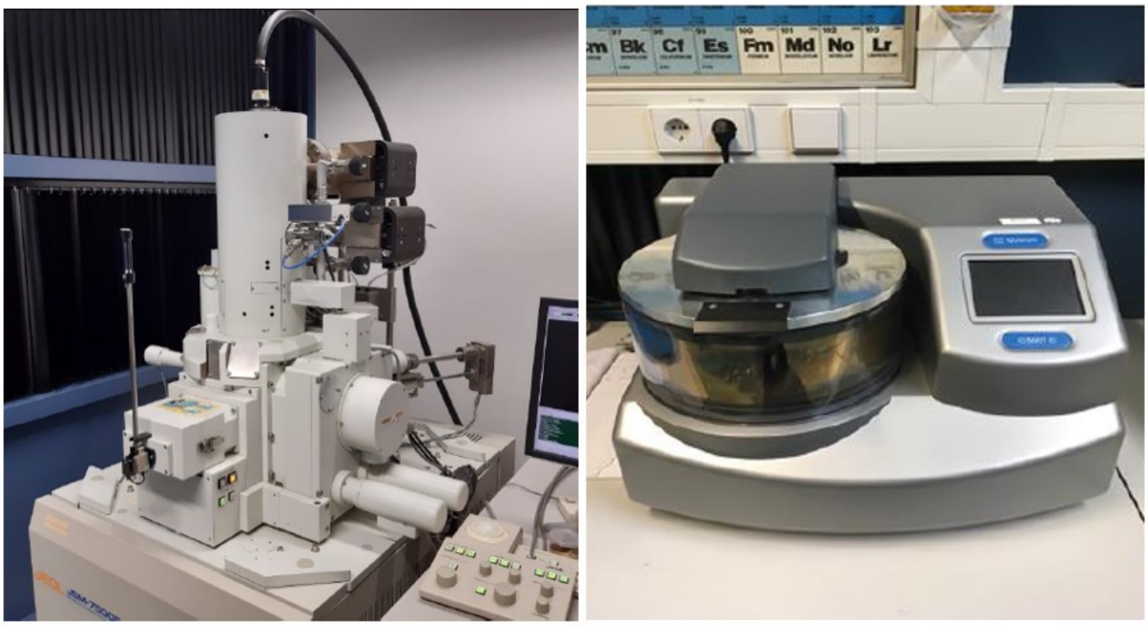

Figure 2.6: SEM setup (left) and sputtering machine (right)

Composite samples fabricated are ductile in general. To observe the actual microstructure of the composite, samples are first immersed in liquid nitrogen for a minute, before they become brittle and break easily while preserving the cross-section microstructure. The samples are then sputtered with gold electrodes before being observed under SEM. The magnetron sputterer in use is the Quorum Q300TD (Figure 2.6 right). Optical images of the top surface of the foams were taken using the Keyence VR-5000 wide-area 3D measuring system which uses a LED light source. The setup is shown in Figure 2.7.

Figure 2.7: Keyence VR-5000

2.3.3. Dielectric measurements

To measure the capacitance and tanδ of the composites at 1 kHz and 1V, an Agilent 4263B LCR meter (Figure 2.8) is used. The measured capacitance of the sample is then used to calculate the dielectric permittivity of the sample after already measuring the area and the sample thickness. The dielectric losses (tanδ), are a good indicator of the lossy nature of the system as it also affects the poling efficiency. Due to difficulty faced in applying electrodes to the highly porous samples as is discussed in section B.4, aluminium plates are instead used as electrodes.

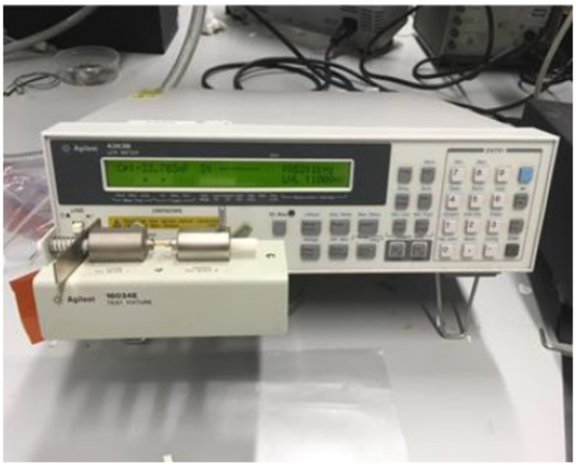

Figure 2.8: LCR meter

2.3.4. Broadband dielectric spectroscopy (BDS)

Broadband dielectric spectroscopy is a spectroscopic technique used to measure the dielectric response of a material at a range of frequencies and temperatures. The temperature is controlled by placing the sample holder inside a cryostat. A single sweep is done for the sample before starting the temperature cycle to look for any errors due to misalignment/improper contact between the sample and the electrodes. The temperature sweep is done from 20-120 °C in steps of 10 °C, while the frequency sweep is from 0.1 to 10^6 Hz. The permittivity and conductivity variation of the composites with temperature and frequency is of great interest. The setup is shown below in Figure 2.9.

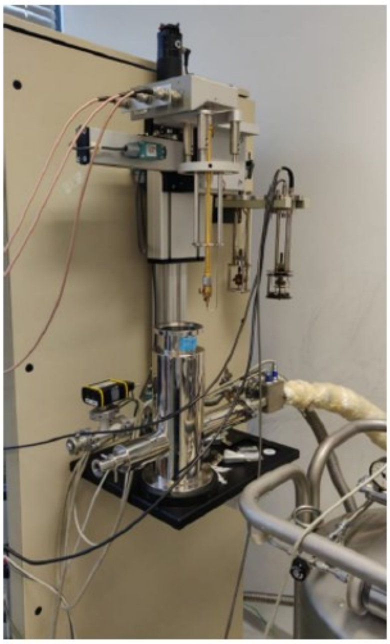

Figure 2.9: BDS setup

2.3.5. Piezoelectric measurements

The piezoelectric measurements are done using a Berlincourt PM300 piezometer (Figure 2.10). The quasi-static measurements are done at a standard frequency of 110 Hz and 0.25 N dynamic force. The value of the dynamic force applied on the piezoelectric disc is insignificant for most systems, provided the stresses produced in inside the material persist in their linear regime. A better charge signal will be produced for higher dynamic forces, eliminating issues caused by signal noise. However, a lower force would also have a much higher chance of the piezoelectric measurements falling inside the linear regime of the material.

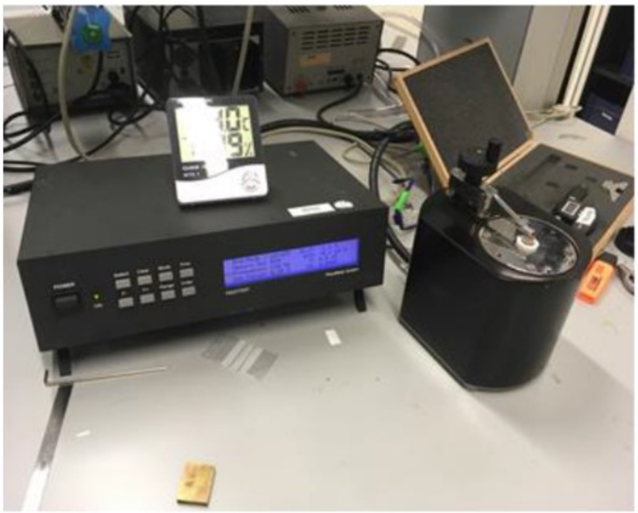

Figure 2.10: Berlincourt piezometer

The pre-load applied to clamp/hold the sample plays a role on the measured d_{33} by this system. Figure 2.11 shows the difference in the d_{33} measured for soft PZT (PC5H) and hard PZT (PC4D) samples. A decrease in the d_{33} is observed for soft-PZT samples with increasing pre-load, the opposite of which is seen for the hard-PZT samples. The pre-load also has a far greater effect on the softer PZT sample, as can be seen from the slope of the curve [5]. Therefore, measurement of the piezoelectric properties of the composites should be done inside their linear stress-strain region, in order to measure reproducible properties. All samples are then measured using Al plates as electrodes, in order to prevent static stress concentrations as discussed in section B.3. This leads to the measurement of an effective d_{33} and not the actual d_{33} of the composite, as the measurement now includes the charges obtained from the d_{31} component. When the sample is compressed uni-axially using an Al plate, both d_{31} and d_{33} values come into play (Figure 1.1), and therefore a direct comparison to other commercial systems isn't done. Since the area of the electrodes now plays a role in the measurement taken, all samples of the size of 20 mm x 20 mm are used for this work.

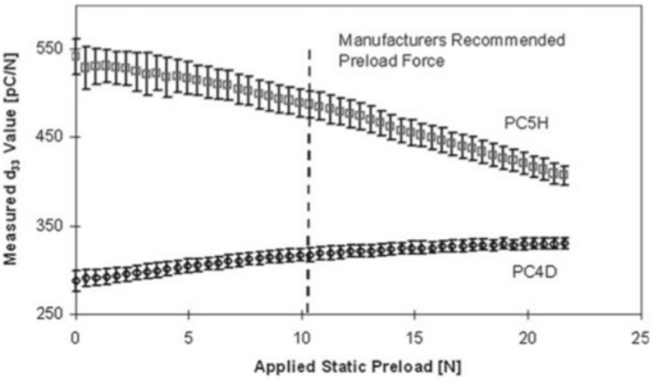

Figure 2.11: Effect of static-pre load on soft (PC5H) and hard (PC4D) PZT [5]

2.3.6. Dynamic mechanical analysis (DMA)

Dynamic-mechanical analysis is done to perform compression testing on the piezoelectric composite foams. This is done to calculate the compressive modulus of these foams, as well as to define the linear stress-strain regime for these foams. Since, the foams are very soft in comparison to other composites and ceramics, describing the linear region is important, as it is the region where the basic piezoelectric equations hold true. The tests are done using Discovery TA RSA-G2 Solids Analyzer. All the samples are cut into 16 mm discs, using a punch die.

The static tests are done at room temperature at different strain rates (0.01 mm/s and 0.005 mm/s). The compressive cell has a maximum loading capacity of 35N, which isn't high enough to define the failure stresses of these foams. Although, it is high enough to define the yield stresses and hence the linear region for these foams. The values obtained for compressive stresses cannot be used for absolute comparisons, as a non-standardized geometry (thickness/diameter ratio) is used. This is due to the fact that piezoelectric composites should be as thin as possible, in order to reduce the voltage required to pole these samples as well as to increase their dielectric breakdown strength. So, making thicker samples, although likely better for compression testing, will be much more difficult if not impossible to pole. Therefore, this testing is done only for relative changes in the mechanical properties of the foams fabricated in different conditions and with different ceramic loadings, as they have similar aspect ratios. The DMA setup is shown below in Figure 2.12.

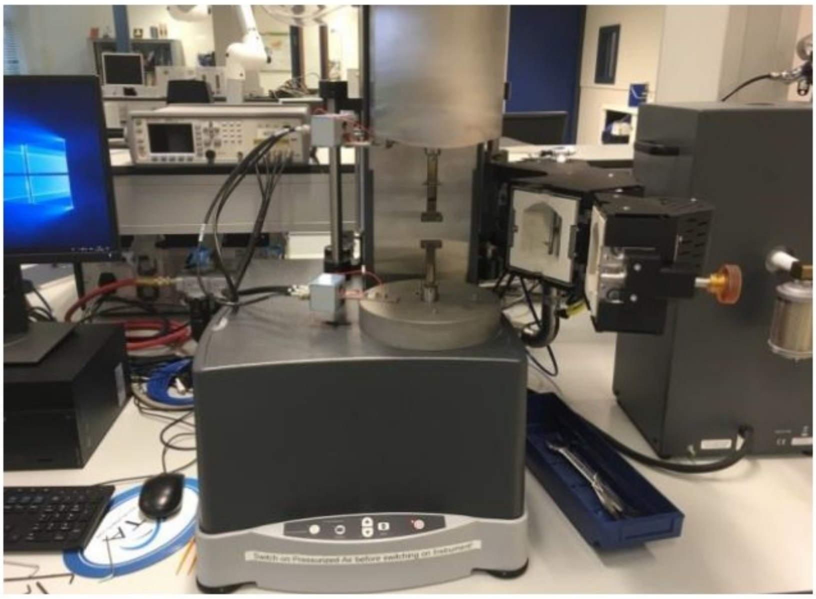

Figure 2.12: DMA setup

2.3.7. FTIR

Fourier Transform Infrared Spectroscopy (FTIR) is a well-defined technique to study the chemical interactions between the polymer and the ceramic phase. For the current study, this technique is used to define the interactions between PVA polymer and $BaTiO_3$ nanoparticles. The samples are measured with PerkinElmer Spectrum 100 FT-IR using transmittance mode. The spectra are obtained in the range between 600-4000 cm^{-1} by performing 64 scans with a resolution of 4 cm^{-1} at room temperature. Further, post-processing is done using Origin. The setup used is shown below in Figure 2.13.

Figure 2.13: FTIR setup

2.4. Corona poling

The poling process is a critical step in obtaining good piezoelectric properties for the composite. This is because, there is a big difference in the dielectric permittivity of the ceramic filler and the polymer matrix, making the electric field distribution inhomogeneous during the poling process and reducing the poling efficiency [3], [28]. The effective field (E_1) experienced by an isolated spherical particle in a polymer matrix is given by :

$$E_1 = \frac{3\varepsilon_p}{\varepsilon_c + 3\varepsilon_p} E_0 \tag{2.2}$$

Where E_0 is the applied electric field, ε_p and ε_c are the dielectric constants of the polymer and the ceramic respectively (52). Due to a high dielectric mismatch between the ceramic and the polymer, this effective field acting on the piezoelectric filler is much smaller. If the composite is poled for a longer time than its dielectric relaxation time (τ), the field distribution in the composite is then dependent on the ratio of electrical conductivity of the polymer and ceramic $\frac{\sigma_p}{\sigma_c}$ [72]. This is because, on longer time scales, the mobility of charges in the matrix plays a vital role in the poling process.

Poling is sped-up by increasing the electrical conductivity of the matrix. Polymers in general, observe an increase in conductivity at elevated temperatures due to their relaxation mechanism. Thus, a polymer matrix with higher conductivity improves the poling efficiency and thereby improves the piezoelectric properties of the composite. Although a higher conductivity also results in higher dielectric losses.

Longer poling times also allow for all the domains to be switched and the polarization to reach a stable value. In the initial stages of the poling process, the conductivity and the dielectric constant of both phases influence the effective electric field on the piezoelectric fillers, which is always much lower than the applied field. The switching of 180 ° domains happens in the initial stages, the rotation of the non-180 ° domains takes a longer time. This is because their rotation is accompanied by local stresses, which require a longer time to develop. The samples are therefore also cooled down under field to prevent significant switching of these domains and to retain a higher remnant polarization. Also, for a poling time that is much longer than the dielectric relaxation time of the composite, the electric field distribution through the composite is controlled by the electrical resistivity instead of the dielectric properties [73], [74].

Increasing the applied electric field also accelerates this process, as then a higher driving force is employed to align these domains. In a random (0-3) composite, the matrix dominates the dielectric properties, the effective field is reduced. So, to overcome these barriers, a combination of a high electric field, poling temperature and poling time is required to pole these composites and obtain a more saturated level polarization [75].

The most common ways of poling piezoelectric composites are contact or corona poling. In contact poling, metal electrodes are in contact on both sides of the composite and the electric field is applied through them. Usually, samples are placed in a silicon bath to prevent the dielectric breakdown of the surrounding medium. This process has its drawbacks [76], as electrodes have to be applied to the sample before the poling process, and poling is very localized to the point of contact. Further issues with localized dielectric breakdowns as well as short-circuit during poling make it a less-attractive for large-scale production.

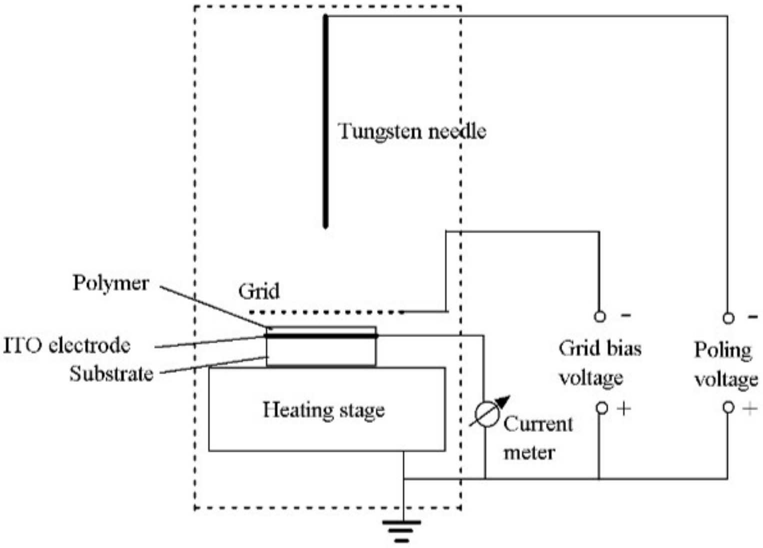

Figure 2.14: Schematic diagram of the corona poling configuration

On the other hand, corona poling is a non-contact method for aligning the ferroelectric domains. The corona poling process is already used for poling non-linear optical (NLO) polymers and electrets [77]. A corona is defined as a self-sustaining discharge when an adequately high voltage is applied between two asymmetrical electrodes. The point-plate configuration is the one used most often in corona poling setups and is shown in Figure 2.14. At a high voltage, the tungsten needles (point) ionize the air, resulting in an ion flux directed at the sample. The resulting ions generate a charge layer on the sample surface, which produces the poling field between the sample and the ground plate below it. Poling samples in this setup results in a very inhomogeneous electric field distribution on the surface layer of the sample. To obtain a more homogenous distribution, a conducting grid is added to the setup to control the surface potential on the surface of the sample. The corona poling setup in use is shown below in Figure 2.15.

Figure 2.15: Corona poling setup

2.4.1. Poling optimization

As can be understood from the previous sections, optimizing the poling conditions is an important criterion in maximizing the piezoelectric properties of these composites. The temperature at which the samples are poled at is dependent on the T$_C$ of the ceramic, the phase composition of the ceramic, the thermal stability of the polymer phase as well as the conductivity of the polymer. The poling temperature and voltage also define the extent to which the ceramic is poled. Piezoelectrics are generally poled near their Curie temperature, as it increases the domain mobility, making it easier to align the domains. Therefore, poling optimization studies are done, to define the poling temperature as well as the grid voltage for the corona poling setup.

Preliminary studies are done to define the pin and grid height from the substrate, as well as the poling time to reduce the number of factors that affect the poling efficiency. The pin voltage is kept consistent for further studies, as there is no visible arcing taking place at the highest possible fields. Also, if samples are poled at a higher temperature, they are then cooled down to near room temperature values under the influence of an electric field. Therefore, for the optimization study, the following parameters are kept consistent :

- Pin voltage : 50 kV
- Pin height : 30 mm
- Grid height : 16 mm (lowest possible in the current setup)
- Poling time : 60 min

The poling temperature is limited by the T$_C$ of the ceramic phase, while the grid voltage is limited to 12 kV as the formation of a parasitic corona discharge between the grid and substrate was observed. Thereby, the samples are poled at three different temperatures: 30 °C, 65 °C and 110 °C. While the grid voltage is varied from 2-12 kV for the given sample thickness.

2.5. Effect of humidity

Some of the samples which were kept outside in the lab, started becoming soft when the humidity increased during the summer where high temperatures combined with frequent rain drove the ambient relative humidity to higher levels. It was noticed that this affected the mechanical and electrical properties of all the samples. Samples became softer and lossier when it started raining. To quantify this behaviour, we made two test chambers at different levels of humidity, measured using a hygrometer.

For this study PVA1 foams with 32 vol.% BT were poled on the same day and then kept in the two separate test setups. The d_{33} after poling for both samples was about 14.2 ± 1 pC/N. The first setup is kept dry at close to 30% relative humidity (RH) inside a vacuum pot with silica desiccant beads. The second is a temporary setup made by using two different sized beakers, the smaller one filled to the brim with water. The bigger beaker is kept upside down and the gaps were covered with paper. The RH for the second setup stabilized at close to 82% RH. Both of the setups are shown below in Figure 2.16. The samples were aged for a week and then their dielectric, piezoelectric and mechanical properties were measured subsequently to observe the effect of humidity

Figure 2.16: Humidity test chambers for low (left) and high (right) humidity

3

Results

This chapter describes the results obtained from the different characterization techniques as well as the piezoelectric response of the composite. Section 3.1 is dedicated to the basic material characterization techniques to define the phase purity & changes in lattice parameters after the poling process (XRD) for the ceramic particles and the chemical interactions between the polymer and ceramic phase (FTIR). Section 3.2 is dedicated to the microstructure of these composites, which also includes density measurements. The dielectric behaviour is described in section 3.3, while the piezoelectric response is shown in section 3.4. The mechanical properties are defined in section 3.5. The properties of the foams are dependent on a variety of factors. The viscosity of the initial PVA slurry (PVA1 and PVA2), the curing cycle, the ceramic filler and its ceramic loading are the parameters varied and discussed further in the subsequent sections. Humidity is another factor that influences the electro-mechanical response of the composite and is explored in each section separately.

3.1. Material characterization

The results of the diffraction and the FTIR studies for the foam composites are presented in the following subsections.

3.1.1. XRD

The phase composition analysis was done using the XRD setup as mentioned in subsection 2.3.1. for both the $BaTiO_3$ and KNLN3 ceramic powders. The XRD plot for BaTiO3 powders is shown below in Figure 3.1. The XRD patterns show the tetragonality of the BaTiO3 powders as signified by the (002) and (200) peaks between 44-46°. A cubic crystal structure retains a single peak, while peak splitting is observed in tetragonal powders. This behaviour is in line with the data provided by the manufacturer.

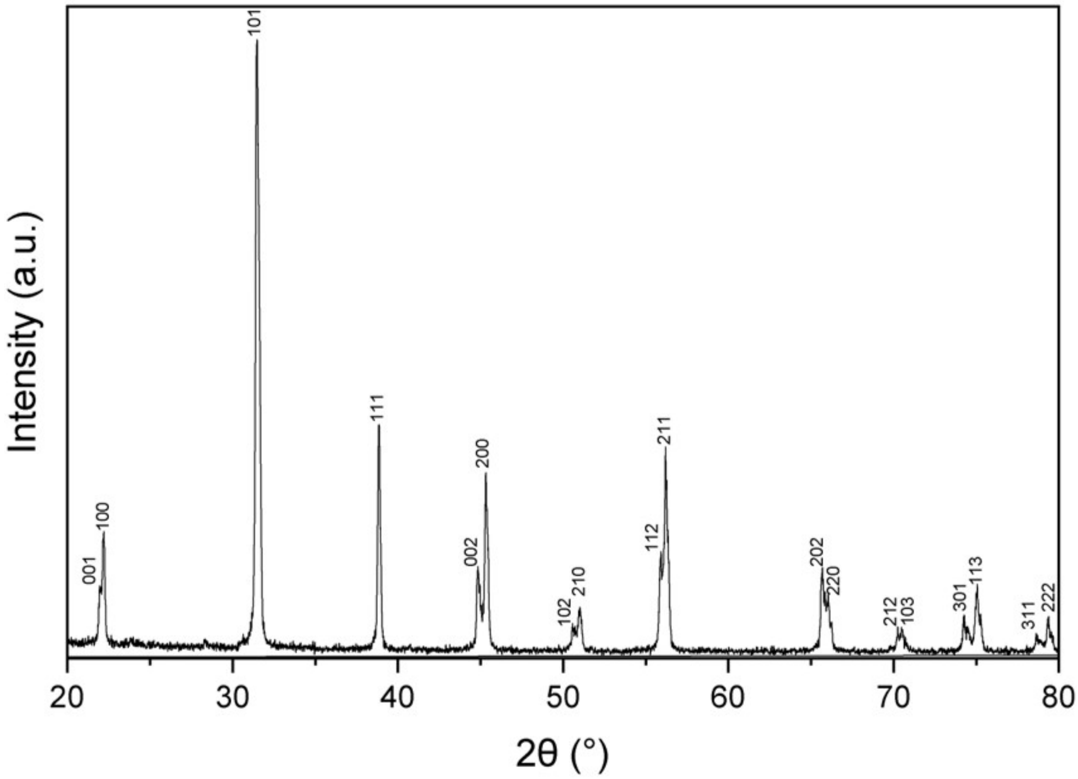

Figure 3.1: XRD pattern for $BaTiO_3$ powders

The XRD plot for KNLN3 powders is shown below in Figure 3.2. The data confirm the presence of single phase KNLN3 with an absence of any peaks indicating secondary phases [71].

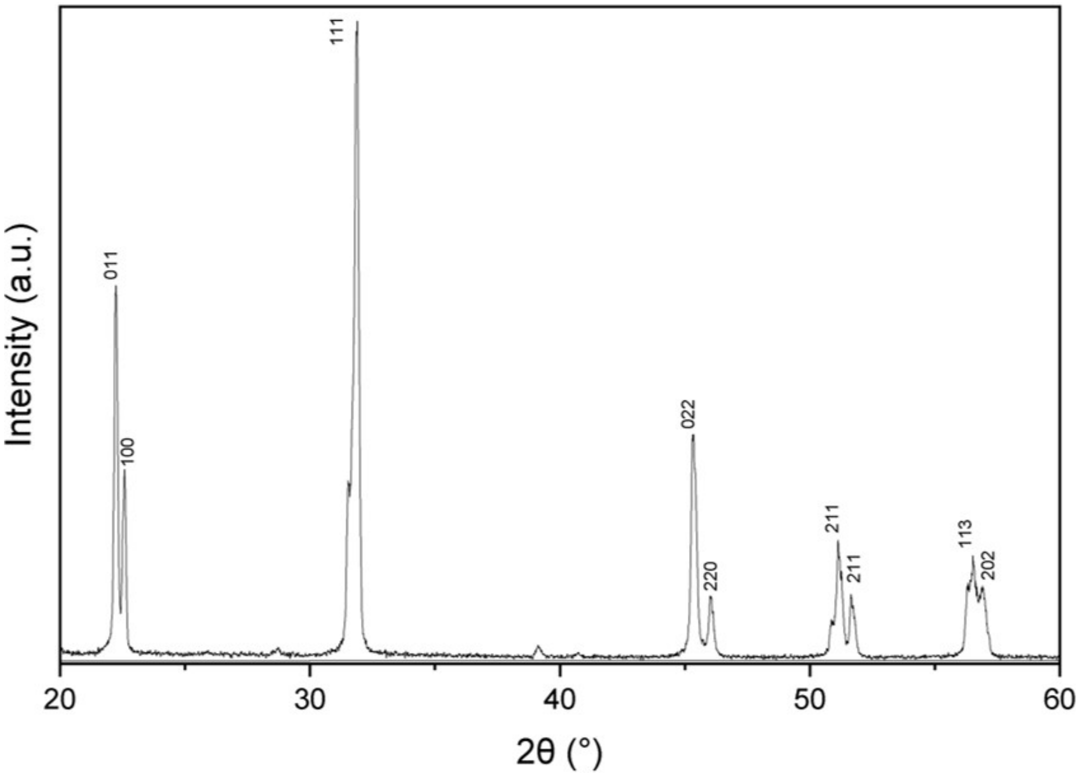

Figure 3.2: XRD pattern for KNLN3 powders

As poling results in a physical change in the position of atoms within the lattice, XRD sees a second potential use in the characterization of the composites to confirm the piezoelectric origins of the observed d_{33} values that are discussed later in this work. It is well accepted that, in the case of $BaTiO_3$ the degree of poling can be largely correlated to the ratio of peak intensities of (002) and (200) reflections [78], [79]. For the XRD studies, PVA1-BT 70/30 (32 vol.% BT) are poled at a pin voltage of 50 kV, grid voltage of 6 kV and for one hour. The grid voltage, set at 6kV is high enough to pole the samples and is optimized for the sample thickness. The samples are poled at three different temperatures, 30 °C, 65 °C [80], and 110 °C. The samples are then cooled down to RT, before the field is turned off. For the sample poled at 30 °C, the cooling down step is not required and the field is turned off directly after one hour. The XRD plot of $BaTiO_3$ and its foam composites is shown below in Figure 3.3.

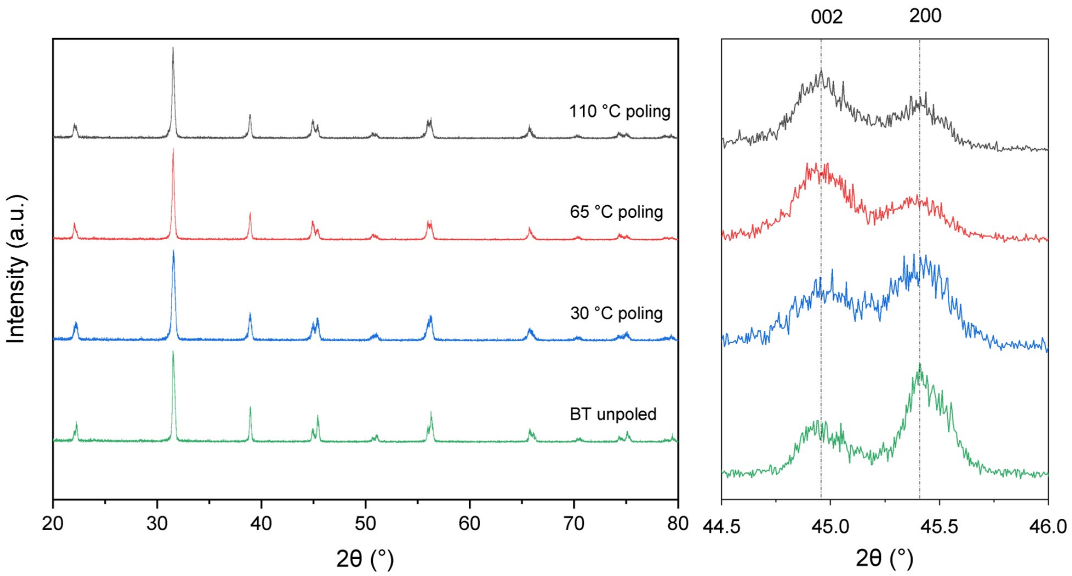

Figure 3.3: XRD plots for unpoled and poled composite at different temperatures

Firstly, the diffraction pattern for the unpoled $BaTiO_3$ corresponds well with the expected pattern for tetragonal $BaTiO_3$ without the presence of any secondary phases. Due to the highly crystalline nature of $BaTiO_3$ and the semi-crystalline nature of PVA, only diffraction peaks corresponding to the ceramic phase are observed in the diffraction patterns. Furthermore, the lack of low angle data (not measured due to the low resolution of the diffractometer at low angles) makes it unlikely that any crystallographic contribution from the polymer would be visible in this pattern. In the right hand figure of Figure 3.3 a zoom on the (002) and (200) peaks for the four patterns is shown. There is a clear change in the peak intensity before and after poling and the ratio of $\frac{I_{002}}{I_{200}}$ peaks increases with temperature. This change in the intensities is attributed to domain reorientation or rotation of single domain or multi domain crystallites. This also is an indicator of an increase in tetragonality of $BaTiO_3$ as expected after poling [81].

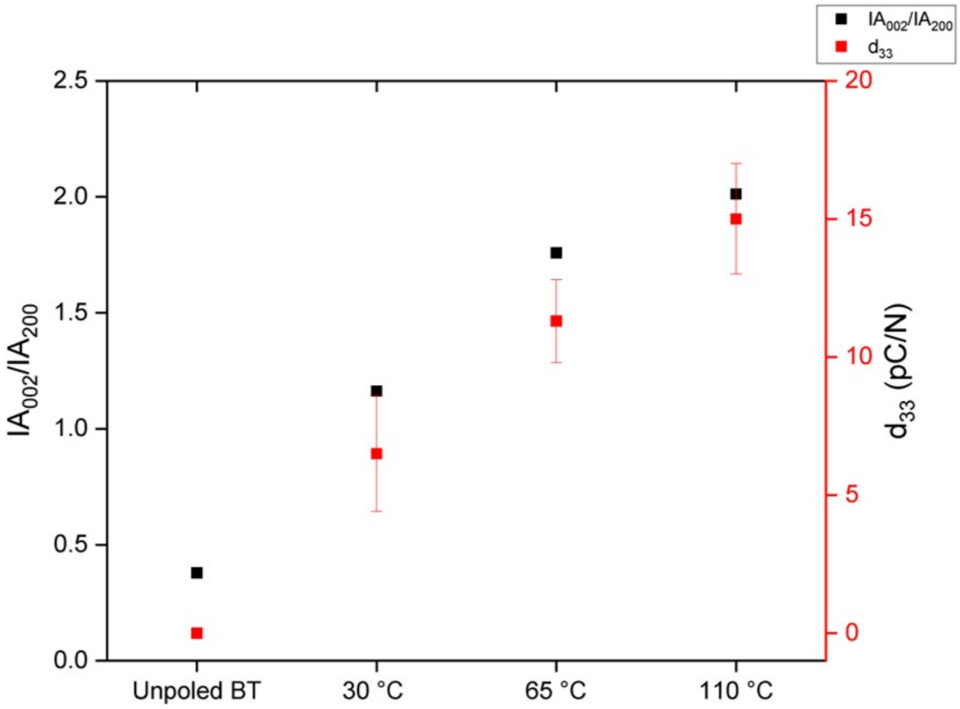

Figure 3.4: Normalized integrated area ratios and d_{33} plot for samples poled at different temperatures

The plot of the normalized integrated area of the (002) and (200) peaks are plotted along with the measured d_{33} for the different poling temperatures. The integrated areas are calculated using the Pseudo-Voigt function in Origin. Integrated areas is a better indicator of changes in the XRD pattern instead of peak intensity, as it accounts for the peak height as well as the area under the peak. The piezoelectric measurements match with the data obtained from the XRD plots in Figure 3.4. The results show that poling BT-PVA1 foams at a temperature of 110 °C, results in better poling. This confirms the observations in section 2.5 on corona poling optimization, that poling just below the T_C and cooling under field is indeed the optimal poling condition.

3.1.2. FTIR

The FTIR for the pure PVA and PVA1-BT foams with different ceramic loadings is shown below in Figure 3.5. Pure PVA shows a characteristic broad peak in the range of 3200-3600 cm^{-1} attributed to the hydroxyl groups present on the PVA surfaces. While the peak at 1710 cm^{-1} is related to the carbonyl group left after the incomplete hydrolysis of poly(vinyl acetate). The peaks between 2800-3000 cm^{-1} are assigned to the symmetric and asymmetric stretching vibrations of the CH_2 groups [82].

The broad O-H peak shifts from 3296.5 cm^{-1} for pure PVA to 3233 cm^{-1} for PVA1-BT 70/30 (32 vol.% loading). With increasing concentration of $BaTiO_3$, there is an increase in shift observed for the O-H vibration peak. It can be credited to the formation of H-bonds between the $BaTiO_3$ nanoparticles and the O-H groups present in PVA. These results indicate the formation of complexes, thereby also improving the interfacial adhesion between the ceramic and the polymer matrix [83], [84].

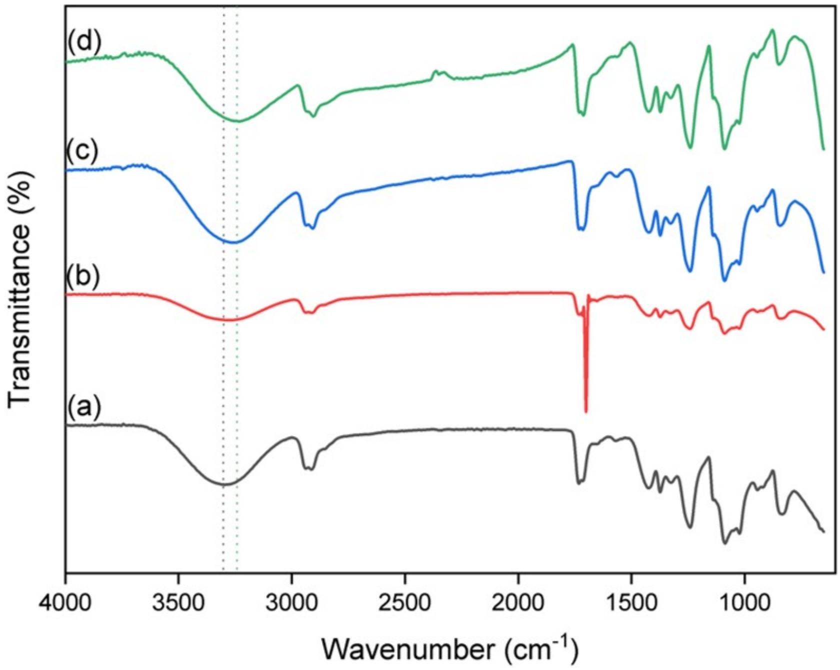

Figure 3.5: FTIR spectra of (a) pure PVA, (b) BT-PVA1 30/70, (c) BT-PVA1 50/50 and (d) BT-PVA1 70/30

3.2. Microstructure & Porosity measurements

Microstructure images (SEM and optical) of the ceramic powders and the foam composites, as well as the porosity measurements are presented in the following subsections.

3.2.1. Microstructure

The ceramic powders selected were observed under SEM to establish the particle shape and size as well as confirm the details provided by the manufacturer. The SEM images of the $BaTiO_3$ particles is shown below in Figure 3.6. The particles size is in the range of 300 nm and shows near-spherical morphology, as described by the manufacturer.

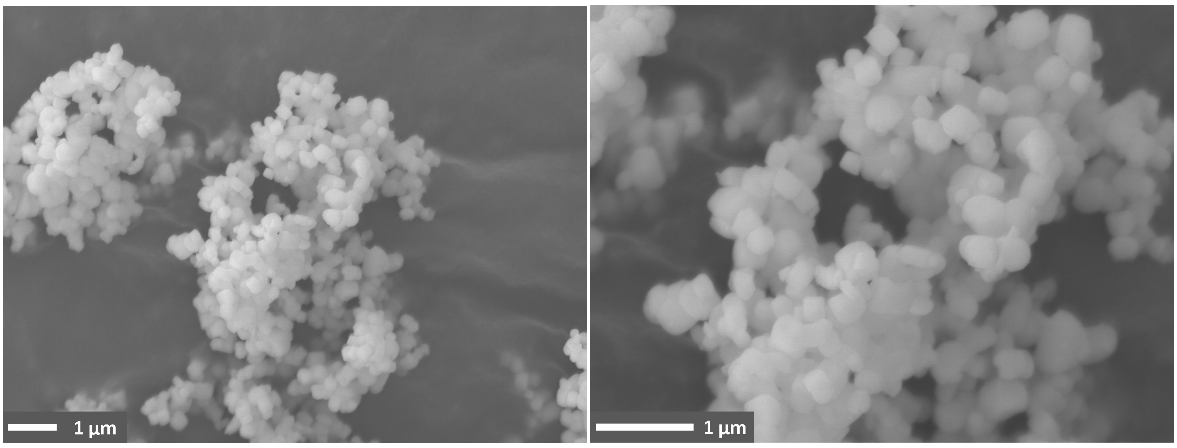

(a) 10,000x magnification

(b) 20,000x magnification

Figure 3.6: SEM image of $BaTiO_3$ particles

SEM images of the two size of KNLN3 powders is shown below in Figure 3.7. The particles show cuboidal morphology and is similar to the results obtained from the literature.

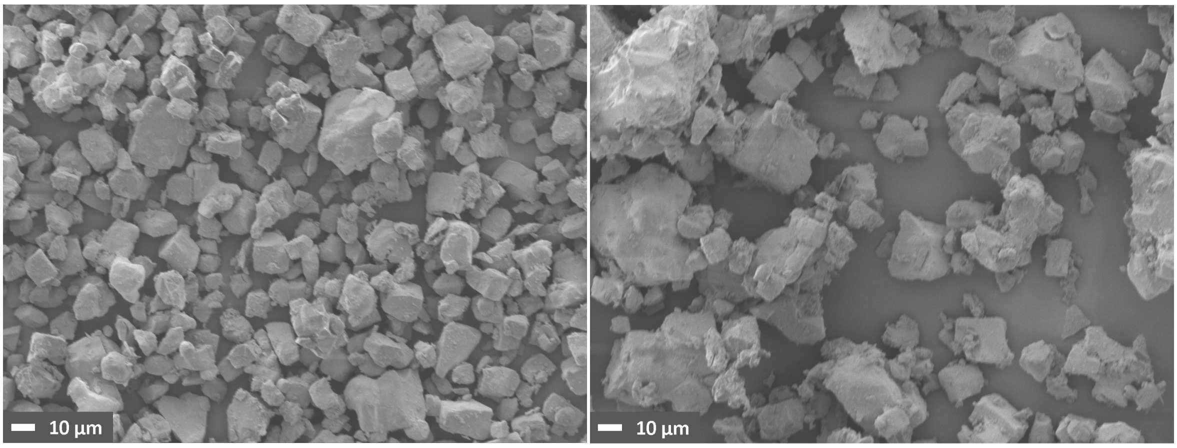

(a) KNLN3(<25 µm)

(b) KNLN3(25-63 µm)

Figure 3.7: SEM images of KNLN3 powders at 500x magnification

In order to investigate the microstructure of the PVA composite foams, SEM images are taken at the foam cross-section while optical imaging is utilized to obtain information about the top surface. A number of parameters are varied during the fabrication process to explore their effects on the overall porosity of the composite and is shown in the following subsections.

Effect of drying cycle

SEM images of the cross-section and optical images of the top surface of PVA1-BT 50/50 (16.9 vol.% BT) cured at RT and 60 °C are shown below in Figure 3.8a and Figure 3.8b. From these images, it is clear that the drying cycle has a major effect on the pore size and morphology. Foams cured at RT show an average pore size between 500-700 µm, while the foam cured at 60 °C have pores in the range of 150-300 µm. There is also a major difference in the pore structure, as the foams cured at 60 °C, have a more interconnected pore network (open pores) in comparison. This difference in pore size and structure can be attributed to the rate of evaporation of water from the wet foam. For foams cured at RT, the pore structure collapses and smaller pores coalesce to form much bigger pores. While in the other case, the wet foam microstructure was preserved to a large extent. Meanwhile, the top surface microstructure is shown in Figure 3.8c and Figure 3.8d. The surface pores in RT cured foams shrink due to the collapse of the structure during the curing cycle, while the foam cured at 60 °C shows similar open-cell morphology to that observed in the cross-section images. The top surface is also less rough for the RT cured foams due to the reduction in open-porosity.

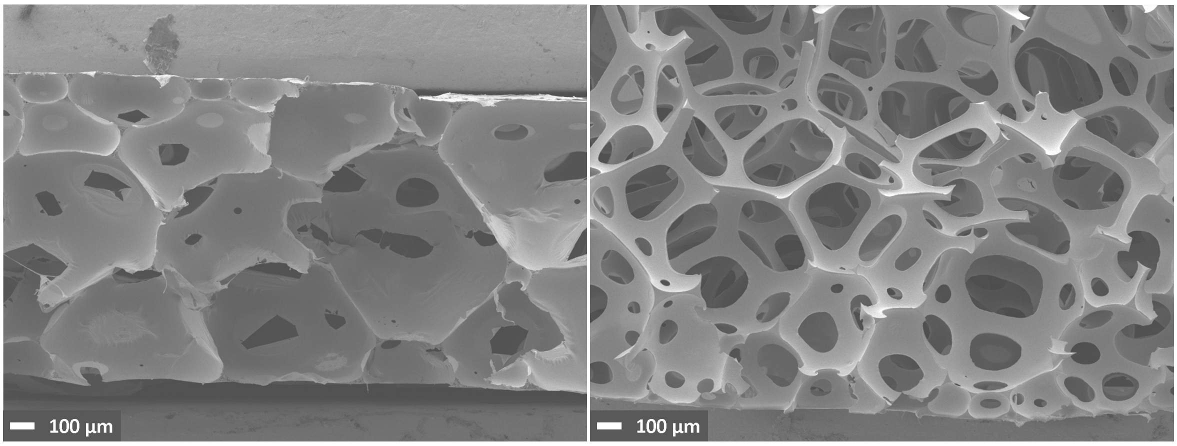

(a) BT-PVA1 50/50 RT cure, 50x SEM

(b) BT-PVA1 50/50 60 °C cure, 50x SEM

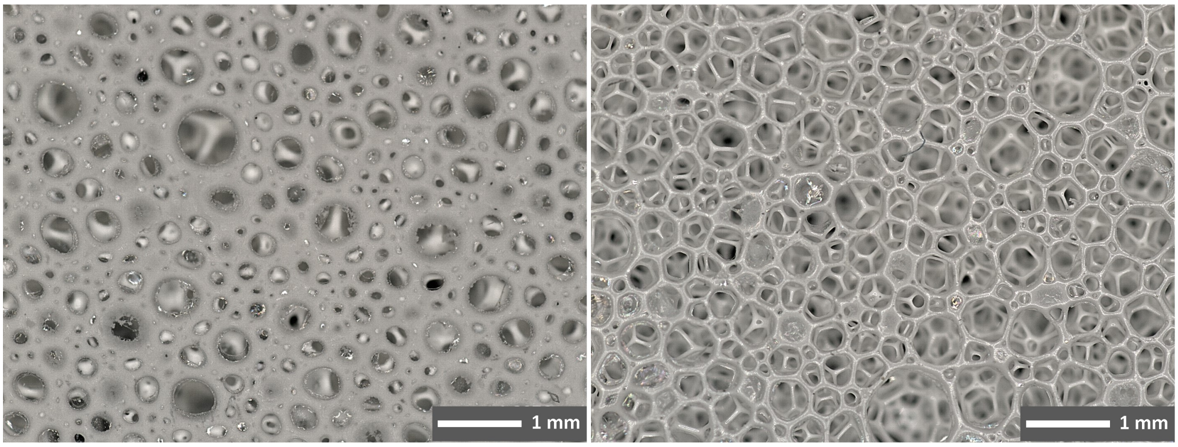

(c) BT-PVA1 50/50 RT cure, 40x OPM

(d) BT-PVA1 50/50 60 °C cure, 40x OPM

Figure 3.8: SEM images (top) at 50x magnification and optical images (bottom) at 40x magnification of BT-PVA1 50/50 RT cure (left) and 60 °C cure (right)

Effect of plasticizer

SEM images of PVA1 foams with same $BaTiO_3$ loading (32.2 vol.%) with and without plasticizer cured at 60 °C is shown below in Figure 3.9a and Figure 3.9b. The addition of plasticizer results in a much more homogeneous pore size distribution (250-470 µm), in comparison to foams without the plasticizer. This can also be attributed to the difference in drying cycles, as foams prepared with the plasticizer take about 10-12 hrs to dry, while the other takes about 2-3 hrs. The reduction in T_G with the addition of BBP (Benzyl butyl phthalate), also affects this drying process. Furthermore, the plasticizer affects the cell structure, as you obtain a microstructure representative of closed-cell foam. While the foam without the plasticizer exhibits a more open-cell structure. The top-surface image is shown in Figure 3.9c andFigure 3.9d, where the plasticized foam has a very smooth surface, while the open-cell structure for the foam without the plasticizer makes it rougher. This can be due to the slow and controlled rate of water evaporation from the plasticized foam, allowing the foam to close the pores at the top surface. However, due to the toxic nature of BBP, it is not used for further experiments as it would prohibit the on-body applications envisaged for these foams. This choice is also explained in the next section.

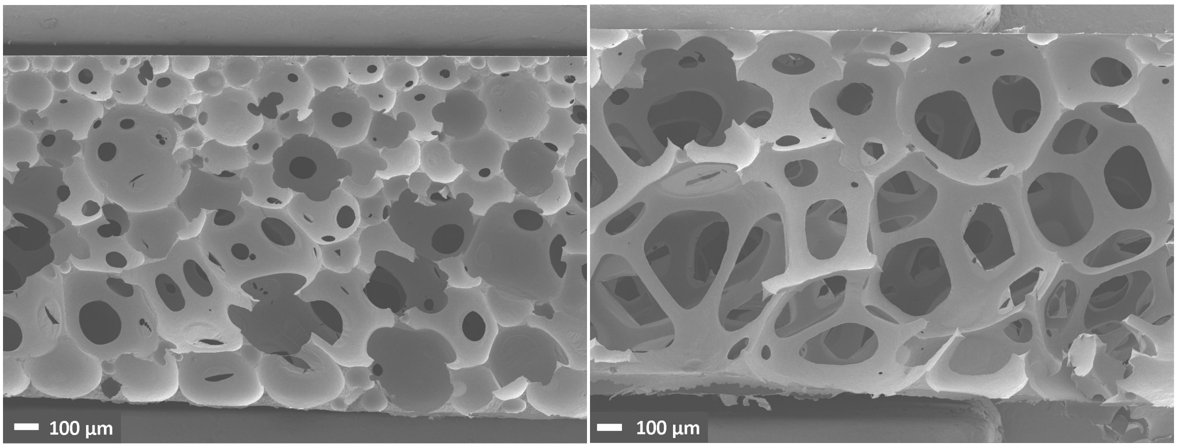

(a) BT-PVA1-BBP40 70/30 60 °C, 50x SEM (b) BT-PVA1 70/30 60 °C, 50x SEM

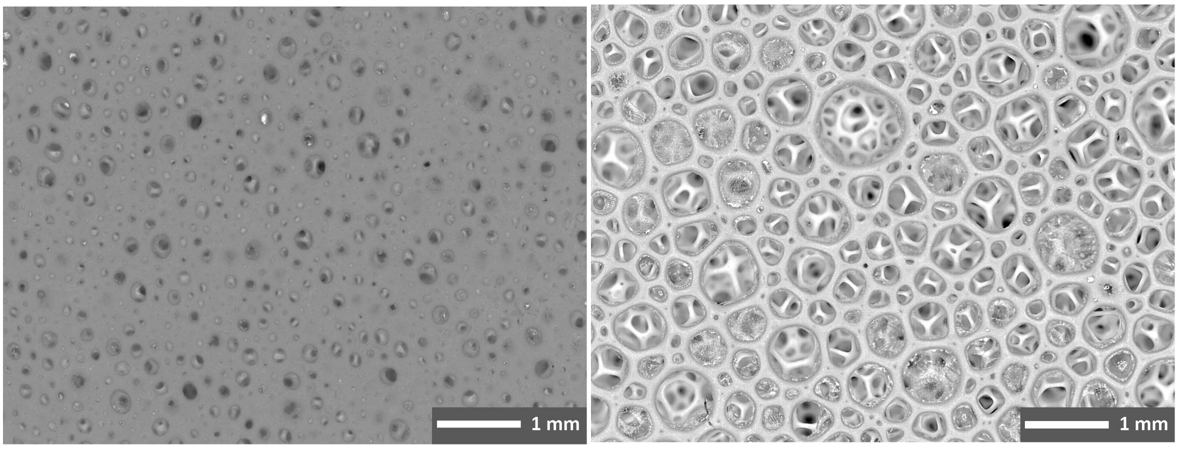

(c) BT-PVA1-BBP40 70/30 60 °C, 40x OPM (d) BT-PVA1 70/30 60 °C, 40x OPM

Figure 3.9: SEM images (top) at 50x magnification and optical images (bottom) at 40x magnification of BT-PVA1 70/30 with 40 wt.% plasticizer (left) and BT-PVA1 70/30 (right), both cured at 60 °C

Effect of PVA:H_2O mass ratio

SEM images of PVA1 and PVA2 foams with same $BaTiO_3$ loading (32.2 vol.%) cured at 60 °C is shown below in Figure 3.10a and Figure 3.10b. The concentration of PVA in water influences the viscosity of the wet foam, the pore structure and porosity, which affects the sample thickness as well as the mechanical properties. The mechanical properties are discussed in the next section, but the overall difference is the foams with higher PVA concentration (PVA2) are stiffer in comparison. A difference in thickness also has an effect on the capacitance of the foam, the thinner the sample, the higher the capacitance.

The difference in the thickness and microstructure can be seen from the Figure 3.10 (top). PVA2 foams are much thinner (≈0.95-1 mm), with an average pore size between 150-300 µm. Although there are some outliers with a few pores exceeding 400 µm in size, and some pores below 50 µm. The smaller pores near the sample bottom can be attributed to the higher viscosity of these foams. PVA2 foams already are more viscous than their counterpart PVA1, a higher ceramic loading affects the drying process, as denser materials tend to settle at the bottom. These foams also show a mix of open and closed cell porosity, that has an effect on the mechanical properties of the foam. PVA1 foams are on average around 1.4 mm thick and softer than their counterparts. The highly porous and interconnected structure can be seen from the SEM images above in Figure 3.10b (right). The bigger pores are between 500-750 µm in size, while the smaller channels (interconnected pores) were about 100-200 µm wide. This sponge-like network of interconnected open pores also affects mechanical properties as well as the overall porosity of the composite foam. The top-surface images are shown in Figure 3.10c and Figure 3.10d. The reduction in size and number of open pores is similar to that observed from the cross-section images and can be attributed to the higher viscosity of the wet polymer foam.

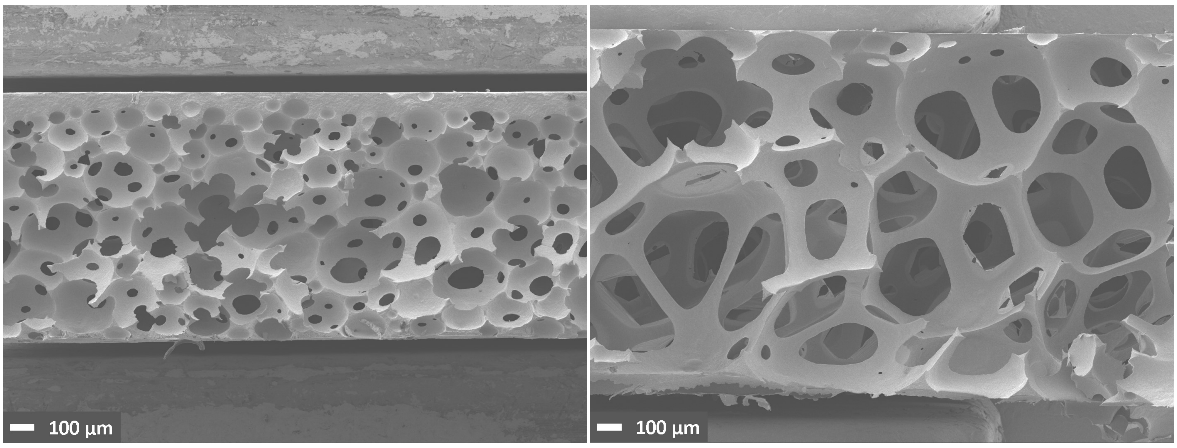

(a) BT-PVA2 70/30 60 °C, 50x SEM

(b) BT-PVA1 70/30 60 °C, 50x SEM

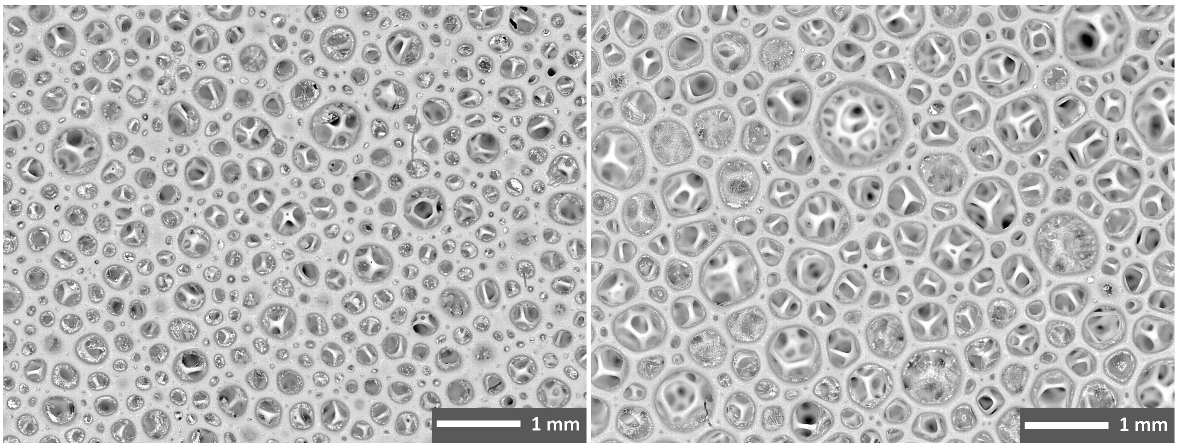

(c) BT-PVA2 70/30 60 °C, 40x OPM

(d) BT-PVA1 70/30 60 °C, 40x OPM

Figure 3.10: SEM images (top) at 50x magnification and optical images (bottom) at 40x magnification of BT-PVA2 70/30 (left) and BT-PVA1 70/30 (right) foams both cured at 60 °C

Effect of ceramic loading ($BaTiO_3$)

The changes in microstructure for PVA2 foams with increasing ceramic loading can be observed from the SEM images in Figure 3.11. Similar trends were also observed in PVA1 foams. The sample thickness stays almost the same (≈1.25-1.3 mm) for the first four ceramic loadings, while at around 32 vol.% BT the thickness reduces a lot (≈0.95-1 mm). This big jump is mainly due to the increase in viscosity of the wet foam at such a high ceramic loading, making it collapse under its own weight during the drying cycle.

The pore sizes in general stay in the same range for the first four foams around 300-400 µm, although with a similar trend of smaller pores (100-150 µm) near the sample bottom. The foam with the highest ceramic loading of 32 vol.% (BT-PVA2 70/30), has a slightly reduced pore size (150-300 µm) as discussed in the previous section. No other major changes in the microstructure have been observed for PVA1 and PVA2 foams with changing ceramic loadings. These trends are also visible in the porosity calculations in the next section. A similar trend is observed for PVA1 foams, but with a more open-cell pore architecture and is shown in appendix.

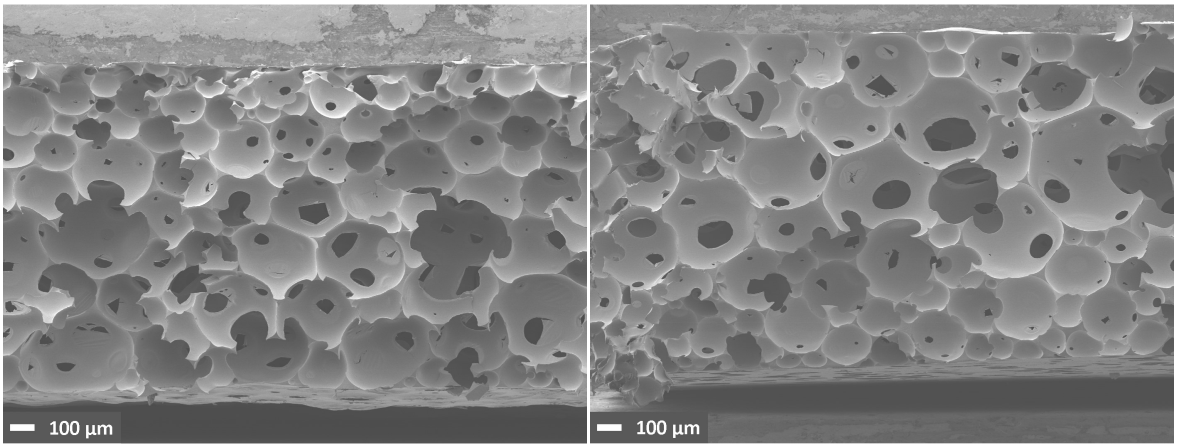

(a) BT-PVA2 30/70 60 °C, 50x SEM (b) BT-PVA2 40/60 60 °C, 50x SEM

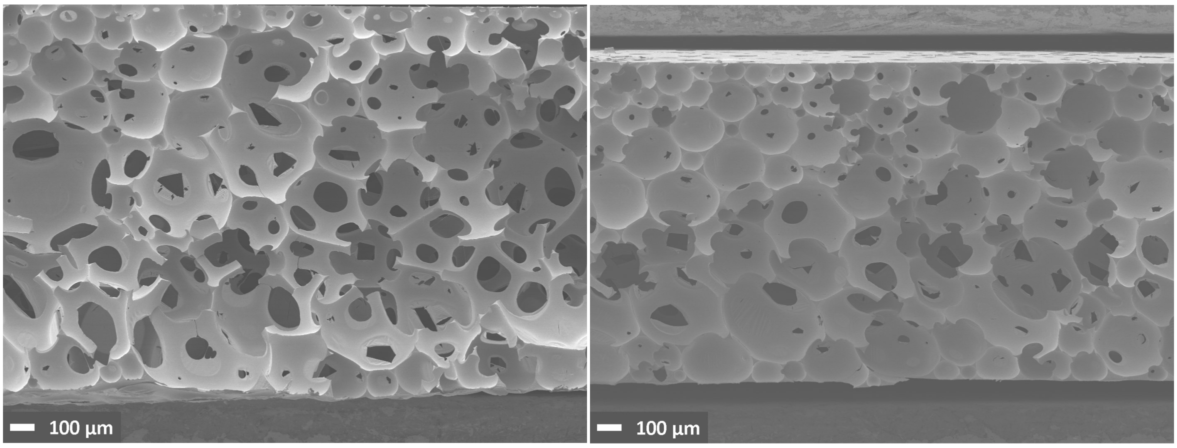

(c) BT-PVA2 50/50 60 °C, 50x SEM (d) BT-PVA2 60/40 60 °C, 50x SEM

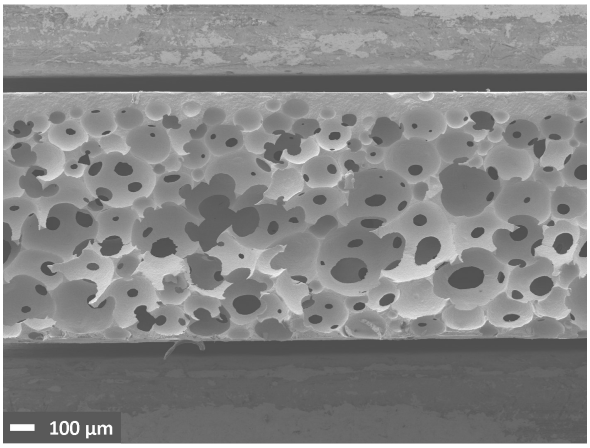

(e) BT-PVA2 70/30 60 °C, 50x SEM

Figure 3.11: SEM images of BT-PVA2 foams with increasing $BaTiO_3$ loadings.

To ensure that there is no significant agglomeration of ceramic particles in these foams, COMPO mode images are taken of the microstructure using a backscattered lens. The brighter regions are the ceramic particles as they have a higher molecular weight, while the polymer phases are darker than them. The dark and thin membranes visible in these SEM images are just pores that did not form and dry completely, as there is no ceramic present in those regions. The SEM images (Figure 3.12) showcase a homogenous distribution of the ceramic filler in the polymer matrix. These images could also be used to indicate the presence of interface porosity inside the pore struts, which act as stress absorbers to reduce the piezoelectric response, and insulation barriers to lower the poling efficiency.

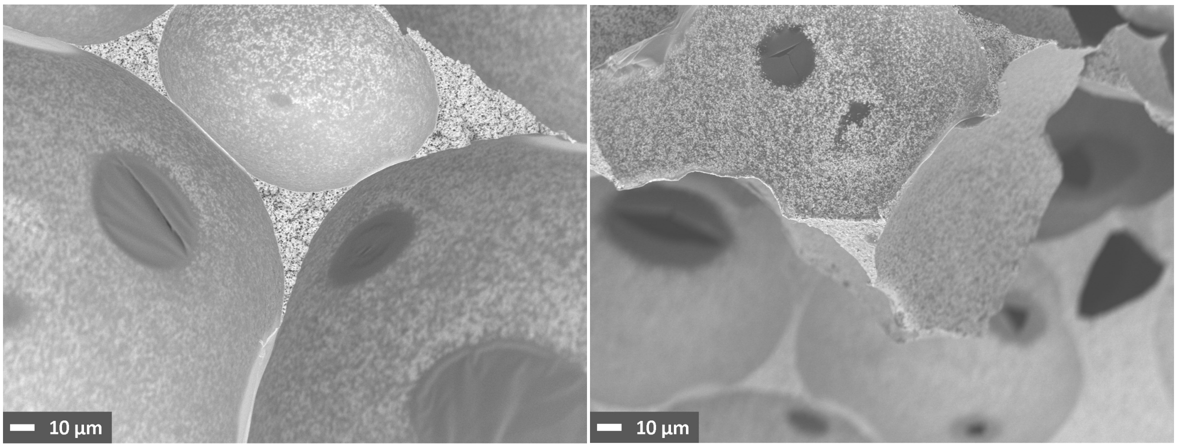

(a) BT-PVA1-BBP40 70/30 60 °C, 500x SEM

(b) BT-PVA1 70/30 60 °C, 500x SEM

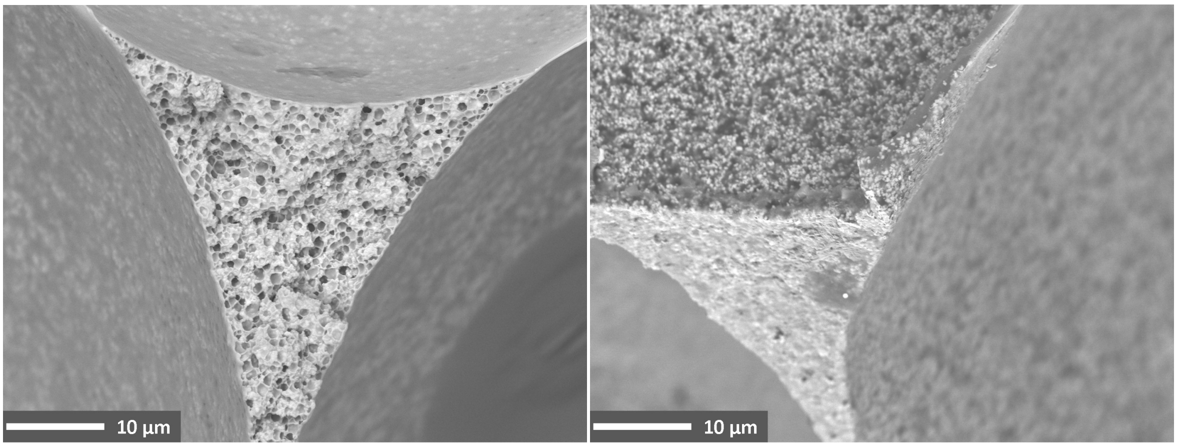

(c) BT-PVA1-BBP40 70/30 60 °C, 2000x SEM

(d) BT-PVA1 70/30 60 °C, 2000x SEM

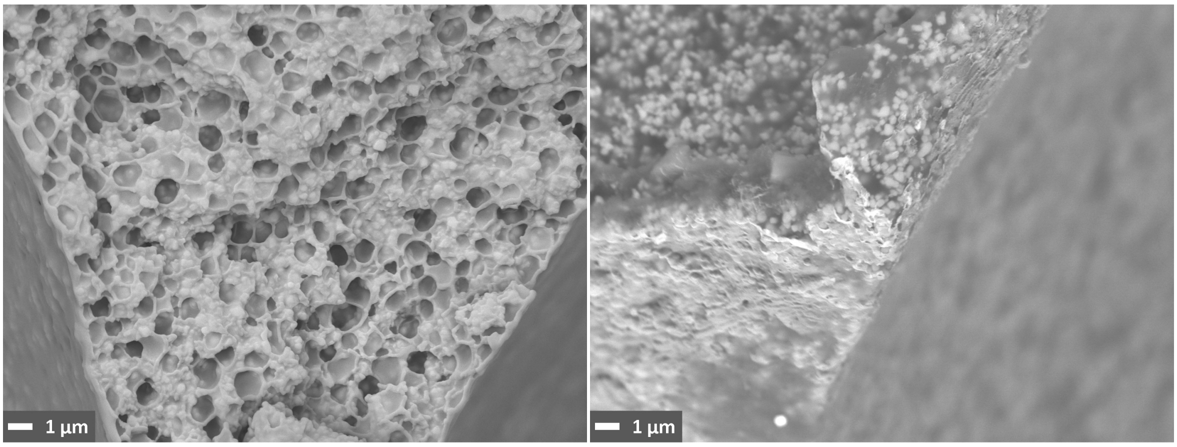

(e) BT-PVA1-BBP40 70/30 60 °C, 5000x SEM

(f) BT-PVA1 70/30 60 °C, 5000x SEM

Figure 3.12: COMPO mode images of BT-PVA1 70/30 with BBP40 (plasticizer) (left) and without plasticizer (right), both cured at 60 °C

Properties of the polymer selected (PVA) varied with a change in curing cycles, the addition of plasticizer and loading of the ceramic filler. Foams cured at RT show a large fluctuation in porosity from sample to sample. For the same foams cured at 60 °C, there is not much of a difference in the values measured. This has a major effect on the reproducibility of the RT cured foams, which further had an effect on the variability in the mechanical and piezoelectric properties of the foams. It can be attributed to the fact that these foams are cured in an open environment. Since the curing cycle of the foams is dependent on the rate and amount of evaporation of water, humidity and temperature on the day have a major effect on their properties (mechanical). The humidity did not affect the sample cured at 60 °C to the same extent, as they are dried inside a closed environment (Heraues 0982 oven). Further discussion of the mechanical and electrical properties of the foams is then limited to foams cured at 60 °C. Discussion of KNLN3 foams is done in the Appendix C.

3.2.2. Porosity measurements

Porosity and relative density measurements are done by calculating the geometric density and comparing it to the theoretical density of the composite. Attempts were made to determine the density using the Archimedes method, but it was not possible as the PVA foams are highly soluble in water and ethanol, while higher alcohols do not penetrate the porous structure. To account for the surface roughness as well as the difficulty in defining the exact dimensions of an open-cell foam, conservative measurements are taken to get an estimate on the lower limit of the porosity. The measurements are done for BT-PVA1 and BT-PVA2 foams with varying ceramic loadings, as explained in the previous section.

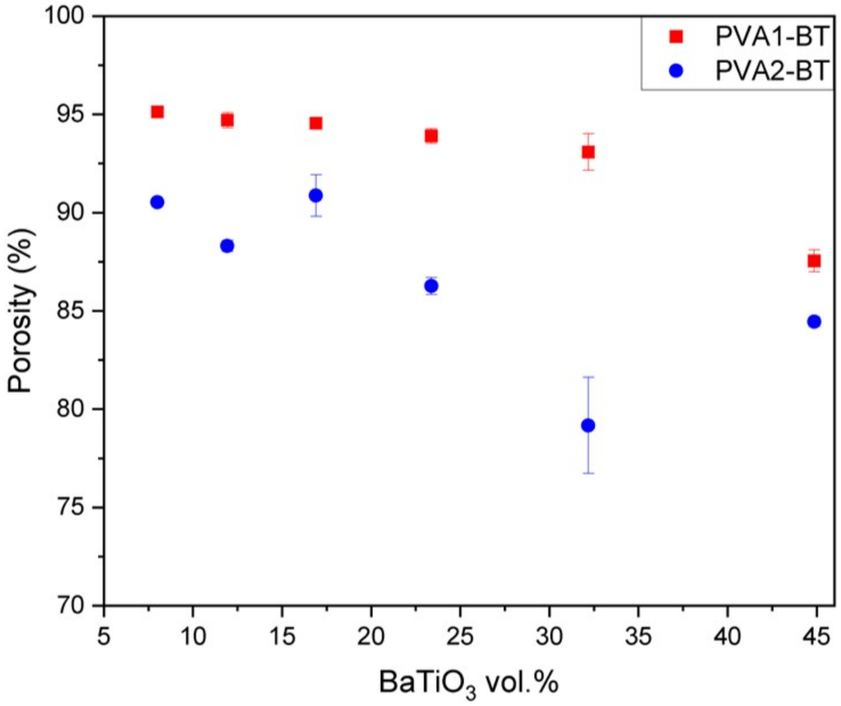

Figure 3.13: Porosity vs $BaTiO_3$ vol.% in BT-PVA foams for different PVA: water mass ratios

Figure 3.13 shows a plot of variation in porosity at different ceramic loadings for two different systems. PVA1 foams show relatively higher porosity than their PVA2 counterparts at the same ceramic loadings, which could also be seen in Figure 3.10 of the previous section. The interconnected structure results in foam with higher porosity. PVA1 foams follow the general trend of a decrease in porosity with an increase in ceramic loading, which can also be established from the SEM images (Figure 3.11). There is a marked decrease in the number and size of channels (interconnected pores) and thickness of struts with increasing ceramic loading. In spite of this, there is a relatively small change in the overall porosity of the foams until 32 vol.% BT loading. The major outlier is the foam with loading at 44 vol.% where the structure predictably collapses and thereby reducing the porosity.

PVA2 foams on the other hand show some scatter in the collected data. There is a big outlier at 32 vol.% where porosity falls below 80% which might be an issue with the specific sample. A slight increase in porosity at 16 vol.% which although doesn't follow the general trend, differs from its neighbouring values by about 2-3% . This small difference in porosity can be due to multiple reasons: human error, variation in porosity at different points of the samples (although accounted for) and sample variability. Another important point of comparison is the foam at 44 vol.% BT. Although the porosity decreases for this foam relative to foams of lower ceramic loading, it doesn't collapse considerably as observed in the PVA1 foam. This is due to the initial PVA slurry being more viscous, allowing the wet foam to prevent it from collapsing even at such high ceramic loadings.

3.3. Dielectric measurement

BDS measurements for pure PVA foams are carried out to describe the dielectric behaviour of the polymer phase and how it changes with temperature and frequency. Furthermore, it is well established that the polymer conductivity has an impact on the poling response of the composite [28]. The variation of dielectric permittivity and AC conductivity for PVA is shown in Figure 3.14. A major increase in both is observed with an increase in temperature, which is in line with data from the literature for PVA based films [60], [63].

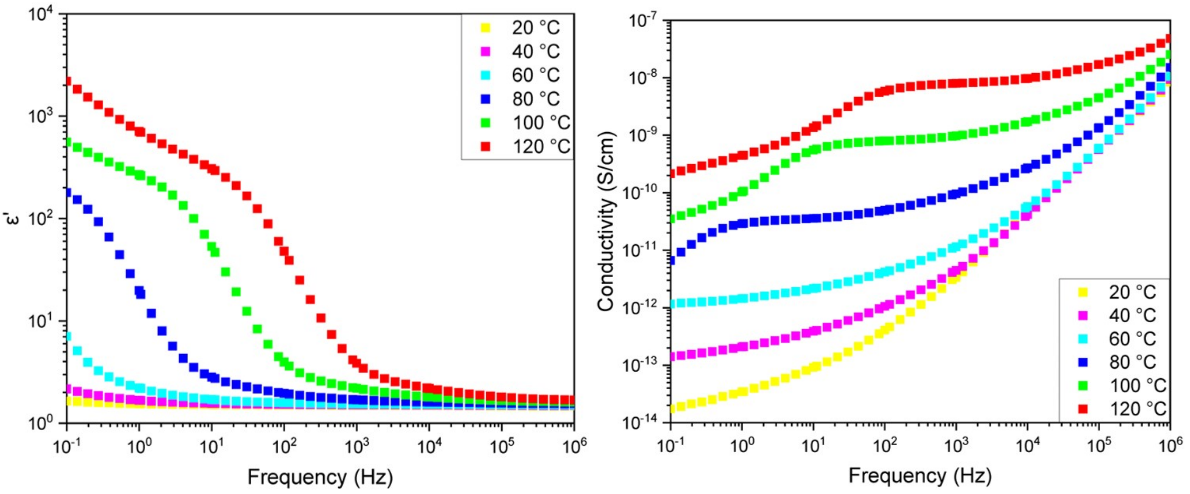

(a) Real permittivity (ε') vs frequency

(b) AC conductivty (σ_{AC}) vs frequency

Figure 3.14: Permittivity and conductivity measurements of PVA foams at different temperatures

A sharp increase in permittivity values (Figure 3.14a) is observed in the low-frequency region with increasing temperatures, while the conductivity plot (Figure 3.14b) indicates the presence of relaxation phenomena in the same region. To define this behaviour, the electric modulus is plotted in Figure 3.15. The dielectric modulus is defined as the inverse of the complex permittivity function and is analogous to the viscoelastic relaxation of polymers [85]. Clear relaxation peaks (Figure 3.15b) are observed at higher temperatures and is attributed to the hopping of ions [86], [87]. The mobility of charge carriers is confined to potential wells (short distance) above the relaxation frequency, while they are highly mobile over long distances below it [88]. With increasing temperatures, the chain mobility increases, shifting the relaxation peaks to higher frequencies [89], [90]. While the peaks are not observed at lower temperatures due to system limitations.

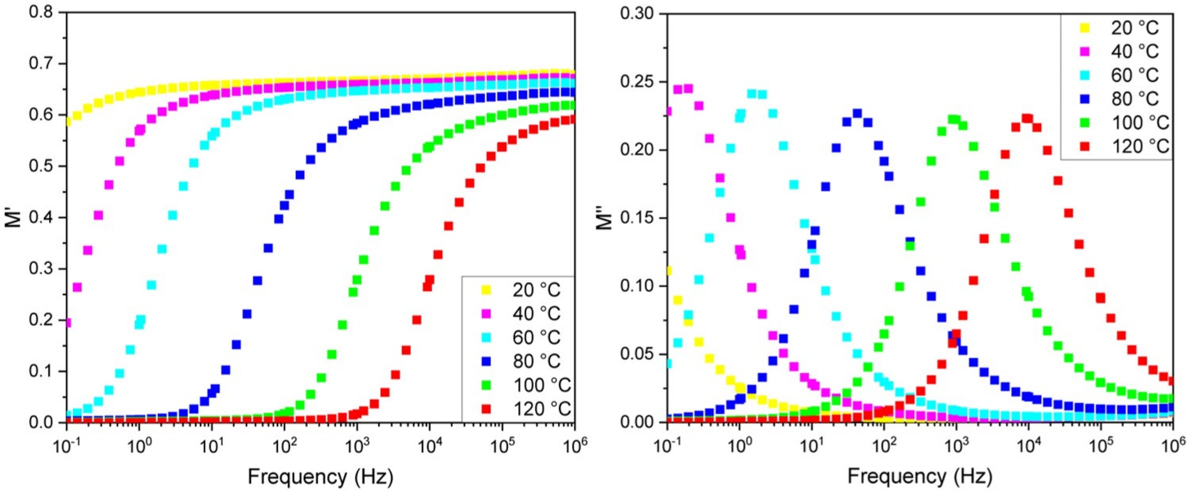

(a) Real dielectric modulus (M') vs frequency

(b) Imaginary dielectric modulus (M") vs frequency

Figure 3.15: Dielectric modulus of PVA foams at different temperatures

This indicates that poling PVA foams at a higher temperature allow for a better poling efficiency, due to an increase in the mobility of charge carriers in the polymer matrix. Therefore, to improve the conductivity of the polymer phase, samples are poled at 110 °C, just below the T$_C$ of the BaTiO$_3$ filler, and cooled under the field to prevent domain realignment. The plot for the relative permittivity and $\tan\delta$ for PVA1 foams is shown below in Figure 3.16. All these measurements are done on a day with RH in the range of 40-42% . The permittivity increase follows the general trend of random composites and reaches a value of 2.57 at 32 vol.% ceramic loading. Note that the vol.% loading mentioned in all these plots is done without accounting for the porosity of the composite. Therefore, if a foam is on average 90% porous, the ceramic loading would account for only 3 vol.% of the total composite. As the dielectric permittivity of a piezoelectric composite is matrix dominated [91]–[93], a major reduction of the permittivity of these composites is expected and observed. The $\tan\delta$ also follows a similar trend of increasing with higher ceramic loading.

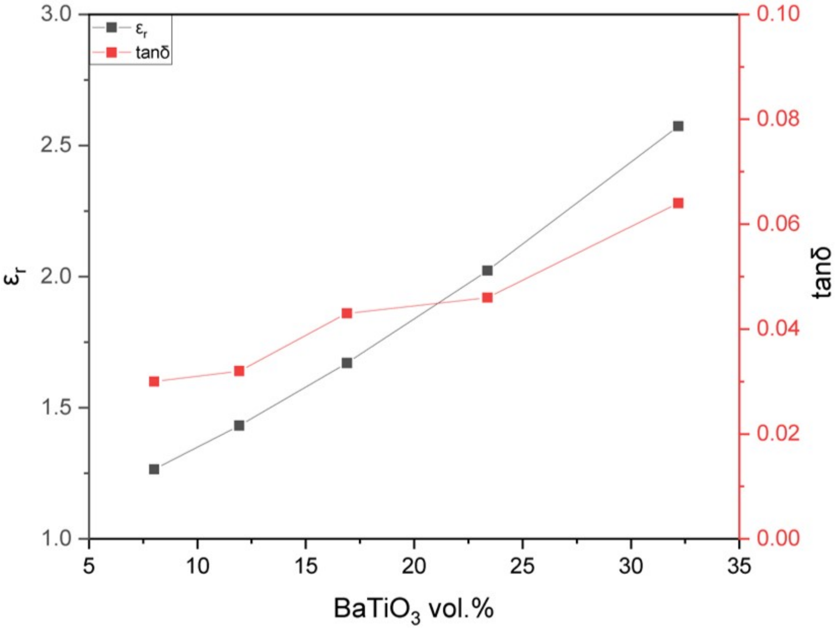

Figure 3.16: Relative permittivity (ε_r) and $\tan\delta$ variation in PVA1 foams with increasing BaTiO3 loading

For the humidity test, samples are removed from the test chamber after ageing for a week. BDS measurements are immediately carried out by using a single frequency sweep at RT to quantify the changes in the dielectric behaviour of these foams (Figure 3.17). A significant increase in the permittivity and tanδ for the sample at 82% RH, is also observed from the LCR meter. A correspondingly large increase is also observed in the conductivity measurements. This indicates that PVA foams are extremely moisture sensitive and their dielectric properties are affected by humidity. Given that PVA is partially water soluble, this is not entirely unexpected.

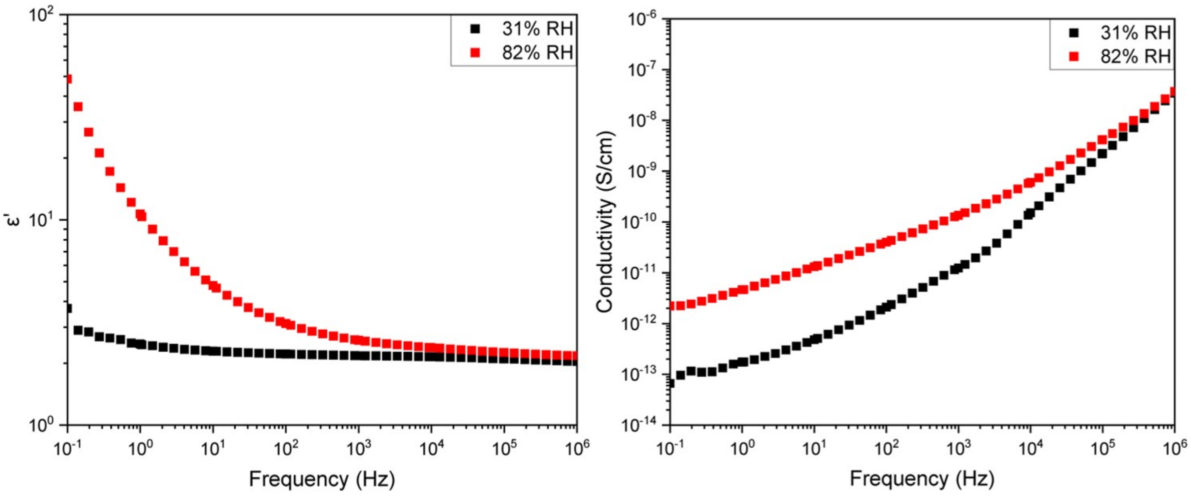

(a) Real permittivity (ε') vs frequency

(b) AC conductivty (σ_{AC}) vs frequency

Figure 3.17: Permittivity and conductivity measurements of PVA foams at different humidity levels

3.4. Piezoelectric measurement

After optimizing the poling temperature, the next step is the grid voltage selection. As mentioned previously, all samples are poled at a pin voltage of 50 kV for one hour at 110 °C before cooling down to RT, which is kept constant throughout the experiments, while the grid voltage is varied. This is because the grid voltage controls the surface charge distribution and the surface potential. Using a low grid voltage results in few ions reaching the sample, due to the low difference in potential between the grid and the substrate. While a high grid voltage may in itself produce a parasitic corona which again results in weak ion bombardment and lower polarization [94]. Therefore, the grid voltage is varied between 2-14 kV, which is dependent on sample thickness. For this study, PVA1-BT 70/30 (32.2 vol.% BT) foams are used.

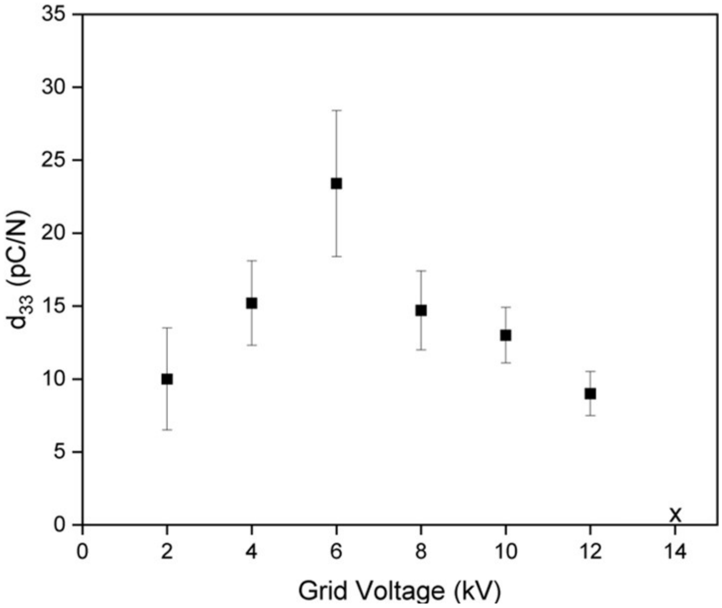

Figure 3.18: Influence of grid voltage on d_{33} for PVA1-BT 70/30 (32.2 vol.% BT) foam

Figure 3.18 shows the distribution of the measured piezoelectric charge coefficient with the grid voltage. Samples could not be poled at voltages above 12 kV as the formation of a parasitic corona discharge is observed at the grid plate (Figure 3.19). The maximum d_{33} is obtained at a grid voltage of 6 kV, which is dependent on the distance between the grid and the sample and the sample thickness. The minimum separation between the grid and sample is 16 mm, while the sample thickness is about 1.3 ± 0.2 mm. This and the fact that the charges released by the corona process penetrate the porous sample and deposit on the pore struts, which in theory could pole the sample better. The struts are on average 10-30 µm thick, which would increase the effective field experienced by the ceramic particles and pole them to a higher degree.

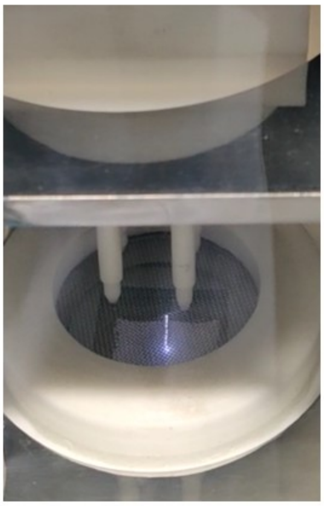

Figure 3.19: Formation of parasitic corona

From the previous sections we can conclude that the dielectric and piezoelectric behaviour is dependent on a number of factors, mainly the permittivity and conductivity of the composite and the piezoelectric response of the ceramic. External factors such as humidity have a major impact on the electrical and mechanical properties of the foam, as PVA is moisture sensitive. Electret behaviour induced via the corona poling method is also another parameter that influences the piezoelectric response of the foams. When some samples are poled at 110 °C for about an hour, they show this behaviour, although it disappears after the first 24 hours of poling. This can be seen in Figure 3.20, where the piezoelectric properties are measured using the Berlincourt setup. All of these factors together affect the electromechanical response of these foams; therefore, it is difficult to isolate individual contributions.

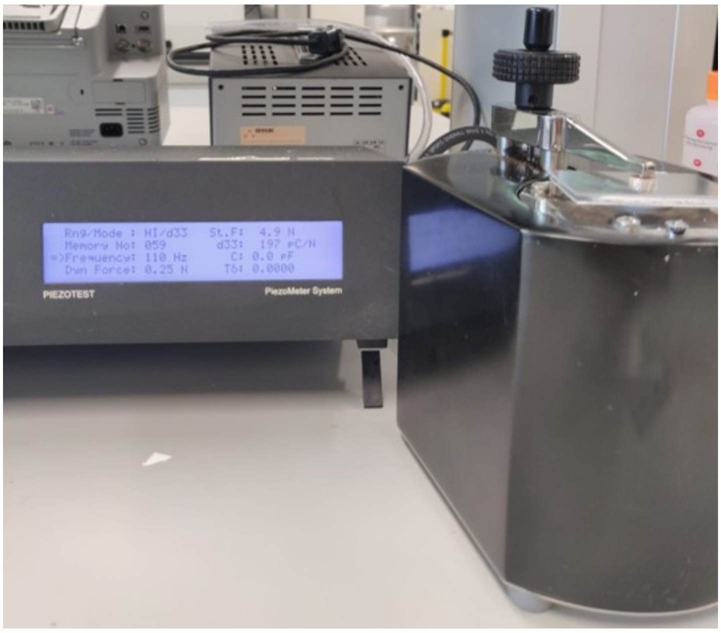

```
  Rng/Mode : HI/d33   St.F:  4.9 N
  Memory No: 059        d33:  197 pC/N
=>Frequency: 110 Hz       C: 0.0 pF
  Dyn Force: 0.25 N      Tδ: 0.0000
```

Figure 3.20: Electret behaviour after poling (d_{33} values in 2nd column-2nd row)

The decay in the d_{33} of these foams isn't significant enough 24 hours after poling, therefore all the measurements are taken on a single day to minimize errors due to changes in humidity and temperature. The plot for the variation of d_{33} and g_{33} for PVA1 foams is shown below in Figure 3.21. The increase in d_{33} with ceramic loadings reaching values as high as 25 pC/N at 32 vol.% ceramic loading.

This major increase in d_{33} can be attributed to multiple factors. First, from the compo-mode images (Figure 3.12), we can observe an excellent distribution of the ceramic particles inside the struts of the foam without any agglomeration. As a result of the high porosity, the ceramic vol.% inside these struts is much higher than it would be inside a non-porous random composite, thereby reducing the interparticle distance. Another consequence of fabricating a porous structure is the reduction of the modulus of the composites, which results in a bigger modulus mismatch. A greater mismatch would mean higher stresses being applied on the ceramic particles (which is true for structured or quasi-structured composites), thereby increasing the piezoelectric response. Also, the formation of electrets, could in theory improve the poling efficiency as they get deposited on the pore walls, thereby poling the ceramic particles present inside the struts to a better extent. The humidity measurements are shown together along with the mechanical properties in the next section as the piezoelectric behaviour is essentially an electromechanical response/phenomenon.

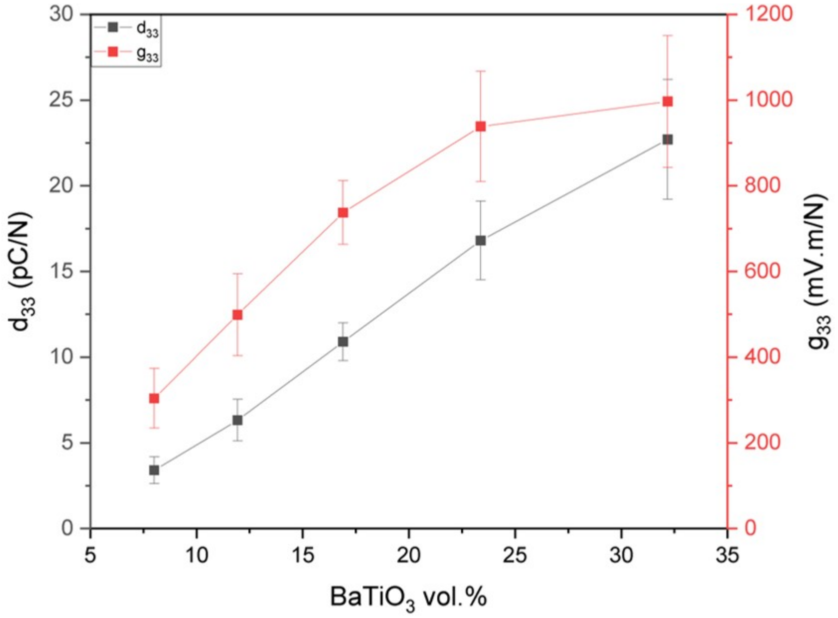

Figure 3.21: d_{33} and g_{33} variation in PVA1 foams with increasing $BaTiO_3$ loading

3.5. Mechanical properties

DMA tests are done to define the mechanical properties of these foams under compression. Samples are prepared using a 16 mm punch die. Since the aspect ratio (t/d) plays an important role in the compressive properties of these foams, samples with similar thicknesses are tested in order to keep it consistent. This is done to get a relative comparison of the mechanical properties, instead of obtaining absolute values. The samples are strained at a rate of 0.01 mm/s and the load cell is limited to a maximum force of 35N.

Figure 3.22 shows the stress-strain behaviour of PVA1 foam at different ceramic loadings. The plot displays the characteristic regions observed in a porous polymer structure as discussed earlier in Figure 1.22. The linear elastic region is followed by a small plateau where the cells collapse. The plastic plateau region can be attributed to the creation of plastic hinges. In the final densification stage, the stress increases rapidly with a slow increase in strain levels. An increase in the compressive modulus, as well as the yield stress, is observed for the foam with higher ceramic loading.

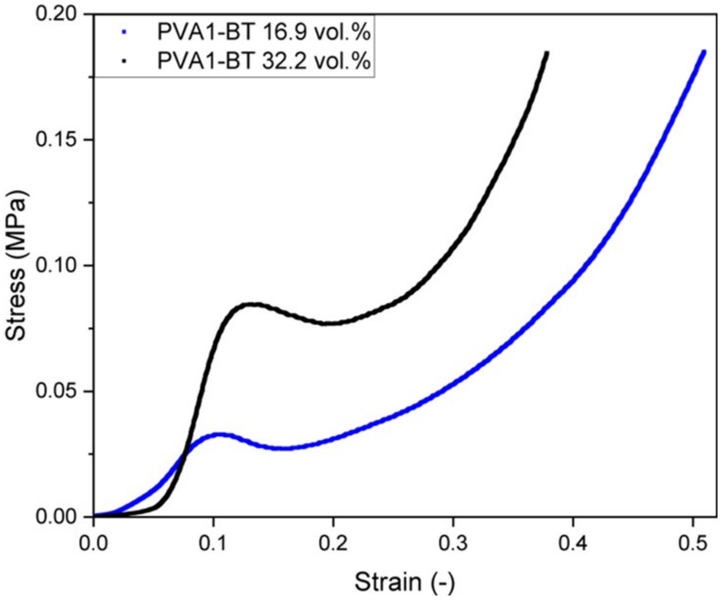

Figure 3.22: Compressive stress-strain curve for PVA1 foam at different ceramic loading

Figure 3.23 represents the stress-strain behaviour of PVA2 at different ceramic loadings. These foams show similar behaviour to that of closed-cell foams without a clear plateau region. This could also be inferred from the difference in microstructure to that of PVA1 foams from Figure 3.10. As the system is limited to a 35N load cell, these foams don't even reach their yield point, so it's difficult to compare the compressive modulus and yield stresses for foams with different ceramic loadings.

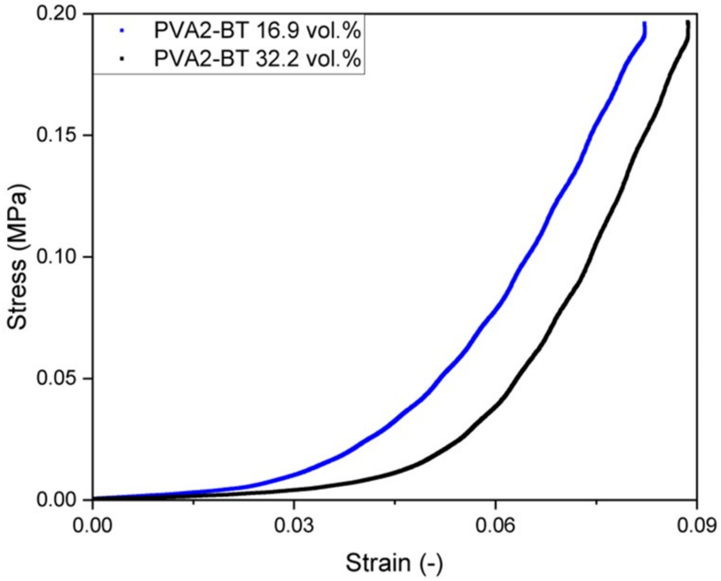

Figure 3.23: Compressive stress-strain curve for PVA2 foam at different ceramic loading

As the PVA2 foams did not reach their yield stresses and their young's modulus could not be defined under the current setup limitations, they are not selected for further study. Along with the fact that there is a relatively large variation in porosity levels of PVA2 foams with increasing ceramic loading (Figure 3.13), a direct comparison is not possible. Therefore only the results from PVA1 foams are interlinked to their piezoelectric properties measured, The modulus values for the PVA1 foams with varying volume fractions of the ceramic are shown below in Figure 3.24. They show an increase in properties with increasing ceramic loading, which would follow the logical conclusion and is consistent with other ceramic-polymer composites.

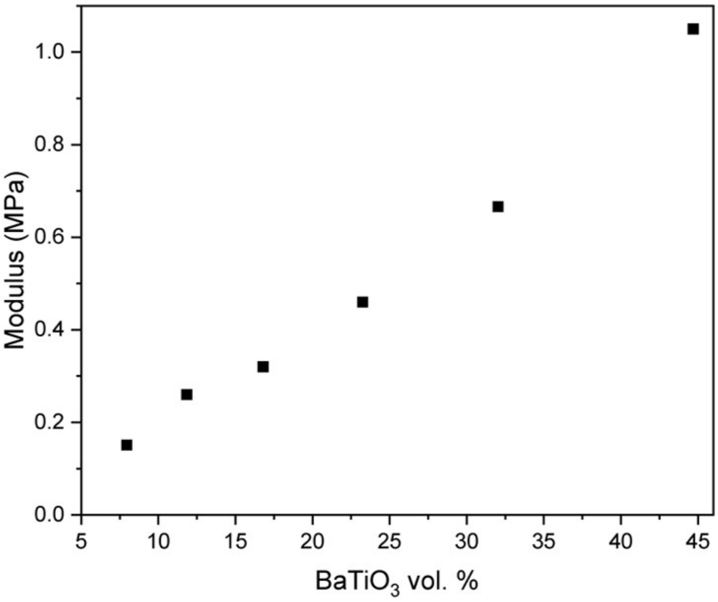

Figure 3.24: Compressive modulus vs ceramic volume fraction for PVA1 foams

Also, to keep the measurement forces consistent for the piezoelectric response, all samples with different ceramic loadings are clamped at a pre-load force of 1N. This is high enough so that the sample doesn't lose contact and rattle. By increasing the area of the sample, the stresses can be reduced and prevent static stress concentrations from affecting the piezoelectric measurements. For the humidity tests, DMA measurements are done for the same samples to quantify the difference in moduli. Since the piezoelectric behaviour is an electromechanical phenomenon, the electromechanical coupling factor *k* gives the efficiency of converting mechanical to electrical energy and vice versa. We can modify Equation 1.8 for a piezoelectric material to be :

$$k = d\sqrt{\frac{E_Y}{\varepsilon}} \tag{3.1}$$

Where E_Y is the modulus/stiffness of the material along the axis of deformation and *d* is the piezoelectric charge constant. In the real world, efficiency cannot be equal to one, so :

$$d < \sqrt{\frac{\varepsilon}{E_Y}} \tag{3.2}$$

Lowering the modulus can, thus, improve the piezoelectric properties, meaning a softer composite will show a much better charge response than a stiffer composite (true for a structured or a quasi-structured composite) [95], [96]. The stress-strain curves for the foams are shown below in Figure 3.25.

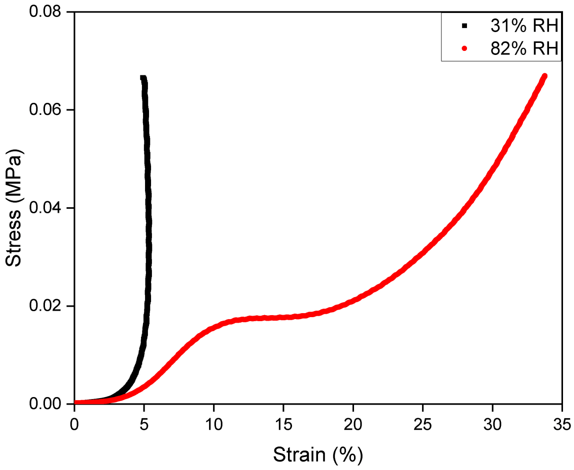

Figure 3.25: The stress-strain curve at different humidity levels

The foam at 81% RH shows elastomeric behaviour, while the stress-strain curve for the foam at 31% RH is similar to that of an elastic-brittle foam. PVA1 foams compressive stress-strain curves at 60% RH is equivalent to that of an elastic-plastic foam, as seen in Figure 1.22. This change in compressive behaviour with a change in the humidity can be attributed to the reduction of mechanical properties of PVA composites with an increase in humidity levels. The compressive modulus is plotted along with the measured d_{33} in Figure 3.26 and they fit the proposed trend from Equation 3.2. Although the modulus for the stiffer foam is an approximation as the composite did not reach its yield stress.

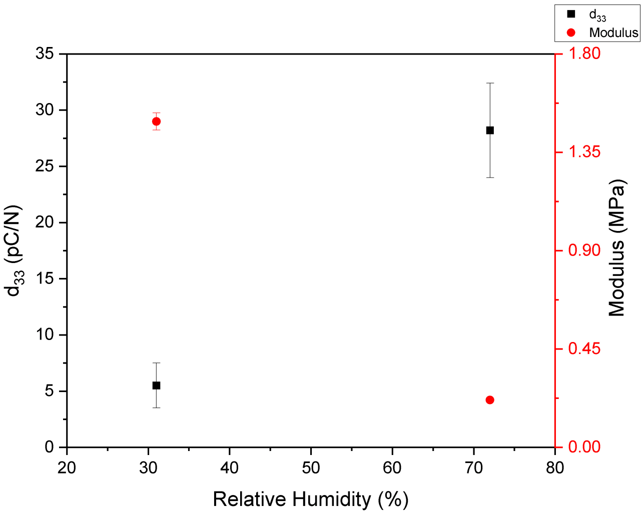

Figure 3.26: d_{33} and compressive modulus for foams at different humidity levels

The results from the previous sections indicate an increase in the permittivity and conductivity of the composite with an increase in the relative humidity. From the results above, we see a clear indication of the reduction of modulus and a great improvement in the measured d_{33} at higher humidity levels. This increase in the measured d_{33} is most interesting as d_{33} tends to reduce with time and a sudden increase due to humidity alone is rare. Although precaution has to be taken, a direct correlation between the increase in measured d_{33} and reduction in modulus is only true for 1-3 structured composites.

For a random composite, this improvement is only possible with increasing connectivity between the ceramic particles (quasi-structured). However, COMPO mode images of the pore strut cross-section (Figure 3.12) illustrate an increased amount of connectivity between the ceramic particles. This is mainly due to the fact that the ceramics are now only restricted to the pore-struts and are not ’randomly’ distributed. Therefore, this increase is attributed to a combination of the reduction in Young’s modulus (resulting in higher stresses applied to the ceramic) and the increased conductivity of the polymer (allowing the charges generated on the ceramic particle surfaces to more easily migrate to the polymer surface).

4

Discussion

The main research objective of this thesis was to further improve on the work done by Hamideh and Kevin on porous PZT-Polyurethane composites. A relatively high g_{33} (about 160 mV.m/N) was obtained for their dielectrophretically structured 1-3 PZT-Polyurethane composites. Although, their systems was still limited by the maximum porosity (60%) of the polymer and the foaming technique used. The maximum g_{33} obtained for our samples is above 1000 mV.m/N, which is about double the next highest piezoelectric sensor in the market currently (PVDF). This great improvement is attributed to the high porosity achieved by the direct foaming technique (≈ 92%), which resulted in a major reduction of the permittivity of the composite. A consequence of a highly porous composite is the reduction of the elastic stiffness, which leads to a higher modulus mismatch between the active piezoceramic and the porous polymer matrix. For a structured composite, this means a softer matrix would impart higher stresses on the piezoelectric ceramic, and therefore a higher d_{33} can be obtained. This two-fold improvement produces a very high voltage response (g_{33}), as shown in the Figure 4.1. All the contributing factors will be discussed separately in the following paragraphs.

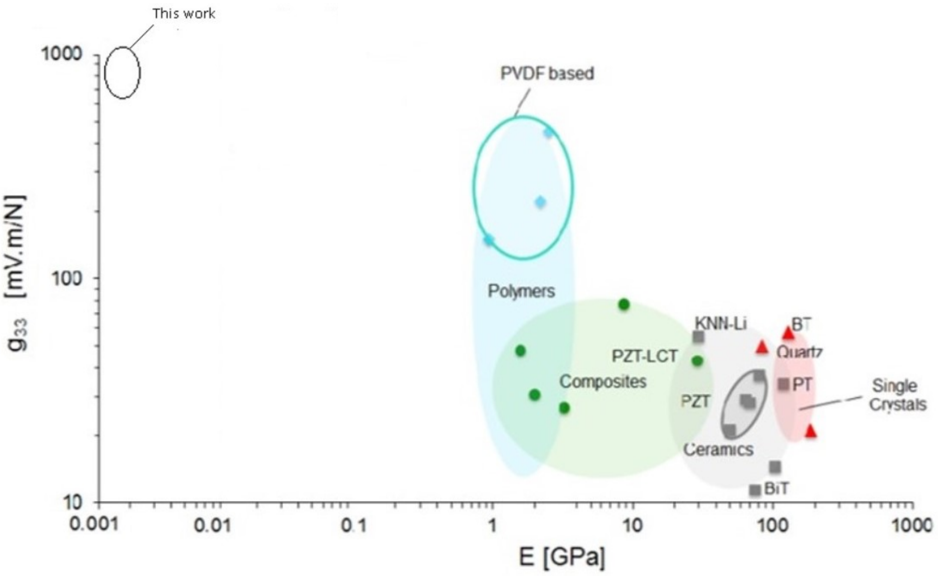

Figure 4.1: g_{33} vs elastic stiffness for all piezoelectric systems

A number of factors influence the piezoelectric voltage response, including the dielectric properties of both the piezoceramic and the polymer phase, the piezoelectric properties of the active piezoeceramic, the adhesion between the two phases, the pore morphology (porosity and microstructure) and the poling technique used. The porosity plays a major role on the dielectric and mechanical properties of the composite, as was explained earlier in the text. For a composite, the dielectric properties of the polymer have a significant effect on its piezoelectric response. As was described earlier in Equation 2.2, the effective electric field experienced by the piezoelectric ceramic is greatly reduced due to the low permittivity polymer matrix, resulting in a much lower poling efficiency. To reduce the mismatch PVA is poled at elevated temperatures to increase its electrical conductivity and can be seen in Figure 3.14. The extremely high permittivity obtained in the low-frequency-high temperature region (Figure 3.16) is a result of the dielectric relaxation of the polymer and is attributed to the ionic hopping mechanism. However, a very high conductivity increases the dielectric losses, making it difficult to pole the samples. This effect was observed in one of the initial trial foams fabricated using Polyethyelene glycol (PEG) as a plasticizer, which could not be poled due to its high conductivity (section B.2). Therefore, it is highly important to optimize the conductivity of the polymer matrix to improve the poling efficiency.

The poling state can be correlated to the relative intensities of the (002) and (200) reflection peaks in the XRD spectrum of $BaTiO_3$ (Figure 3.3). The increase in the ratio of the $\frac{I_{002}}{I_{200}}$ peaks with temperature is an indicator for an increase in tetragonality of the $BaTiO_3$ crystal structure. This rise in tetragonality is reflected in the measured d_{33} (Figure 3.4), and is the reason why all samples are poled at 110 °C. This increase in tetragonality is attributed to the higher domain mobility of $BaTiO_3$ at temperatures close to its T_C, resulting in an increase in piezoelectric properties. Grid poling optimization for the corona poling setup is done to maximize the d_{33} of the composite, as a non-optimized voltage leads to weak ion-bombardment and a lower d_{33}. For the batch of samples used in this study, the thickness is kept consistent and the properties are measured after ageing for a day. The highest values are obtained at a grid voltage of 6 kV, much greater than that obtained in literature for random composites. There is some electret contribution to the piezoelectric response, as extremely high d_{33} values are observed sometimes just after poling (Figure 3.20), although they decay after 24 hrs. The relatively high d_{33} values can also be then attributed to the subsequent charging of the piezoactive ceramic by electrets present on the pore struts.

Another consequence of porosity is that the randomly distributed ceramic particles are now restricted to the pore struts, which are on average about 10-20 μm thick. It results in a much lower inter-particle distance between the ceramic particles. This means that the composite exhibits a higher amount of parallel connectivity and therefore the modulus mismatch between the ceramic and polymer matrix enhances the piezoelectric charge coefficient d_{33}. We also have to take into account that the measured charge coefficient includes contributions from the d_{31} component. Since electrodes could not be applied on these composites, as explained in section B.4, Al plates are used as electrodes. Therefore, an effective piezoelectric charge constant is measured instead, including contributions from both d_{33} and d_{31} as they are coupled via the Poisson's constant (Equation 1.7).

The thin struts also means that particles bigger than 2-3 μm will agglomerate and collapse the struts, resulting in sedimentation as seen for KNLN3 composites in Figure C.1 and discussed in the Appendix C. Although, the density and the volume fraction of the ceramic loading as well as the viscosity of the foam slurry will also affect foam stability. This is also the reason why $BaTiO_3$ particles worked the best in this study, as they were small enough to not affect the foam stability to a great extent. This can be inferred from the porosity measurements for PVA1 foams (Figure 3.13), where foams upto 32 vol.% loading had porosities in the region of 92-94% , and a significant drop was only observed for the highest loading (44 vol.%). As was explained earlier in subsection 1.1.1, the dielectric and piezoelectric properties of $BaTiO_3$ are grain size dependent (Figure 1.9). Further decrease of particle size for improved foam stability and better distribution would not improve the piezoelectric properties, as $BaTiO_3$ below 200 nm has a cubic crystal structure and is therefore paraelectric. For $BaTiO_3$ the optimum grain size is about 0.7-1 μm, which could be the range where the best properties for the foam could be obtained, although it could not be done during this study, and is part of the recommendations.

A negative consequence of introducing porosity is the interface porosity present between the two different phases due to poor adhesion (Figure 3.12). It leads to the formation of insulation barriers which greatly reduce the poling efficiency of the composite, meaning the active piezoceramic has a lower piezoelectric response. Interface porosity also act as stress absorbers resulting in lower stresses applied on the piezoceramic, and therefore a lower piezoelectric response.

As the data is collected over a span of several months, the humidity varied a lot during the summer and winter seasons. To account for the whole spectrum of d_{33} values measured during this period, a box plot is shown in Figure 4.2. During the humid days, d_{33} values as high as 45 pC/N were measured, although there is also a significant increase in the permittivity as well as the $\tan\delta$ losses. It is difficult to isolate the different factors mainly conductivity, permittivity, modulus and the poling efficiency which affect the piezoelectric behaviour of the composite since they are electromechanically coupled to each other.

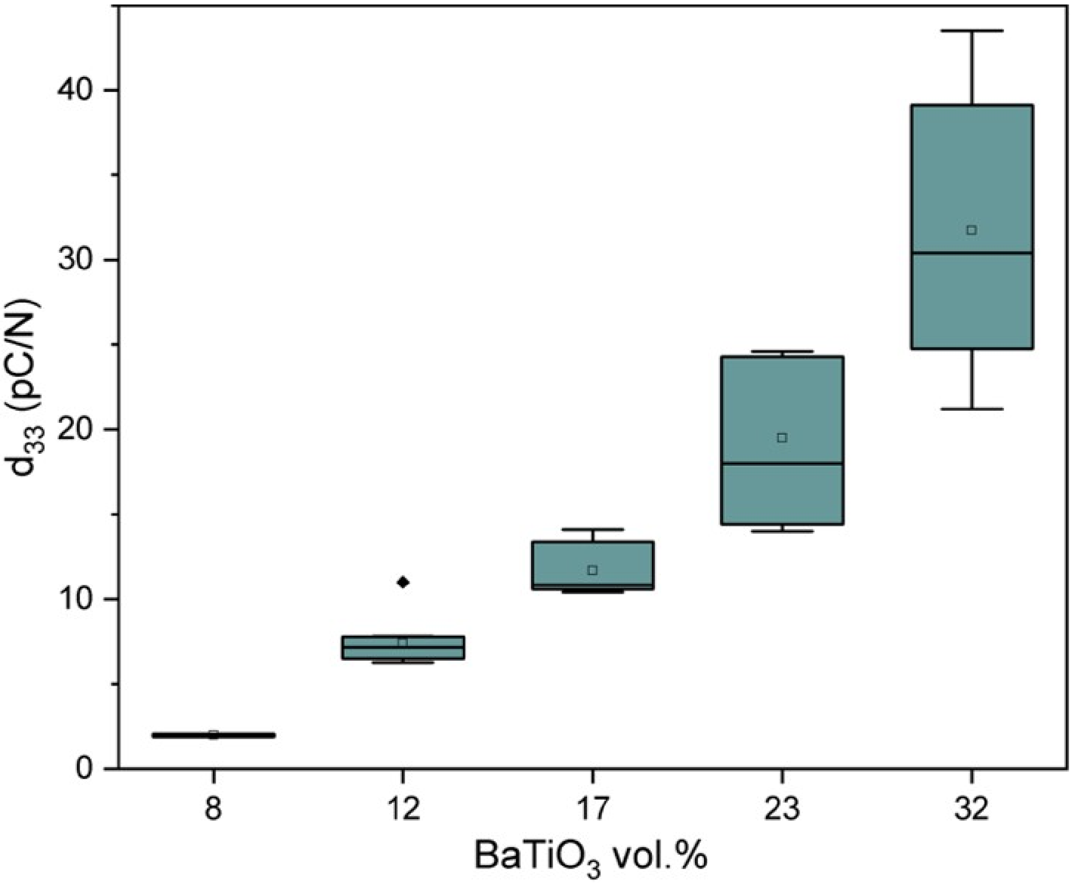

Figure 4.2: Boxplot of all d_{33} data collected for PVA1 foams with porosities in the 90-90% range

The discussion of the dielectric and piezoelectric properties above is important, in order to define the high g_{33} values obtained for the porous composites. The high poling efficiency is attributed to multiple factors: optimized grid voltage, absence of interface porosity and the conductivity of polymer matrix. While poling $BaTiO_3$ at a higher temperature increases the tetragonality of the ceramic, and therefore its d_{33}. The mechanical properties of the foam contribute to the modulus mismatch, while the particle size and distribution define the overall piezoelectric response. The permittivity is controlled by the porosity at RT, which for the highest loading is about 2.5. Such a low value of permittivity has a major impact on the calculated g_{33}, as it now exceeds the 1000 mV.m/N mark, and has values twice as better than the sensors used in the industry currently (PVDF). With increasing humidity levels, the increase in d_{33} is offset by the jump in the relative permittivity of the composite, and therefore a lower value of g_{33} is obtained. The optimum humidity level to maximize the piezoelectric voltage response is in the range of 55-60% RH.

Although these composites are extremely soft with modulus in the kPa region, they cannot be used for applications requiring sensing of high mechanical loads/stresses. The best use-case could be for a touch or a vibration sensor, in order for the material to have a linear electromechanical response. As it was explained earlier, humidity has major implications on the electromechanical response of these composites, so either they should be used in a closed environment or crosslinked for commercial applications (section B.1).

5

Conclusions

To improve on the current generation of piezoelectric sensor technology, an avenue to explore is the reduction of the dielectric constant of a piezoelectric composite. This can be achieved by including the third phase with a low dielectric constant, such as air, to create a so-called “tri-phase” composite. The inclusion of air results in a porous structure which reduces the dielectric permittivity of the composite significantly, while not having a major impact on the piezoelectric charge constant (d_{33}) of the composite.

PVA foams are fabricated using the direct foaming technique which resulted in porosities greater than 90% . As the dielectric permittivity is a matrix dominated property, this high porosity leads to a major reduction in the dielectric constant of the foam composite. Although cell anisotropy was not achieved using this fabrication process, the high porosity still reduced the permittivity to a great extent. Big size KNLN3 (25-63 μm) used during the foaming process resulted in sedimentation and collapse of the microstructure. Therefore, only BT particles (300 nm) were used for further study, with ceramic loadings up to 32 vol.% . The corona poling process employed resulted in the formation of electrets, charging the cellular structure and improving the poling efficiency of the piezoelectric foams. Another consequence of fabricating a porous structure is the reduction of the modulus of the composites, which results in a bigger modulus mismatch. The poling efficiency was significantly improved by poling at a higher temperature and an optimized grid voltage. The piezoelectric voltage response for the PVA1-BT composites crossed the 1000 mV.m/N mark and has successfully demonstrated the effect of porosity on the piezoelectric properties of the composite.

Bibliography

[1] A. D. B. Ferreira, P. R. Nóvoa, and A. T. Marques, “Multifunctional material systems: A state-of-the-art review,” *Composite Structures*, vol. 151, pp. 3–35, 2016.

[2] G. Gautschi, “Piezoelectric sensors,” in *Piezoelectric Sensorics*, Springer, 2002, pp. 73–91.

[3] J. Holterman and W. Groen, *An Introduction to piezoelectric materials and applications*. Stichting Applied Piezo, 2013.

[4] J. Curie and P. Curie, “Développement par compression de l’électricité polaire dans les cristaux hémièdres à faces inclinées,” *Bulletin de minéralogie*, vol. 3, no. 4, pp. 90–93, 1880.

[5] M. Stewart and M. G. Cain, “Direct piezoelectric measurement: The berlincourt method,” in *Characterisation of Ferroelectric Bulk Materials and Thin Films*, Springer, 2014, pp. 37–64.

[6] H. Khanbareh, “Expanding the functionality of piezo-particulate composites,” 2016.

[7] R. G. Ballas, *Piezoelectric multilayer beam bending actuators: Static and dynamic behavior and aspects of sensor integration*. Springer Science & Business Media, 2007.

[8] W. Cao, “The strain limits on switching,” *Nature materials*, vol. 4, no. 10, pp. 727–728, 2005.

[9] J. Li, R. Rogan, E. Üstündag, and K. Bhattacharya, “Domain switching in polycrystalline ferroelectric ceramics,” *Nature materials*, vol. 4, no. 10, pp. 776–781, 2005.

[10] E. Subbarao, M. McQuarrie, and W. Buessem, “Domain effects in polycrystalline barium titanate,” *Journal of Applied Physics*, vol. 28, no. 10, pp. 1194–1200, 1957.

[11] D. Berlincourt and H. H. Krueger, “Domain processes in lead titanate zirconate and barium titanate ceramics,” *Journal of Applied Physics*, vol. 30, no. 11, pp. 1804–1810, 1959.

[12] T. Takenaka and H. Nagata, “Current status and prospects of lead-free piezoelectric ceramics,” *Journal of the European Ceramic Society*, vol. 25, no. 12, pp. 2693–2700, 2005.

[13] M. Acosta, N. Novak, V. Rojas, *et al.*, “Batio3-based piezoelectrics: Fundamentals, current status, and perspectives,” *Applied Physics Reviews*, vol. 4, no. 4, p. 041 305, 2017.

[14] D. Ghosh, A. Sakata, J. Carter, *et al.*, “Domain wall displacement is the origin of superior permittivity and piezoelectricity in batio3 at intermediate grain sizes,” *Advanced Functional Materials*, vol. 24, no. 7, pp. 885–896, 2014.

[15] Y. Tan, J. Zhang, C. Wang, G. Viola, and H. Yan, “Enhancement of electric field-induced strain in batio3 ceramics through grain size optimization,” *physica status solidi (a)*, vol. 212, no. 2, pp. 433–438, 2015.

[16] Y. Tan, J. Zhang, Y. Wu, *et al.*, “Unfolding grain size effects in barium titanate ferroelectric ceramics,” *Scientific reports*, vol. 5, no. 1, pp. 1–9, 2015.

[17] H. Takahashi, Y. Numamoto, J. Tani, and S. Tsurekawa, “Piezoelectric properties of batio3 ceramics with high performance fabricated by microwave sintering,” *Japanese journal of applied physics*, vol. 45, no. 9S, p. 7405, 2006.

[18] T. R. Shrout and S. J. Zhang, “Lead-free piezoelectric ceramics: Alternatives for pzt?” *Journal of Electroceramics*, vol. 19, no. 1, pp. 113–126, 2007.

[19] Y. Guo, K.-i. Kakimoto, and H. Ohsato, “Phase transitional behavior and piezoelectric properties of (na 0.5 k 0.5) nb o 3–li nb o 3 ceramics,” *Applied physics letters*, vol. 85, no. 18, pp. 4121–4123, 2004.

[20] Y. Saito, H. Takao, T. Tani, *et al.*, “Lead-free piezoceramics,” *Nature*, vol. 432, no. 7013, pp. 84–87, 2004.

[21] J.-F. Li, K. Wang, F.-Y. Zhu, L.-Q. Cheng, and F.-Z. Yao, “(k, na) nbo 3-based lead-free piezoceramics: Fundamental aspects, processing technologies, and remaining challenges,” *Journal of the American Ceramic Society*, vol. 96, no. 12, pp. 3677–3696, 2013.

[22] N. K. James, D. B. Deutz, R. K. Bose, S. van der Zwaag, and P. Groen, “High piezoelectric voltage coefficient in structured lead-free (k, na, li) nbo3 particulate—epoxy composites,” *Journal of the American Ceramic Society*, vol. 99, no. 12, pp. 3957–3963, 2016.

[23] H. Kawai, “The piezoelectricity of poly (vinylidene fluoride),” *Japanese journal of applied physics*, vol. 8, no. 7, p. 975, 1969.

[24] A. M. Vinogradov, S. C. Schumacher, and E. M. Rassi, “Dynamic response of the piezoelectric polymer pvdf,” *International Journal of Applied Electromagnetics and Mechanics*, vol. 22, no. 1-2, pp. 39–51, 2005.

[25] R. Sun, L. Wang, Y. Zhang, and C. Zhong, “Characterization of 1-3 piezoelectric composite with a 3-tier polymer structure,” *Materials*, vol. 13, no. 2, p. 397, 2020.

[26] H. J. Lee and S. Zhang, “Design of low-loss 1-3 piezoelectric composites for high-power transducer applications,” *IEEE transactions on ultrasonics, ferroelectrics, and frequency control*, vol. 59, no. 9, pp. 1969–1975, 2012.

[27] E. N. Silva and N. Kikuchi, “Design of piezocomposite materials and piezoelectric transducers using topology optimization—part iii,” *Archives of Computational Methods in Engineering*, vol. 6, no. 4, pp. 305–329, 1999.

[28] V. L. Stuber, T. R. Mahon, S. Van Der Zwaag, and P. Groen, “The effect of the intrinsic electrical matrix conductivity on the piezoelectric charge constant of piezoelectric composites,” *Materials Research Express*, vol. 7, no. 1, p. 015 703, 2019.

[29] R. Newnham, D. Skinner, and L. Cross, “Connectivity and piezoelectric-pyroelectric composites,” *Materials Research Bulletin*, vol. 13, no. 5, pp. 525–536, 1978.

[30] F. D. Ma and Y. U. Wang, “Depolarization field effect on dielectric and piezoelectric properties of particulate ferroelectric ceramic-polymer composites,” *Journal of Applied Physics*, vol. 117, no. 12, p. 124 101, 2015.

[31] D. Van den Ende, B. Bory, W. Groen, and S. Van der Zwaag, “Improving the d 33 and g 33 properties of 0-3 piezoelectric composites by dielectrophoresis,” *Journal of Applied Physics*, vol. 107, no. 2, p. 024 107, 2010.

[32] S. A. Wilson, G. M. Maistros, and R. W. Whatmore, “Structure modification of 0–3 piezoelectric ceramic/polymer composites through dielectrophoresis,” *Journal of Physics D: Applied Physics*, vol. 38, no. 2, p. 175, 2005.

[33] V. L. Stuber, D. B. Deutz, J. Bennett, *et al.*, “Flexible lead-free piezoelectric composite materials for energy harvesting applications,” *Energy Technology*, vol. 7, no. 1, pp. 177–185, 2019.

[34] D. B. Deutz, N. T. Mascarenhas, S. van der Zwaag, and W. A. Groen, “Enhancing energy harvesting potential of (k, na, li) nbo3-epoxy composites via li substitution,” *Journal of the American Ceramic Society*, vol. 100, no. 3, pp. 1108–1117, 2017.

[35] B. Krause, G.-H. Koops, N. F. van der Vegt, M. Wessling, M. Wübbenhorst, and J. van Turnhout, “Ultralow-k dielectrics made by supercritical foaming of thin polymer films,” *Advanced materials*, vol. 14, no. 15, pp. 1041–1046, 2002.

[36] C. J. M. M. Dias, *Ferroelectric composites for pyro-and piezoelectric applications*. Bangor University (United Kingdom), 1994.

[37] K. C. Khemani and A. C. S. Staff, *Polymeric foams*. ACS Publications, 1997.

[38] N. Chand and J. Sharma, “Influence of porosity on resistivity of polypropylene foams,” *Journal of cellular plastics*, vol. 48, no. 1, pp. 43–52, 2012.

[39] W. Cao, Q. Zhang, and L. E. Cross, “Theoretical study on the static performance of piezoelectric ceramic-polymer composites with 1-3 connectivity,” *Journal of applied physics*, vol. 72, no. 12, pp. 5814–5821, 1992.

[40] ——, “Theoretical study on the static performance of piezoelectric ceramic-polymer composites with 2-2 connectivity,” *IEEE transactions on ultrasonics, ferroelectrics, and frequency control*, vol. 40, no. 2, pp. 103–109, 1993.

[41] Q. Zhang, W. Cao, H. Wang, and L. E. Cross, “Characterization of the performance of 1–3 type piezocomposites for low-frequency applications,” *Journal of applied physics*, vol. 73, no. 3, pp. 1403–1410, 1993.

[42] H. Khanbareh, S. Van der Zwaag, and W. Groen, “Effect of dielectrophoretic structuring on piezoelectric and pyroelectric properties of lead titanate-epoxy composites,” *Smart Materials and Structures*, vol. 23, no. 10, p. 105 030, 2014.

[43] H. G. Lee and H. G. Kim, “Influence of microstructure on the dielectric and piezoelectric properties of lead zirconate-polymer composites,” *Journal of the American Ceramic Society*, vol. 72, no. 6, pp. 938–942, 1989.

[44] K. C. Kao, “5 - electrets,” in *Dielectric Phenomena in Solids*, K. C. Kao, Ed., San Diego: Academic Press, 2004, pp. 283–326, ISBN: 978-0-12-396561-5. DOI: `https://doi.org/10.1016/B978-012396561-5/50015-3`. [Online]. Available: `https://www.sciencedirect.com/science/article/pii/B9780123965615500153`.

[45] S. Bauer, R. Gerhard, and G. M. Sessler, “Ferroelectrets: Soft electroactive foams for transducers,” 2004.

[46] S. Bauer, “Piezo-, pyro-and ferroelectrets: Soft transducer materials for electromechanical energy conversion,” *IEEE Transactions on Dielectrics and Electrical Insulation*, vol. 13, no. 5, pp. 953–962, 2006.

[47] Y. Zhang, C. R. Bowen, S. K. Ghosh, *et al.*, “Ferroelectret materials and devices for energy harvesting applications,” *Nano Energy*, vol. 57, pp. 118–140, 2019.

[48] X. Zhang, L. Wu, and G. M. Sessler, “Energy harvesting from vibration with cross-linked polypropylene piezoelectrets,” *AIP Advances*, vol. 5, no. 7, p. 077 185, 2015.

[49] M.-G. Kang, W.-S. Jung, C.-Y. Kang, and S.-J. Yoon, “Recent progress on pzt based piezoelectric energy harvesting technologies,” in *Actuators*, Multidisciplinary Digital Publishing Institute, vol. 5, 2016, p. 5.

[50] S. A. Wilson, R. P. Jourdain, Q. Zhang, *et al.*, “New materials for micro-scale sensors and actuators: An engineering review,” *Materials Science and Engineering: R: Reports*, vol. 56, no. 1-6, pp. 1–129, 2007.

[51] M. Wegener, W. Wirges, and R. Gerhard-Multhaupt, “Piezoelectric polyethylene terephthalate (petp) foams–specifically designed and prepared ferroelectret films,” *Advanced Engineering Materials*, vol. 7, no. 12, pp. 1128–1131, 2005.

[52] M. Wegener, E. Tuncer, W. Wirges, *et al.*, “Ferroelectrets: Highly anisotropic electrically charged polymer foams for electromechanical transducer applications,” in *IEEE Ultrasonics Symposium, 2004*, IEEE, vol. 2, 2004, pp. 1138–1141.

[53] N. Mills, *Polymer foams handbook: engineering and biomechanics applications and design guide*. Elsevier, 2007.

[54] L. J. Gibson, “Cellular solids,” *Mrs Bulletin*, vol. 28, no. 4, pp. 270–274, 2003.

[55] D. Eaves, *Handbook of Polymer Foams*. Rapra Technology Limited, 2004, ISBN: 9781847350541. [Online]. Available: `https://books.google.nl/books?id=jhB6AQAACAAJ`.

[56] H. L. Chan, P. Ng, and C. Choy, “Effect of poling procedure on the properties of lead zirconate titanate/vinylidene fluoride-trifluoroethylene composites,” *Applied physics letters*, vol. 74, no. 20, pp. 3029–3031, 1999.

[57] B. Ploss, B. Ploss, F. G. Shin, H. L. Chan, and C. Choy, “Pyroelectric or piezoelectric compensated ferroelectric composites,” *Applied Physics Letters*, vol. 76, no. 19, pp. 2776–2778, 2000.

[58] A. Briddick, P. Li, A. Hughes, F. Courchay, A. Martinez, and R. L. Thompson, “Surfactant and plasticizer segregation in thin poly (vinyl alcohol) films,” *Langmuir*, vol. 32, no. 3, pp. 864–872, 2016.

[59] C. M. Hassan and N. A. Peppas, “Structure and applications of poly (vinyl alcohol) hydrogels produced by conventional crosslinking or by freezing/thawing methods,” *Biopolymers· PVA hydrogels, anionic polymerisation nanocomposites*, pp. 37–65, 2000.

[60] R. Nangia, N. K. Shukla, and A. Sharma, “Preparation, structural and dielectric properties of solution grown polyvinyl alcohol (pva) film,” in *IOP Conference Series: Materials Science and Engineering*, IOP Publishing, vol. 225, 2017, p. 012 044.

[61] E. A. Van Etten, E. S. Ximenes, L. T. Tarasconi, I. T. Garcia, M. M. Forte, and H. Boudinov, “Insulating characteristics of polyvinyl alcohol for integrated electronics,” *Thin Solid Films*, vol. 568, pp. 111–116, 2014.

[62] N. Peppas, “Hydrogels in medicine and pharmacy, vol 2, polymers,” *Boca Raton, FL: CRC*, 1987.

[63] P. B. Bhargav, V. M. Mohan, A. Sharma, and V. N. Rao, “Structural, electrical and optical characterization of pure and doped poly (vinyl alcohol)(pva) polymer electrolyte films,” *International Journal of Polymeric Materials*, vol. 56, no. 6, pp. 579–591, 2007.

[64] S. Rajendran and O. Mahendran, “Experimental investigations on plasticized pmma/pva polymer blend electrolytes,” *Ionics*, vol. 7, no. 4, pp. 463–468, 2001.

[65] M. M. Coleman and P. C. Painter, “Hydrogen bonded polymer blends,” *Progress in polymer science*, vol. 20, no. 1, pp. 1–59, 1995.

[66] M. Avella, M. Cocca, M. Errico, and G. Gentile, “Biodegradable pvoh-based foams for packaging applications,” *Journal of cellular plastics*, vol. 47, no. 3, pp. 271–281, 2011.

[67] Y. Pan, W. Wang, C. Peng, K. Shi, Y. Luo, and X. Ji, “Novel hydrophobic polyvinyl alcohol–formaldehyde foams for organic solvents absorption and effective separation,” *RSC Advances*, vol. 4, no. 2, pp. 660–669, 2014.

[68] N. Zhao, L. H. Mark, C. Zhu, *et al.*, “Foaming poly (vinyl alcohol)/microfibrillated cellulose composites with co2 and water as co-blowing agents,” *Industrial & Engineering Chemistry Research*, vol. 53, no. 30, pp. 11 962–11 972, 2014.

[69] Y. Jia, S. Bai, C. B. Park, and Q. Wang, “Effect of boric acid on the foaming properties and cell structure of poly (vinyl alcohol) foam prepared by supercritical-co2 thermoplastic extrusion foaming,” *Industrial & Engineering Chemistry Research*, vol. 56, no. 23, pp. 6655–6663, 2017.

[70] R. J. Pugh, “Particle-stabilized foams,” in *Bubble and Foam Chemistry*. Cambridge University Press, 2016, pp. 269–306. DOI: `10.1017/CBO9781316106938.009`.

[71] S. Anandakrishnan, “Optimization of scale-up of knln piezocomposites: For flexible haptic feedback applications,” 2020.

[72] C. Wong, Y. Wong, and F. G. Shin, “Effect of interfacial charge on polarization switching of lead zirconate titanate particles in lead zirconate titanate/polyurethane composites,” *Journal of applied physics*, vol. 92, no. 7, pp. 3974–3978, 2002.

[73] J. Mendiola, C. Alemany, B. Jimenez, and E. Maurer, “Poling of (pb, la)(zr, ti) o 3 ferroelectric composite,” *Journal of materials science letters*, vol. 4, no. 11, pp. 1383–1386, 1985.

[74] M. C. Chure, P. C. Chen, L. Wu, B. H. Chen, and K. K. Wu, “Influence of poling conditions on the characteristics of pzt ceramics,” in *Advanced Materials Research*, Trans Tech Publ, vol. 284, 2011, pp. 1375–1380.

[75] N. K. James, “Piezoelectric and dielectric properties of polymer-ceramic composites for sensors,” 2015.

[76] D. Waller and A. Safari, “Corona poling of pzt ceramics and flexible piezoelectric composites,” *Ferroelectrics*, vol. 87, no. 1, pp. 189–195, 1988.

[77] S. Fedosov, A. Sergeeva, T. Revenyuk, and A. Butenko, “Application of corona discharge for poling ferroelectric and nonlinear optical polymers,” *arXiv preprint arXiv:0705.0177*, 2007.

[78] S. Dalle Vacche, D. Damjanovic, V. Michaud, and Y. Leterrier, “Interface-dominated time-dependent behavior of poled poly (vinylidene fluoride–trifluoroethylene)/barium titanate composites,” *Materials*, vol. 13, no. 1, p. 225, 2020.

[79] S. Dalle Vacche, Y. Leterrier, V. Michaud, D. Damjanovic, A. B. Aebersold, and J.-A. E. Månson, “Effect of interfacial interactions on the electromechanical response of poly (vinylidene fluoride-trifluoroethylene)/batio3 composites and its time dependence after poling,” *Composites Science and Technology*, vol. 114, pp. 103–109, 2015.

[80] Z. Wang and F. Narita, “Corona poling conditions for barium titanate/epoxy composites and their unsteady wind energy harvesting potential,” *Advanced Engineering Materials*, vol. 21, no. 7, p. 1 900 169, 2019.

[81] H.-I. Hsiang, K.-Y. Lin, F.-S. Yen, and C.-Y. Hwang, “Effects of particle size of batio3 powder on the dielectric properties of batio3/polyvinylidene fluoride composites,” *Journal of materials science*, vol. 36, no. 15, pp. 3809–3815, 2001.

[82] H. S. Mansur, C. M. Sadahira, A. N. Souza, and A. A. Mansur, “Ftir spectroscopy characterization of poly (vinyl alcohol) hydrogel with different hydrolysis degree and chemically crosslinked with glutaraldehyde,” *Materials Science and Engineering: C*, vol. 28, no. 4, pp. 539–548, 2008.

[83] T. Soliman, M. Zaki, M. Hessien, and S. I. Elkalashy, “The structure and optical properties of pva-batio3 nanocomposite films,” *Optical Materials*, vol. 111, p. 110 648, 2021.

[84] S. Ningaraju, A. G. Prakash, and H. Ravikumar, “Studies on free volume controlled electrical properties of pva/nio and pva/tio2 polymer nanocomposites,” *Solid State Ionics*, vol. 320, pp. 132–147, 2018.

[85] N. G. McCrum, B. E. Read, and G. Williams, “Anelastic and dielectric effects in polymeric solids,” 1967.

[86] I. Hodge, K. Ngai, and C. Moynihan, “Comments on the electric modulus function,” *Journal of non-crystalline solids*, vol. 351, no. 2, pp. 104–115, 2005.

[87] F. Tian and Y. Ohki, “Electric modulus powerful tool for analyzing dielectric behavior,” *IEEE Transactions on Dielectrics and Electrical Insulation*, vol. 21, no. 3, pp. 929–931, 2014.

[88] A. S. Ala’eddin and P. Poopalan, “Ac conductivity and dielectric relaxation behavior of sol-gel baxsr1-xtio3 thin films,” *Journal of Materials Science & Technology*, vol. 27, no. 9, pp. 802–808, 2011.

[89] E. A. Van Etten, E. S. Ximenes, L. T. Tarasconi, I. T. Garcia, M. M. Forte, and H. Boudinov, “Insulating characteristics of polyvinyl alcohol for integrated electronics,” *Thin Solid Films*, vol. 568, pp. 111–116, 2014.

[90] J. Betzabe Gonzalez-Campos, Z. Y. Garcia-Carvajal, E. Prokhorov, *et al.*, “Revisiting the thermal relaxations of poly (vinyl alcohol),” *Journal of applied polymer science*, vol. 125, no. 5, pp. 4082–4090, 2012.

[91] T. Yamada, T. Ueda, and T. Kitayama, “Piezoelectricity of a high-content lead zirconate titanate/polymer composite,” *Journal of Applied Physics*, vol. 53, no. 6, pp. 4328–4332, 1982.

[92] N. Jayasundere and B. Smith, “Dielectric constant for binary piezoelectric 0-3 composites,” *Journal of Applied Physics*, vol. 73, no. 5, pp. 2462–2466, 1993.

[93] N. Jayasundere, B. Smith, and J. Dunn, “Piezoelectric constant for binary piezoelectric 0-3 connectivity composites and the effect of mixed connectivity,” *Journal of applied physics*, vol. 76, no. 5, pp. 2993–2998, 1994.

[94] S. K. Mahadeva, J. Berring, K. Walus, and B. Stoeber, “Effect of poling time and grid voltage on phase transition and piezoelectricity of poly (vinyledene fluoride) thin films using corona poling,” *Journal of physics D: applied physics*, vol. 46, no. 28, p. 285 305, 2013.

[95] B. Newman, J. Scheinbeim, and A. Sen, “The effect of plasticizer on the piezoelectric properties of unoriented polyvinylidene fluoride films,” *Ferroelectrics*, vol. 57, no. 1, pp. 229–241, 1984.

[96] M. Moody, C. Marvin, and G. Hutchison, “Molecularly-doped polyurethane foams with massive piezoelectric response,” *Journal of Materials Chemistry C*, vol. 4, no. 20, pp. 4387–4392, 2016.

[97] S. H. Gehrke, “Synthesis, equilibrium swelling, kinetics, permeability and applications of environmentally responsive gels,” *Responsive gels: volume transitions II*, pp. 81–144, 1993.

[98] J. G. Lyons, L. M. Geever, M. J. Nugent, J. E. Kennedy, and C. L. Higginbotham, “Development and characterisation of an agar–polyvinyl alcohol blend hydrogel,” *Journal of the mechanical behavior of biomedical materials*, vol. 2, no. 5, pp. 485–493, 2009.

[99] N. Samadi, M. Sabzi, and M. Babaahmadi, “Self-healing and tough hydrogels with physically cross-linked triple networks based on agar/pva/graphene,” *International journal of biological macromolecules*, vol. 107, pp. 2291–2297, 2018.

[100] D. S. Wang, “Plasticizers in rigid polyurethane foam,” *Journal of Cellular Plastics*, vol. 15, no. 3, pp. 144–151, 1979.

[101] A. Zoller and A. Marcilla, “Soft pvc foams: Study of the gelation, fusion, and foaming processes. i. phthalate ester plasticizers,” *Journal of Applied Polymer Science*, vol. 121, no. 3, pp. 1495–1505, 2011. DOI: `https://doi.org/10.1002/app.33671`. [Online]. Available: `https://onlinelibrary.wiley.com/doi/abs/10.1002/app.33671`.

[102] F. H. Falqi, O. A. Bin-Dahman, M. Hussain, and M. A. Al-Harthi, “Preparation of miscible pva/peg blends and effect of graphene concentration on thermal, crystallization, morphological, and mechanical properties of pva/peg (10 wt%) blend,” *International Journal of Polymer Science*, vol. 2018, 2018.

[103] E. Mousa, Y. Hafez, and G. M. Nasr, “Optical study on pva/peg blend doped with nano-silica,” *Journal of Electronic Materials*, vol. 50, no. 5, pp. 2594–2604, 2021.

[104] K. A. Tawab, M. Magida, and S. M. Ibrahim, “Effect of ionizing radiation on the morphological, thermal and mechanical properties of polyvinyl alcohol/polyethylene glycol blends,” *Journal of Polymers and the Environment*, vol. 19, no. 2, pp. 440–446, 2011.

[105] P. Liu, W. Chen, C. Liu, M. Tian, and P. Liu, “A novel poly (vinyl alcohol)/poly (ethylene glycol) scaffold for tissue engineering with a unique bimodal open-celled structure fabricated using supercritical fluid foaming,” *Scientific reports*, vol. 9, no. 1, pp. 1–12, 2019.

[106] D. Yin, A. Xiang, Y. Li, H. Qi, H. Tian, and G. Fan, “Effect of plasticizer on the morphology and foaming properties of poly (vinyl alcohol) foams by supercritical co 2 foaming agents,” *Journal of Polymers and the Environment*, vol. 27, no. 12, pp. 2878–2885, 2019.

[107] L. Wucherer, J. C. Nino, F. Basoli, and E. Traversa, “Synthesis and characterization of batio3-based foams with a controlled microstructure,” *International Journal of Applied Ceramic Technology*, vol. 6, no. 6, pp. 651–660, 2009.

[108] I.-W. Chen and X.-H. Wang, “Sintering dense nanocrystalline ceramics without final-stage grain growth,” *Nature*, vol. 404, no. 6774, pp. 168–171, 2000.

[109] X.-H. Wang, X.-Y. Deng, H.-L. Bai, *et al.*, “Two-step sintering of ceramics with constant grain-size, ii: Batio3 and ni–cu–zn ferrite,” *Journal of the American Ceramic Society*, vol. 89, no. 2, pp. 438–443, 2006.

[110] T. Karaki, K. Yan, and M. Adachi, “Barium titanate piezoelectric ceramics manufactured by two-step sintering,” *Japanese Journal of Applied Physics*, vol. 46, no. 10S, p. 7035, 2007.

[111] T. Xu and C.-A. Wang, “Effect of two-step sintering on micro-honeycomb batio3 ceramics prepared by freeze-casting process,” *Journal of the European Ceramic Society*, vol. 36, no. 10, pp. 2647–2652, 2016.

[112] T. Ikegami, S.-I. Matsuda, Y. Moriyoshi, and H. Suzuki, “Normal grain growth in porous and dense compacts,” *Journal of Materials Science*, vol. 17, no. 10, pp. 2855–2860, 1982.

[113] C. Greskovich and K. Lay, “Grain growth in very porous al2o3 compacts,” *Journal of the American Ceramic Society*, vol. 55, no. 3, pp. 142–146, 1972.

[114] M. Mehr, J. Pineiro, B. D. Santos, and J. C. Nino, “Suppressed grain growth in highly porous barium titanate foams by two-step sintering,” *Journal of the American Ceramic Society*, vol. 100, no. 2, pp. 539–545, 2017.

A

PU-BT composites

For this composite, polyurethane has been chosen as the polymeric phase, since it is easy to make a porous structure with good mechanical properties through a side reaction that one of the monomers: diisocyanate undergoes with water, producing CO_2 gas and urea. This reaction is detailed in the next section. This chapter is done as a preliminary step to verify the piezoelectric and dielectric properties of these porous composites and use them as a starting point to further improve the piezoelectric voltage coefficient.

A.1. Fabrication process

Smooth-on-Econ Crystal Clear^{TM} 202 EU Polyurethane is used as the two-component polymer system. The diisocyanate selected is 4,4'-methylenedicyclohexyl diisocyanate (Part A) and the polyol is Phenylmercuric oleate (Part B), mixed in a ratio of 100:90 by weight. Adding water to the diisocyanate component results in the release of CO_2 and the formation of poly-urea-urethane through the process shown inFigure A.1. The release of CO_2 is key to the formation of pores with low dielectric constants and can be controlled by varying the addition of water.

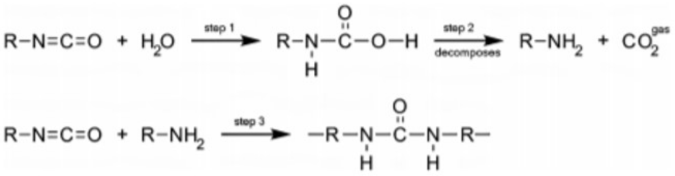

The r

Figure A.1: Reaction of the isocyanate component with water

To make the composite, Part B is speed mixed at 3500 rpm for 2 min with (0.5 wt.% of part A) H_2O, this amount of water is in µL range. While Part A is mixed separately with the ceramic filler ($BaTiO_3$). Part B is then introduced into A and speed mixed again for 2 min, before tape casting at a height of 1 mm onto an aluminium substrate coated with a release agent. The samples are cured at 65 °C for 2h followed by post-curing at 100 °C for another 2h before demolding, according to the manufacturer's guidelines. Figure 2.1 shows the tape-casting setup (right) and speed mixer (left) used to fabricate the foam. Foams with ceramic loadings higher than 20% are not made due to difficulty in mixing the individual components, leading to agglomeration of the ceramic particles. This is mainly due to the high initial viscosity of the polyol and the diisocyanate components, making them difficult to mix and subsequently cast.

The samples are initially poled using the contact poling setup. Due to the sample surface roughness and variation in thickness, they were difficult to pole. Even some samples which are poled using this process have very low piezoelectric properties. This led to the decision to pole the samples using the corona poling setup. Since it is a non-contact setup, the issues with surface roughness and thickness variation did not affect the poling efficiency to a major extent. All samples are then subsequently poled for one hour at 90 °C at a pin voltage of 50kV and grid voltage of 2 kV.

The samples are then removed from the poling setup and sputtered with gold to apply the electrodes to measure the dielectric and piezoelectric properties. The measurements are done about 24h after the poling process to remove the effects of surface charge etc.

A.2. Results & Discussion

A.2.1. Microstructure

SEM images of the porous microstructure for 10 and 15 vol.% polyurethane-BT composites is shown below in Figure A.2. The pore size remains the same in the region of 150-300 µm. Although the depth of the pores in the 15 vol.% sample is higher, leading to better interconnectivity of these pores. The results exhibit the fact that the overall porosity is controlled by the amount of H_2O added to the mix. The porosity remains consistent for these samples with some through pores present in the 15 vol.% BT samples. These results are consistent with the findings from the work done by Kevin and Hamideh [6]. The foams also exhibit closed-cell morphology which can be observed from the SEM images.

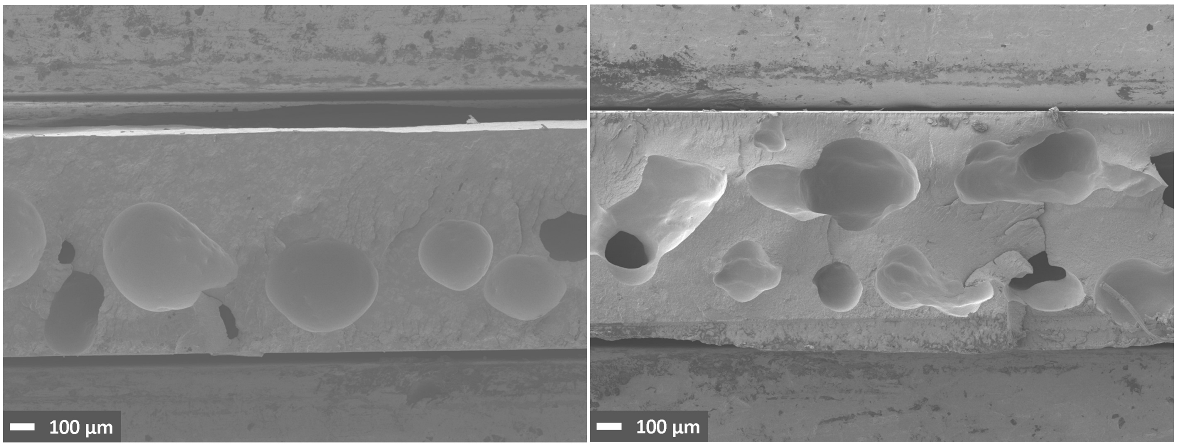

(a) PU-(0.5 wt.% A) H_2O-10 vol.% BT, 50x magnification

(b) PU-(0.5 wt.% A) H_2O-15 vol.% BT, 50x magnification

Figure A.2: SEM images of porous BT-Polyurethane composite cross-section

A.2.2. Dielectric and piezoelectric measurements

Having confirmed the successful creation of pores in the microstructure the investigation of the dielectric and piezoelectric properties of the composites is the next logical step. To that end, the tanδ and the ε_r of several polyurethane composites with different levels of added water are shown in Figure A.3. From this, it is clear that the addition of large air pores has indeed reduced the overall dielectric constant of the system. The tanδ stays consistently below 0.05 for all the ceramic loading of the samples measured. The samples are on average around 60% porous.

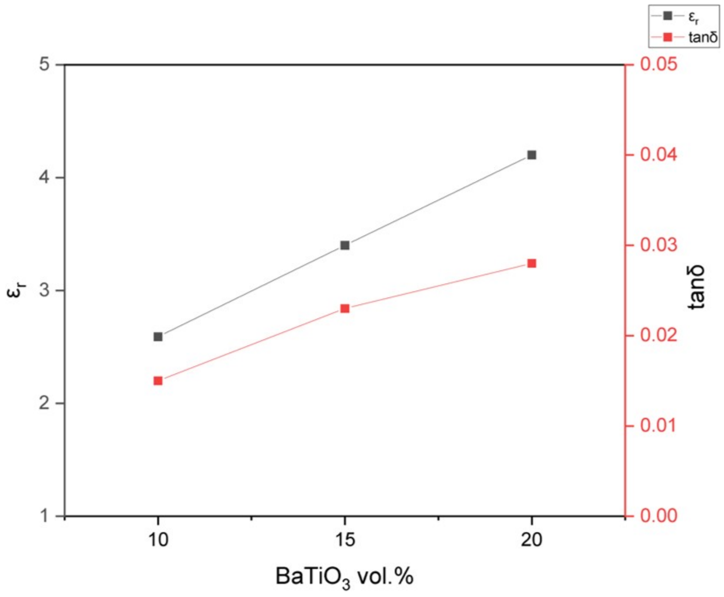

Figure A.3: Dielectric constant and $\tan\delta$ at different BaTiO3 ceramic loadings

The variation of d_{33} with ceramic loading is shown in Figure A.4. It follows the general trend of an increase in d_{33} with increasing ceramic loading as expected of a 0-3 type composite (59). Furthermore, by comparing the d_{33} values for porous and non-porous polyurethane-based systems it is evident that the addition of pores does not have an appreciable impact on the piezoelectric performance of the system. However, due to the reduction in the ε_r caused by the air, the g_{33} of the system increases significantly. The maximum achievable g_{33} of 105 mV.m/N is found at the highest ceramic loading used (20%). This is mainly due to the overall reduction in the dielectric constant. For higher loadings, there is an improvement in the d_{33}, although the dielectric constant also increases. This proportional increase in both factors result in the same increasing trend but with the curve flattening near 20% . Another important thing to note is the fact that the volume percentages showcased in these plots are for bulk composites and not porous composites.

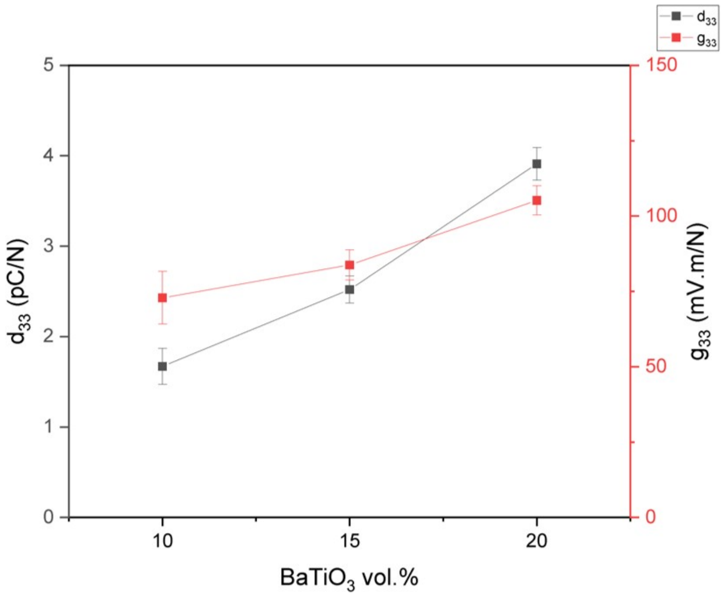

Figure A.4: d_{33} and g_{33} at different BaTiO3 ceramic loadings

A.3. Conclusions

The porous composites foams were fabricated to replicate the work done by Hamideh (6), and to verify the changes in properties observed. To obtain the required porosity, 0.5 wt.% of part A amount of water was added to react with the diisocyanate (A) and release CO2. Samples with varying volume fractions of $BaTiO_3$ (10, 15 and 20%) were fabricated using tape-casting. Higher loading samples were difficult to fabricate due to the already high viscosity of the individual components of the polymer (polyurethane) and the ceramic phase. Samples were poled using the corona poling setup for one hour at room temperature, due to difficulties with the contact poling setup as mentioned previously. The samples were on average 60% porous, in-line with the values obtained from the literature. As a result, the linear increase in the dielectric constant can be attributed to the increase in the ceramic loading, as observed in Figure 29. The highest g_{33} was obtained at the lowest ceramic loading considered in the study at 113 mV.m/N. The gradual increase in g_{33} with ceramic loading is expected as the increase in permittivity is compensated by the increase in d_{33}, although the curve flattens at higher loadings.

The polymer matrix and the foaming techniques used limits the pore morphology and the overall porosity of the composite. As was stated in subsection 1.3.1, a more anisotropic pore structure leads to a much higher reduction in the permittivity values, which was not possible in the system used. Another limiting factor is that the polymer matrix was hard/brittle, making it difficult to exploit the modulus mismatch between the polymer and the ceramic phase. A softer polymer matrix would in theory impart higher stresses on the ceramic particles relative to a stiffer polymer matrix, resulting in higher piezoelectric properties measured at the same force. The samples were also not poled efficiently in this setup, as the conductivity mismatch of the two phases resulted in a lower poling efficiency. Even poling samples at 110 °C, did not result in better piezoelectric performance, making the polymer matrix unsuitable.

B

Experimental trials

Before concluding all the work done during this thesis, this section adds a bit of context to why some choices were made regarding the final foam composites and the different methods which were tried initially and failed leading to the final system. The first three sections : section B.1, section B.2 and section B.3 describe the trials for obtaining the final foam composite (Agarose, PEG, and PVA samples locally compressed). The section B.4 is dedicated to the application of electrodes to the foam composite and section B.5 is for the sintering trials.

B.1. PVA hydrogel

As is mentioned earlier in section 1.4, for PVA to be used in commercial applications, it has to be crosslinked. There are multiple ways of doing so which include chemical crosslinking, gamma radiation and physical crosslinking by crystallite formation. The first method was discarded due to issues related to toxicity, while the second was because of issues related to setup and the inefficiency of this method. For this trial, the third method of using a physical crosslinking agent was used. A polysaccharide, Agarose is selected due to its bio-compatibility and gelling properties [97]. For this work, hydrogels are prepared based on the work by Lyons et al. [98] and Samadi et al. [99]. The final result of the two methods is shown in the Figure B.1 : left -just after fabrication, right after drying. The hydrogels shrank during the deswelling cycles and the samples were extremely stiff. For poling at higher temperatures, this led to a low-porosity stiff hydrogel that could not be poled. Therefore this concept was discarded.

(a) After swelling (b) After drying/deswelling

Figure B.1: PVA-Agarose hydrogel with BT (10 vol.%)

B.2. PVA-PEG foam

Polymer foam fabrication is done using a plasticizer and a surfactant system. In general, phthalates are used as plasticizers during the foaming process [100], [101], however due to their highly toxic nature research has been heading towards more environment friendly polymers. An option is to use polyethylene glycol (PEG) as a plasticizer due to its good blending/miscibility properties with rigid polymers and its bio-compatibility [102], [103]. This allows it to act as a plasticizer for PVA during the foaming process although above a certain concentration it is immiscible and leads to phase separation [104]. This polymer system is commonly foamed using supercritical CO_2 [105], [106], which is not possible with the current setup. Since water also acts as a plasticizer for PVA, it is used in addition to PEG during the direct foaming process. The resulting foam composite is shown in Figure B.2. The composites were then poled using the corona poling process, and had their piezoelectric properties subsequently measured. The samples were poled very weakly. This led to the discovery that the foam were highly conductive even at room temperatures, and therefore could not be poled properly.

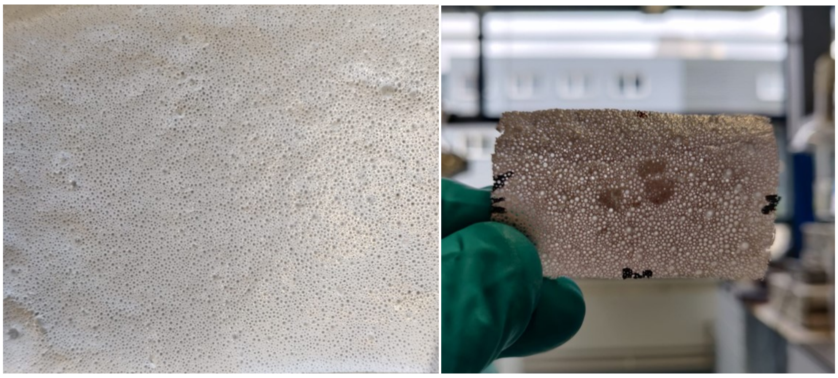

Figure B.2: PVA-PEG (90/10 wt.%) with BT (10 vol.%)

B.3. PVA foam compression

The piezoelectric properties are measured using the berlincourt setup as mentioned in subsection 2.3.5 and shown in Figure 1.2. As the foams are much softer in comparison to ceramics and other polymer-ceramic composites, it results in dimples on the surface while taking measurements as shown in Figure B.3. To prevent stress concentrations, samples are compressed evenly using a thin aluminium plate to obtain reproducible piezoelectric measurements.

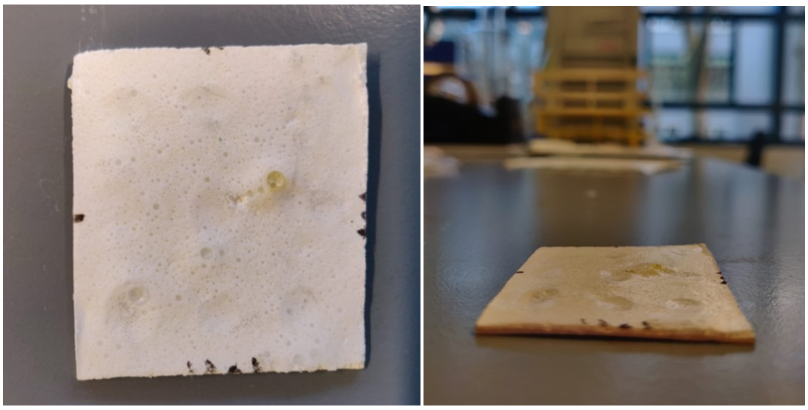

Figure B.3: Dimples on foam composites after compression

B.4. Electrodes

For dielectric and piezoelectric measurements, electrodes are applied on the top and bottom surface of the piezoelectric. Since the foam composite has a lot of open pores on the surface, it gets a bit tricky. If samples are sputtered (Figure B.4a), which is usually done for all piezoelectrics, there is a chance the system might short due to to the possibility of a through pore (pore connecting the top and bottom surface). Therefore different methods were trialled to apply electrodes. The second trial was done using a conductive silver paste, which was cast (50 µm thick layer) on the Al substrate. To prevent the paste from seeping through due to gravity, the sample was placed on top of the casted paste and co-cured at 90 °C for one hour. Although, applying electrodes before poling using the corona setup results in the samples sticking to the grid, while after poling results in reduced piezoelectric properties. Also, the conductive paste did not completely adhere to the sample surface, and therefore this concept was discarded.

The next trials were done using a thin layer (50 µm) of either epoxy or PDMS followed by sputtering the samples. Both of these polymer systems were unsuccessful in properly adhering to the surface. PDMS films had a lot of air gaps (Figure B.4b), while the epoxy system used was quite stiff and penetrated the pores completely. The last trial was done using carbon black dissolved in PVA slurry followed by co-curing with the composite, which resulted in the partial dissolution of the composite. Therefore, all measurements are then done using Al plates as top and bottom electrodes.

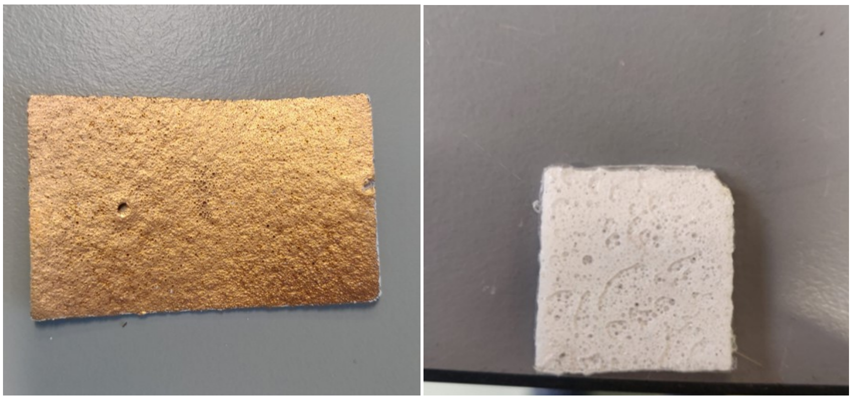

(a) Gold-sputtered electrodes (b) PDMS film on foam composite

Figure B.4: Different trials for applying electrodes

B.5. Sintered BT foams

Initial sintering experiments are done after the foam fabrication process to obtain a porous sintered ceramic. Conventional sintering practices do not allow for control over the grain size for a porous structure [107]. If there is less grain growth, you retain the porous microstructure of the original foam composite, but the sintered body obtained is very soft and fragile. While, in the case of high grain growth, the porous structure collapses. To control grain growth, two-step sintering is a prominent technique used for bulk samples. The first stage is for bonding between adjacent particles and formation and growth of necks with limited densification, Followed by the second step which includes annealing at a lower temperature to control/limit the grain growth and allow for densification [108]–[111]. An example of a sintering cycle is shown below in Figure B.5a. The second stage temperature should be below the kinetic window to suppress grain growth and is shown in Figure B.5b for $BaTiO_3$ systems.

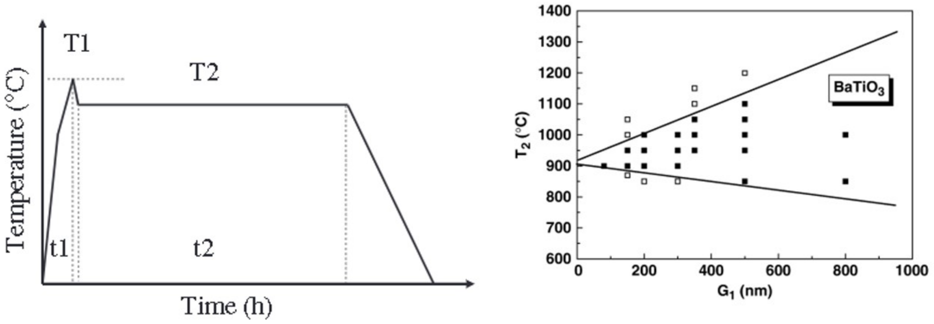

(a) A typical two-step sintering cycle [110]

(b) Kinetic window for $BaTiO_3$ (G1 - initial grain size (particle size in our case)) [109]

Figure B.5: Two-step sinter process

Although, this technique has been mainly used for bulk green bodies, as the grain growth mechanisms differ for porous structures [112], [113]. Porous structures face issues related to thermal shocks, cracks and collapse of the structure during the fast heating/cooling cycles [114]. Therefore, for this work, a two-step sinter cycle is followed for the foam composites with the highest ceramic loadings to check the viability of this process. An example of the sintering process of the foam composite pre-sinter (Figure B.6a), after the sinter (Figure B.6b) and the open pore-structure of foam (Figure B.6c), is shown below.

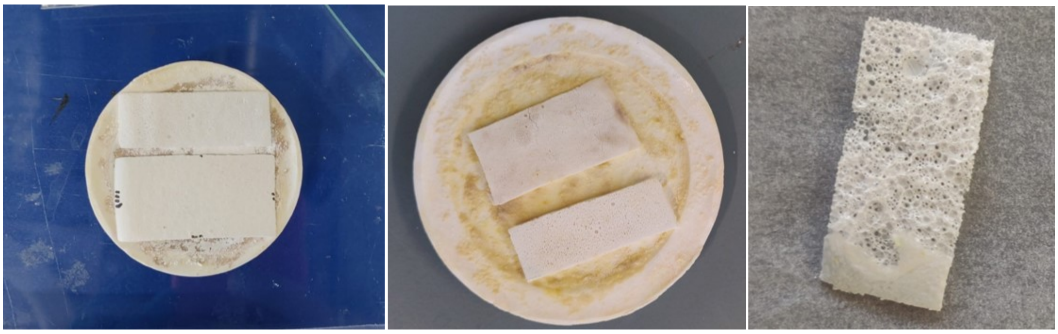

(a) Before sinter

(b) After sinter

(c) Porous structure after sinter

Figure B.6: Two-step sinter process

For this work, the two-step sinter cycle is modified from the work by Mehr et al. [114], as the foaming technique used is different. The sintered foams shown above are quite fragile as can be seen in Figure B.6c, even after multiple sintering optimizations for grain size and density. This is due to a multitude of reasons mainly due to the low initial volume fraction of the ceramic in the foam slurry and oven related limitations regarding the fast heating/cooling rates. Some examples of SEM images of the microstructure obtained is shown below in Figure B.7. The first trial with a single step sinter (Figure B.7a) resulted in almost no grain growth and a very soft foam that breaks upon slight force. Sintering at temperatures above 1325 °C for a long duration (one hour) results in abnormal grain growth, where grains grew to sizes in the range of about 100 µm (Figure B.7b). Although the foams were quite strong, their microstructure collapsed and the grain size retained is not useful for the required piezoelectric properties (Figure 1.9). The two-step sinter process resulted in foams with grain sizes in the region of 5-8 µm (Figure B.7c and Figure B.7d), although they were still quite soft for actual use in a sensor, and therefore are discarded.

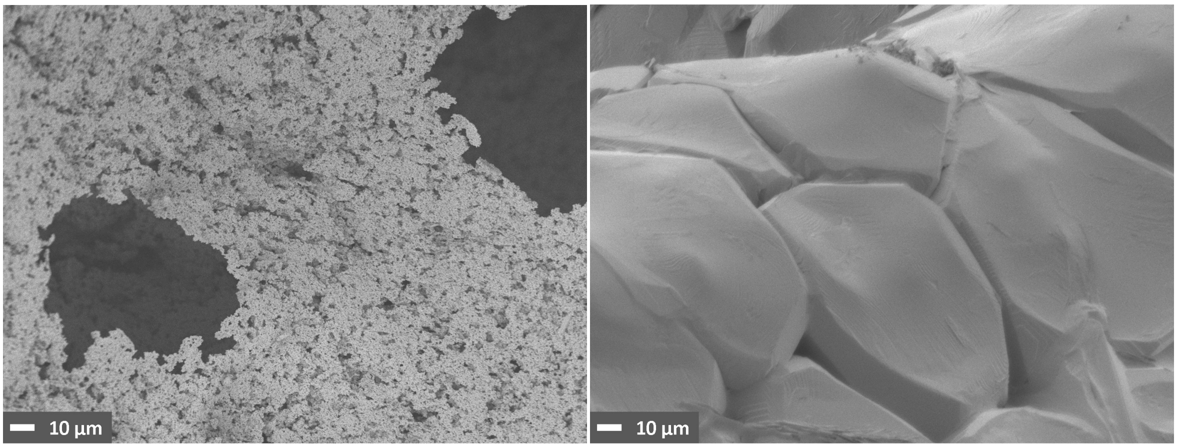

(a) Single-step sinter 1200 °C

(b) Single-step sinter 1350 °C

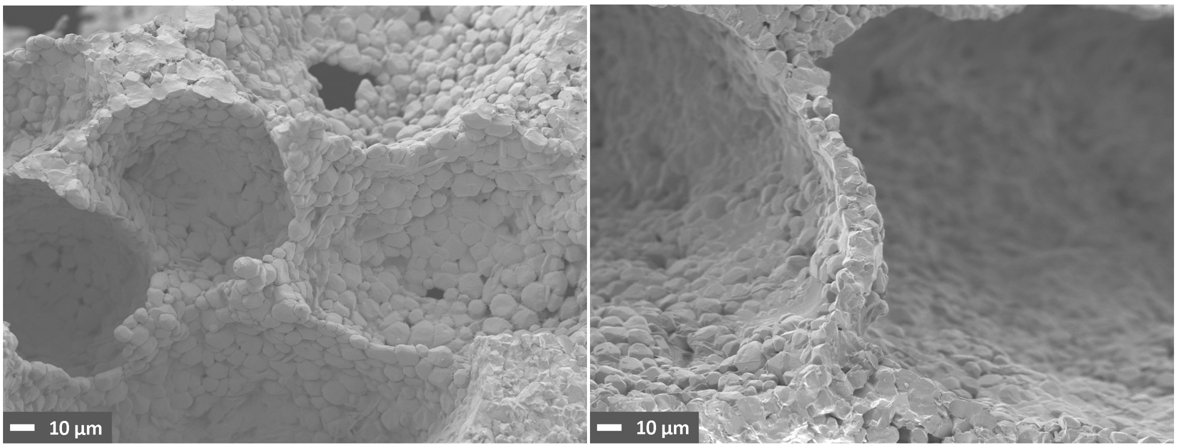

(c) Two-step sinter 1050/1375/1150 °C - pore structure

(d) Two-step sinter 1050/1375/1150 °C - thin strut

Figure B.7: SEM images of BT foams at 500x magnification

C

KNLN3-PVA foams

Due to the successful trials with BT-PVA1 and PVA2 foams, new experiments were done with the KNLN3 powders at the highest ceramic loadings, to compare the effect of ceramic filler and particle size on the microstructure and piezoelectric properties. The ceramic fillers were divided into two different size ranges according to the sieve used: <25 µm and 25-63 µm. We could already observe from the SEM images in the previous section that the average strut thickness was in the range of 10-30 µm. Particles above this size range thus had a visible effect on the microstructure of the foam as shown in Figure C.1

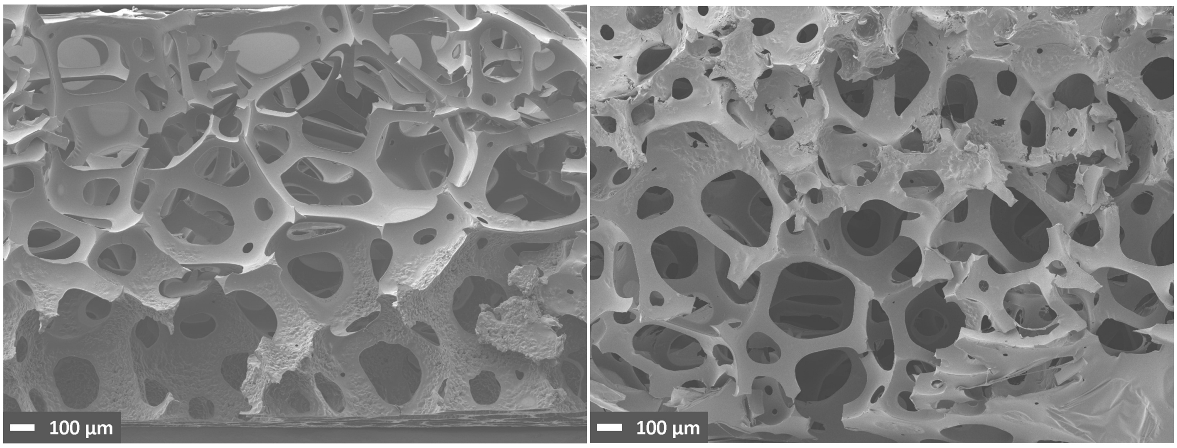

(a) KNLN3 (<25 µm) foam, 50x magnification

(b) KNLN3 (25-63 µm) foam, 50x magnification

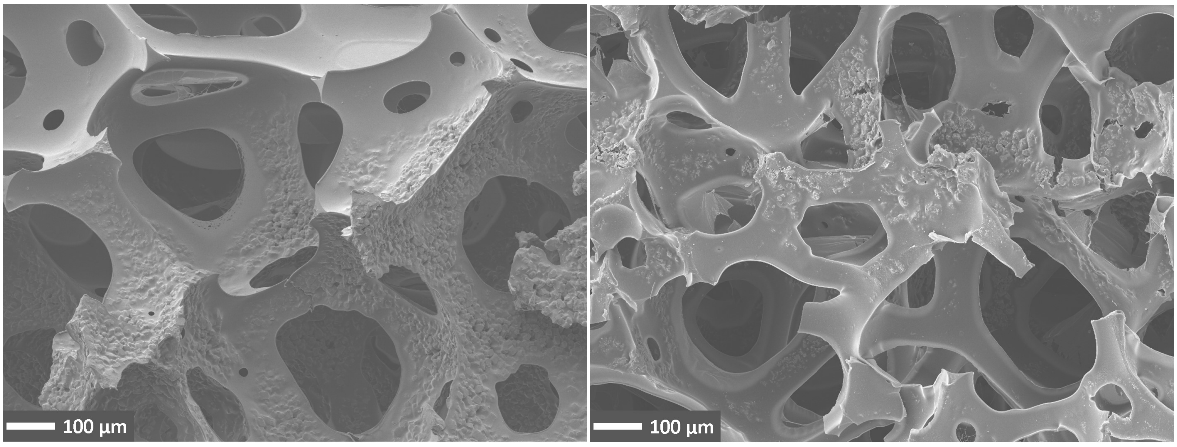

(c) KNLN3 (<25 µm), 100x magnification

(d) KNLN3 (25-63 µm) foam, 100x magnification

Figure C.1: SEM images of KNLN3-PVA1 70/30 60 °C foams

Visible sedimentation could be observed in the foams for both cases, which also affected the collapse of the foam structure. This was not observed for $BaTiO_3$ foams even at high ceramic loadings as the particle size was in the nanometer range (300 nm), even though $BaTiO_3$ has a higher density than that of KNLN3. Since the particle size played a major role in the foam stability as well as sedimentation, further trials were not done for these foams, and just the piezoelectric measurements were taken for these samples. Future studies should investigate the performance of KNLN3 with a smaller particle size to truly evaluate its performance.